Mechanobiology of biofilms : impact of mechanical factors on bacterial proliferation by an experimental approach in vitro

Margaux Blondel

RÉPUBLIQUE FRANÇAISE
Liberté Égalité Fraternité

Université de Toulouse

Doctorat de l'Université de Toulouse

préparé à Toulouse INP

Mécanobiologie des biofilms : influence de facteurs mécaniques sur la prolifération bactérienne par une approche expérimentale in-vitro

---

Thèse présentée et soutenue, le 30 mai 2024 par

Margaux BLONDEL

École doctorale
MEGEP - Mécanique, Energétique, Génie civil, Procédés

Spécialité
Génie mécanique, mécanique des matériaux

Unité de recherche
IMFT - Institut de Mécanique des Fluides de Toulouse

Thèse dirigée par
Pascal SWIDER et Sophie PALIERNE

Composition du jury
Mme Elvire SERVIEN, Présidente, Université Claude Bernard Lyon 1
Mme Véronique VIATEAU, Rapporteuse, École Nationale Vétérinaire d'Alfort
M. Georges JACQUET-RICHARDET, Rapporteur, INSA Lyon
M. Thibaut CACHON, Examinateur, VetAgro Sup
M. Pascal SWIDER, Directeur de thèse, Université Toulouse III - Paul Sabatier
Mme Sophie PALIERNE, Co-directrice de thèse, École Nationale Vétérinaire de Toulouse

Membres invités
Mme Yara Abidine, Toulouse INP

Acknowledgements

I would like to express my gratitude to all the people who contributed in one way or another to this work.

First of all, I would like to thank warmly my thesis director, Professor Pascal Swider, without whom this thesis would never have seen the light. Thank you so much for having given me the opportunity to work once again with you and your research team and for trusting me during these three years. I cannot thank you enough for everything you brought me, for all your listening, for your precious advice and for your unfailing support.

I would also like to express my sincere gratitude to Doctor Yohan Davit for having accepted my work to be part of his global research project. I am also utterly indebted to the Ecole Nationale Vétérinaire de Toulouse (ENVT) and to VetAgro Sup, both of which supported me in my research project and enabled me enriching my professional experience thanks to their trusted collaboration.

I am extremely grateful to Doctor Yara Abidine for her precious help in this work. What a surprise when we met again in Purpan! It was a pleasure working with you once again! Thank you for your time and for your availability during this thesis, and for all your help and encouragements in the difficult moments.

A heartfelt thanks to Clara Toulouze for her help and commitment when it came to testing the experimental setup with bacteria. Many thanks for the time you spent to show me how to proceed and for the interesting discussions we had on the subject. I would also like to thank Massinissa Benbelkacem and all the colleagues I met during the time spent in Purpan, who brought their encouragements and advice every time it was needed. Their help has been extremely precious as well.

I am grateful to Jérôme Briot for his ideas regarding the conception and fabrication of the mechanical device, as well as to Professor Frederic Lachaud for his collaboration in the conception of the finite element numerical models and to Stefano Lun Kwong Leon for his implication regarding 3D printing and manufacturing.

A profound thank you to my family for their constant support and for their love. Thank you so much for being on my side in this intense adventure and for your encouragements.

Abstracts

Abstract: Postoperative infection is a dreaded complication in human and veterinary orthopedics which can be associated with significant consequences in terms of morbidity, costs and recurrence. Its eradication is difficult, especially due to the development of biofilms on implants used. As a matter of fact, bacteria within a biofilm are tolerant to antibiotics, thus explaining the high number of therapeutic failures when antibiotic therapy alone is used. Investigating factors that could affect biofilm development, and particularly exploring the impacts of the solid and fluid mechanical stresses to which a healing bone is permanently submitted, could allow developing therapeutic strategies alternative to antibiotics and minimize the risk of antibiotic resistances.

The main hypothesis of this work consisted in supposing that a mechanical stimulus could modify bacterial proliferation and biofilm formation.

The first part of this work is based on describing the clinical aspects of bacterial infection in human and veterinary orthopedic surgery, as well as the mechanisms of biofilm formation. A multiscale approach of the mechanobiology underlying biofilm development is then discussed, starting from the bacterium to reach the biological tissue, and the therapeutic strategies alternative or additional to antibiotics are presented. In the second part, the original experimental workbench developed in this study is presented. A microfluidic device capable of sustaining a bending moment while still allowing bacterial biofilm growth was conceived. It consisted in a chip containing a microchannel molded into PDMS bonded to a flexible PETG coverslip. A mechanical system capable of generating a cyclic bending moment of controlled frequency and amplitude (0 – 2.5 Hz and 0 – 3.10 mm, respectively) was also conceived. The equations governing the kinematical response of the device were provided. The third part of the document presents and discusses the preliminary results of the *in vitro* study. To quantify biofilm development, PDMS chips were inoculated with a strain of *P. aeruginosa* containing a fluorescent protein-expressing plasmid. The microfluidic devices thus inoculated were then submitted to a bending moment (dynamic condition), and the static response was used as control. Imaging with epifluorescence microscopy was performed to compare fluorescence in the static chips with that in the dynamic chips.

Preliminary results showed that cyclic bending may influence biofilm development. On the one hand, biofilms formed rather randomly along the microchannels submitted to bending, contrary to those formed in the static microchannels during the same period of time. On the other hand, biofilms size and fluorescence intensity were also affected by bending, with intensity remaining unchanged between microscopic images obtained at 24h and at 48h and size increasing. Compared to static results, this latter observation suggests that bending may alter biofilm composition, especially by decreasing bacterial concentration.

In conclusion, the methodology presented in this thesis tends towards validating the initial hypothesis regarding the mechanobiological susceptibility of biofilms, in particular under steady state dynamical stimuli. This work suggests a reproducible experimental framework allowing to assess the impact of a dynamic cycle on bacterial biofilm development, and eventually to test therapeutic strategies in a controlled environment.

Key words: Biofilm, Mechanobiology, Microfluidics, *Pseudomonas aeruginosa*, Infection, Dynamic loading, Experimental methods

Résumé : L'infection postopératoire est une complication redoutée tant en chirurgie orthopédique humaine que vétérinaire, pouvant avoir des conséquences lourdes en termes de morbidité, de coûts et de récidives. Son éradication est particulièrement difficile, notamment à cause du développement de biofilms sur les implants utilisés. Les bactéries au sein d'un biofilm sont en effet tolérantes aux antibiotiques, ce qui explique les nombreux échecs thérapeutiques lorsqu'une antibiothérapie seule est utilisée. L'exploration des facteurs influant sur le développement de ces biofilms, en particulier l'impact de contraintes mécaniques fluides et solides auxquelles l'os en cours de cicatrisation est en permanence soumis, permettrait de développer des stratégies thérapeutiques alternatives aux antibiotiques, et de minimiser les risques d'antibiorésistances.

L'hypothèse centrale de ce travail a consisté à supposer qu'un stimulus mécanique pouvait modifier la prolifération bactérienne et la formation du biofilm.

La première partie de cette thèse s'attache à décrire les aspects cliniques de l'infection bactérienne en chirurgie orthopédique humaine et vétérinaire, ainsi que les mécanismes de formation d'un biofilm. La mécanobiologie sous-jacente au développement d'un biofilm est ensuite discutée dans une approche multi-échelle, de la bactérie au tissu biologique, et les stratégies thérapeutiques complémentaires ou alternatives aux antibiotiques sont présentées. La deuxième partie présente le dispositif expérimental original développé dans cette étude. Un dispositif micro-fluidique pouvant être soumis à un moment de flexion et permettant la formation d'un biofilm bactérien a été conçu. Ce dispositif a consisté en l'assemblage d'une puce contenant un micro-canal moulé dans du PDMS, et d'une lamelle flexible en PETG. Un système mécanique générant une force de flexion cyclique de fréquence et d'amplitude contrôlables (0 – 2.5 Hz et 0 – 3.10 mm, respectivement) a également été conçu. Les équations gouvernant la réponse cinématique du dispositif ont été fournies. La troisième partie du document présente et discute les résultats préliminaires obtenus dans l'étude *in vitro*. Afin de quantifier le développement du biofilm, les puces en PDMS ont été inoculées avec une souche de *P. aeruginosa* contenant un plasmide exprimant une protéine fluorescente. Les dispositifs microfluidiques ainsi inoculés ont ensuite été soumis à un moment de flexion (condition dynamique), et la réponse statique a été utilisée comme contrôle. La microscopie en épifluorescence a permis de comparer la fluorescence des puces dynamiques à celle des puces statiques.

Les résultats préliminaires ont montré que la flexion cyclique pouvait impacter le développement des biofilms. D'une part, les biofilms se sont formés de façon aléatoire le long des micro-canaux soumis à la flexion, contrairement à ceux formés dans les micro-canaux statiques pendant ce même laps de temps. D'autre part, la taille et l'intensité de la fluorescence des biofilms formés ont également été impactées par la flexion, l'intensité restant inchangée entre les images capturées à 24h et 48h mais la taille augmentant. En comparaison avec les résultats statiques, cette dernière observation suggère que la flexion pourrait altérer la composition des biofilms, en particulier en diminuant la concentration bactérienne.

En conclusion, la méthodologie proposée dans ce travail de thèse tend à valider l'hypothèse initiale au regard de la sensibilité mécanobiologique des biofilms bactériens, en particulier sous stimuli mécaniques à l'état d'équilibre. Ce document propose un cadre expérimental reproductible permettant d'évaluer l'impact d'un cycle dynamique sur le développement d'un biofilm bactérien, et éventuellement de tester des stratégies thérapeutiques dans un environnement contrôlé.

Mots clés : Biofilm, Mécanobiologie, Microfluidique, *Pseudomonas aeruginosa*, Infection, Chargement dynamique, Méthodes expérimentales

Table of contents

List of figures

List of tables

General introduction

Surgical site infection (SSI) is a common postoperative complication, occurring in approximately 1-3% human patients (Calderwood et al. 2023). Orthopedic surgery carries the highest risk of postoperative SSI, as up to 20% of orthopedic patients can be affected (Motififard et al. 2021). SSI is more common after surgical treatment of open fractures than closed fractures, with a risk ranging from 8.5% to 14.9% when one-stage treatment can be performed (Gopal et al. 2000), and exceeding 30% when multiple-staged surgeries are needed (Mathews et al. 2015). It can lead to delayed bone healing, permanent functional loss and, in up to 17.6% cases, amputation (Papakostidis et al. 2011). Surgical revision is required in more than 80% of SSI cases in orthopedics, and success rates vary between 70 and 90% (Thakore et al. 2015). Economic outcomes associated with orthopedic postoperative SSI are consequent. Indeed, treatment costs associated with these orthopedic complications are more than 2.5 times higher compared to patients without a postoperative SSI (Badia et al. 2017), with a difference in health and social care cost exceeding £1,500 (Png et al. 2022; Parker et al. 2018). This difference is in part due to the cost associated to revision procedures and to prolonged hospital stays (Badia et al. 2017). In veterinary orthopedics, the incidence of SSI is similar to what is described in human orthopedics, but can reach up to 30% after surgical repair of an open or a closed fracture in dogs (Gieling et al. 2019). The consequences can be as disastrous as those observed in human patients, and can necessitate amputation in extreme cases.

Treatment of postoperative SSI in orthopedics is a challenge for the surgeon. This is in part due to the development of bacterial biofilms on implants used for bone fixation (Costerton, Stewart, and Greenberg 1999; Kennedy et al. 2022). Biofilms are complex microbial communities, developing on interfaces usually comprising a liquid phase and encased in a self-secreted polymer matrix (Costerton, Stewart, and Greenberg 1999). Their formation is a multi-step process, and begins when a bacterium adheres to a surface. Some substrates, like implants, are more amenable to bacterial adhesion (Filipović et al. 2020). Biofilms developing on the surface of an implant eventually induce an inflammatory response in the host, and may cause implant failure. Currently, antibiotics are commonly prescribed as first-line treatment when SSIs are diagnosed after orthopedic surgery. However, their systematic and unreasonable use and their inefficiency in eradicating infections once a biofilm has formed have led to the emergence of multidrug-resistant organisms (Gieling et al. 2019; Bowler, Murphy, and Wolcott 2020). Antibiotic resistances are a cause for concern nowadays, and therapeutic alternatives to antibiotics are needed given the slow rate of new drug development (Bowler, Murphy, and Wolcott 2020; Connaughton et al. 2014; Simpkin et al. 2017).

In this context, investigating bacterial biofilm formation may allow the emergence of alternative therapeutic strategies that do not rely solely on antibiotics. As cartilage and bone tissues are reactive environments, the exploration of the roles played by biophysical factors may be of particular interest. However, the influence of mechanics on biofilm development has little been studied so far (Jara et al. 2020; Xiao, Xu, and Li 2021; Araújo et al. 2019). Mechanical constraints play key roles in the regulation of many biological processes (Dumont and Prakash 2014). Bacteria are sensitive to mechanical stimuli via numerous receptors and effectors, which allow them to adapt, deform, adhere to or detach from a support (Araújo et al. 2019; Chawla et al. 2020). It also seems that some mechanical stimuli may promote biofilm development as a defensive strategy in a hostile environment (Bottagisio et al. 2020).

In this project, we hypothesized that a mechanical stimulus could influence biofilm growth. We conceived a mechanical device that allowed submitting bacteria and biofilms to cyclic mechanical loading and we compared biofilm growth using fluorescence microscopy.

The present document is divided into three chapters. Firstly, we present a state-of-the-art of bacterial biofilm mechanobiology and its implications for treating orthopedic infection. In the

second chapter, we describe the experimental setup that we have elaborated to expose the substrate of a bacterial biofilm to a bending moment. In the third chapter, we present the first results obtained with this setup as we assess the effect of bending on biofilm growth. At last, we shall conclude and expose the perspectives brought by this project for future studies.

Chapter I:
Understanding and overcoming biofilm-associated infections in orthopedic surgery

1. Introduction

In this chapter, the clinical aspects of SSIs in bone tissue are presented in both animals and humans, and the mechanisms underlying bacterial biofilm formation are described. The role mechanical factors play on biofilm development is then discussed at different scales: bacterial microscopic scale, biofilm mesoscopic scale and fracture/implant macroscopic scale. Finally, research strategies in complement or alternative to antibiotics are presented.

Part of this chapter has been published as a review article (Blondel et al. 2024). The article can be found at the end of this work.

2. Clinical aspects of bacterial infection in orthopedic surgery

Implants are indispensable in orthopedic surgery, but they are considered as foreign materials by the body. Furthermore, the local inflammatory environment is modified secondary to trauma, and further amplified by disruption of the skin barrier related to material implantation. These factors collectively increase the risk of bacterial contamination at the surgical site. Once bacteria adhere to an implant, they form surface-adhering biofilms, which exhibit not only tolerance to the host defense and to antibiotics, but also mature over time, preventing bone healing through cytokine mediated osteoclast activation and bone resorption (Moriarty et al. 2022). Bone healing is also influenced by bacterial toxins, which may play detrimental roles in shifting the host response toward bacterial clearance or exaggerated pro-inflammatory response. They can contribute to mechanisms leading to biofilm formation and dispersion (Saeed et al. 2021).

The sequence of events in osteosynthesis-associated infection is described in Figure 1.

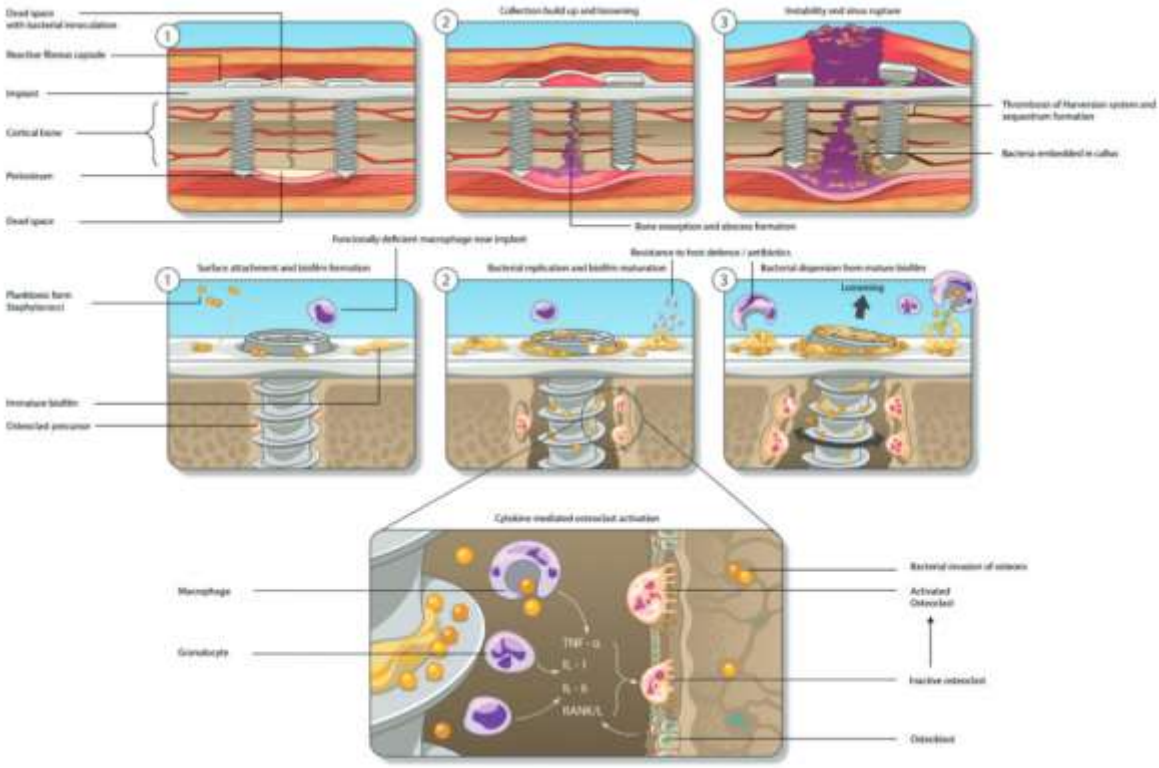

Figure 1: Sequence of events occurring in osteosynthesis-associated infection (from Fang et al. 2017)

2.1 Prevalence of bacterial isolates

Monomicrobial infections involving *Staphylococcus aureus* are most prevalent in human and animal orthopedic patients (González-Martín et al. 2022; Depypere et al. 2022). In fact, *S. aureus* is the most commonly isolated bacterium causing SSIs regardless of time to onset of infection, with the methicillin-resistant strain more frequently encountered than the methicillin-

sensitive strain (Gieling et al. 2019; Depypere et al. 2022; Fang et al. 2017a; Morgenstern et al. 2021). This Gram-positive bacterium is capable of forming biofilms on an implant or on necrotic bone, of forming abscesses in soft tissues and in bone marrow, and of penetrating into cells and colonizing the osteocyte-canaliculi network of cortical bone. Other skin commensal bacteria can also cause SSIs, such as coagulase-negative staphylococci, *Corynebacterium* and *Propionibacterium* as well as enterococci, enterobacterales, streptococcus, and *Candida spp* (González-Martín et al. 2022; Depypere et al. 2022). In human patients, SSIs developing within 2 weeks of surgery are mainly polymicrobial and frequently include enterobacterales and *Enterococcus spp.* (Depypere et al. 2022). Furthermore, the Gram-negative bacteria *Pseudomonas aeruginosa* are also frequently involved, primarily due to their minimal nutritional needs, their tolerance to relatively high temperatures and their resistance to various antibiotics (Shrestha et al. 2022). It is worth noting that *P. aeruginosa* is responsible for more recurrences and therapeutic failures than *S. aureus*, and that an increased number of multi-resistant *P. aeruginosa* infections is reported (Fang et al. 2017a). Anaerobes present more frequently in polymicrobial infections, but remain rarely isolated overall (Depypere et al. 2022; Gitajn et al. 2022).

2.2 Infection in bone healing

Bone healing occurs by one of two different repair mechanisms: primary bone healing or secondary bone healing (Foster et al. 2021). The degree of fracture reduction, the biological environment of the fracture and the stability obtained at the fracture site once the implant is placed determine whether a fractured bone heals through primary or secondary bone healing. Primary bone healing occurs when stability of the construct is absolute and when strain at the fracture site has been eliminated, which implies anatomic reduction of the fracture, compression of bone fragments and rigid fixation. When mechanical strain at the fracture site exceeds 2%, secondary bone healing occurs and involves formation of a bone callus (Foster et al. 2021).

Stability at the fracture not only determines the type of bone healing, but it is also closely linked to bone infection. Bone infection promotes instability and non-union, but an unstable fracture site can also predispose to bone infection (Figure 1) (Foster et al. 2021). Indeed, clinical and experimental evidence show that a stable internal fixation of a fractured bone leads to less septic complications than an unstable fixation (Sabaté Brescó et al. 2017; Friedrich and Klaue 1977). In fact, stability at the fracture site is considered compromised if bone infection persists for more than two weeks (Foster et al. 2021).

2.3 Diagnosis of postoperative orthopedic SSI

The diagnosis of postoperative SSIs primarily relies on clinical signs, which can vary depending on the bacteria involved, the route of infection and the stage of bone healing. Main complaints in human patients include pain, local erythema and soft tissue swelling, and can be accompanied by wound dehiscence, fistula formation, purulent discharge and fever (Fang et al. 2017a). Clinical signs in animals are somewhat similar and include lameness, swelling, heat, pain upon palpation and draining tracts (Gieling et al. 2019). As in humans, pyrexia is not a consistent finding (Gieling et al. 2019).

Additional diagnostic imaging examinations may support the diagnosis of SSIs in human and veterinary patients (Gieling et al. 2019; Fang et al. 2017a). While radiography can provide information on bone healing and implant stability, it has low sensitivity and specificity in

detecting acute osteomyelitis and only strongly correlates to bone infection when performed 1-2 weeks or greater following infection (Funk and Copley 2017; Jennings et al. 2023). Advanced imaging modalities, such as high-resolution imaging or positron emission tomography, may therefore be necessary (Jennings et al. 2023).

However, a definitive diagnosis of bone infection requires bacterial analysis of deep samples, such as bone or soft tissue (Gieling et al. 2019; Fang et al. 2017a; McNally et al. 2020). In human or animal patients suspected of developing bacterial infection secondary to orthopedic surgery, bacterial analysis on five or more deep tissue/implant samples should be performed (González-Martín et al. 2022; Depypere et al. 2022). Infection is confirmed when either a single positive culture test identifies a virulent pathogen, or at least two positive bacterial cultures isolate the same pathogens (Metsemakers et al. 2018).

2.4 Management of postoperative orthopedic SSI

In both human and veterinary medicine, treating bone infection presents a significant challenge for the orthopedic surgeon due to various factors that contribute to the persistence and resilience of these infections. The nature of implants, providing ideal surfaces for bacterial colonization, exacerbates this challenge. Bacteria that colonize fracture sites, such as *S. aureus*, are difficult to eradicate given their virulence and their capacity to form biofilms (Zimmerli and Sendi 2017; Cheung, Bae, and Otto 2021). Several factors contribute to the development of bacterial biofilms at a fracture site, notably by impairing both adaptive and innate host immunity. These include fracture type (open or closed), bacterial strains involved, type of implant, degree of soft tissue trauma, and environmental and physicochemical conditions (such as necrotic debris, hypoxia, attenuated immune response, fluid flow, circulating proteins). In veterinary medicine, age, American Society of Anesthesiologists (ASA) physical status, wound classification, anesthesia and surgery time, the use of surgical implants, the use of perioperative antimicrobial prophylaxis and/or postoperative antibiotics, the timing of preoperative hair clipping, the number of people present in the operating theater, hypotension and the presence of endocrine disease are the most frequently reported risk factors (Stetter et al. 2021). In human medicine, other patient-related factors such as hypothermia, hypoxia, hypertension, as well as smoking, diabetes, cardiac failure, previous surgeries and immunodeficiency can also impact the development of bone infections (Filipović et al. 2020; Foster et al. 2021; Stetter et al. 2021; Y.-K. Wu, Cheng, and Cheng 2019).

Treatment of SSIs associated with implants is a challenge for the surgeon, mainly because infections around implants will frequently lead to the formation of a biofilm (Costerton, Stewart, and Greenberg 1999; Kennedy et al. 2022). In most cases, biofilm elimination requires orthopedic implant removal. However, this cannot be considered an option until bone healing is completed, and amputation should only be considered as a last resort. Therefore, the purposes of treating SSIs are to not only eradicate the infection but also promote successful healing, while minimizing the risks associated with antibiotic resistance. The initial therapeutic approach is identical in human and veterinary patients, and consists in combining surgical debridement under general anesthesia to systemic antibiotic administration, associated if needed with local antibiotic therapy. Broad-spectrum antibiotics are initially selected to provide coverage against a wide range of bacteria, and antibiotic therapy may be adjusted eventually according to sensitivity testing. However, the systematic and excessive use of antibiotics and their relative inefficiency once a biofilm has formed have led to the emergence of multidrug resistant organisms (Gieling et al. 2019; Bowler, Murphy, and Wolcott 2020). Nowadays, antibiotic resistance is considered a major public health issue (Bowler, Murphy, and Wolcott 2020),

especially as antibiotic resistance genes are transmissible by horizontal gene transfer (Uruén et al. 2020). To address this issue, new efforts are directed towards determining the minimal biofilm eradication concentration (MBEC), which is more relevant than the minimal inhibitory concentration (MIC) used for planktonic bacteria (Okae et al. 2022; Tillander et al. 2022). The MBEC takes into account the unique characteristics of bacteria within biofilms and aims to identify antibiotic concentrations that can effectively eliminate biofilm-associated infections.

Postoperative orthopedic SSIs are a major health issue in human and veterinary medicine. SSIs are difficult to diagnose but mainly challenging to treat. This challenge is in part due to the formation of biofilms on implants. Bacteria developing within a biofilm are tolerant to antibiotics, thus explaining the possible emergence of multidrug resistant organisms when antibiotics are used once a biofilm has formed. Bacterial proliferation and biofilm growth are complex multi-factorial processes. In this context, investigating bacterial biofilm formation may allow the emergence of alternative therapeutic strategies that do not rely solely on antibiotics.

3. Mechanisms of bacterial biofilm formation

Bacterial biofilm formation is a dynamic and multifactorial process. A biofilm is a community of microorganisms coated with a hydrated matrix rich in self-produced extracellular polymeric substances (EPS) and in contact with a surface (Costerton, Stewart, and Greenberg 1999). EPS are composed of proteins, polysaccharides, lipids and extracellular DNA providing mechanical resistance, protection against antibiotics and immune cells, tolerance to dehydration, and constitute a carbon source to microorganisms (Shrestha et al. 2022).

All bacteria are capable of forming biofilms but the mechanisms governing adhesion to a surface, growth and maturation, and dispersion are inherent to each bacterium (Shrestha et al. 2022). Indeed, bacterial genotype determines its ability to form a biofilm on a given surface and each bacterium has a preferred surface and an optimal pH and temperature for growth. For example, *S. aureus* adheres particularly well to metal, which explains why it is the most common isolate found in postoperative orthopedic SSIs (Gieling et al. 2019; Morgenstern et al. 2021; Fang et al. 2017b).

Biofilm formation is commonly considered to occur in four main stages as described in Figure 2: (1) reversible to irreversible bacterial adhesion to a surface; (2) bacterial growth and biofilm formation; (3) biofilm maturation and (4) detachment and dispersion of bacteria (Y.-K. Wu, Cheng, and Cheng 2019; Sauer et al. 2022).

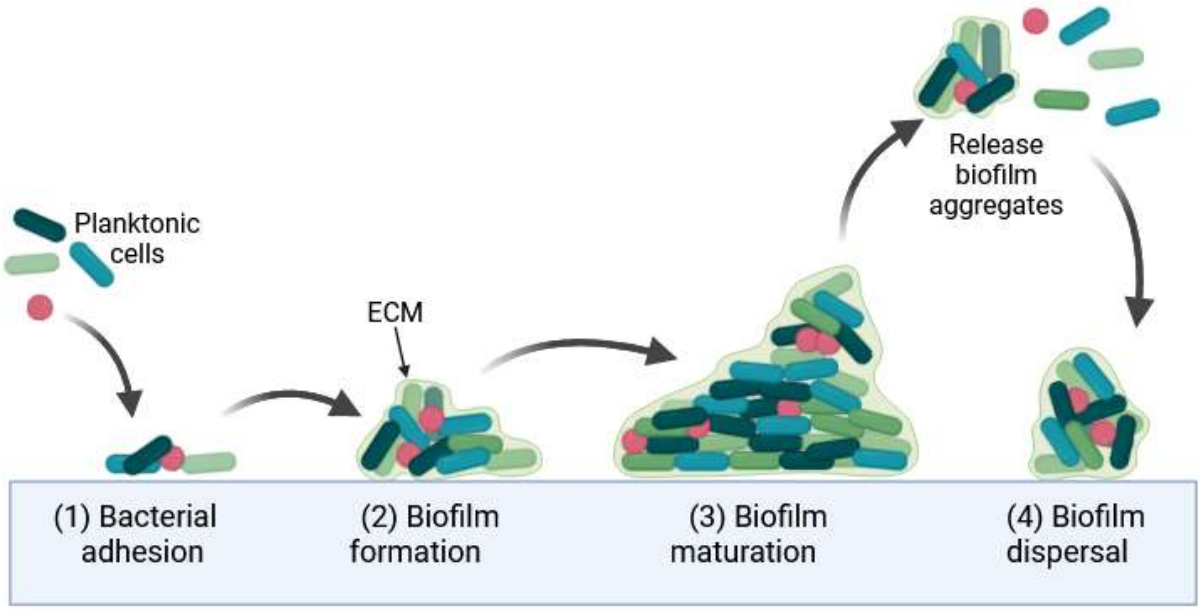

Figure 2: Stages of biofilm formation

3.1 Bacterial adhesion

Biofilm development is initiated by the adhesion of bacteria onto a surface due to physical forces such as Van der Waals forces and electrostatic interactions. Reversible adhesion of the bacterium to the surface occurs due to weak interactions involving mechanosensing, the ability

of a cell to sense mechanical cues of its microenvironment, including surface properties (Filipović et al. 2020; Krsmanovic et al. 2021). After mechanotransduction of the sensed signal, production of intracellular signaling molecules occurs, thus fortifying the adhesion and making it irreversible (Krsmanovic et al. 2021).

Adhesion onto the surface is influenced not only by the bacterium itself, but also by the environmental characteristics and the surface properties (Fang et al. 2017b; Cordero, Munuera, and Folgueira 1996). Indeed, components of bacterial surfaces may affect initial adhesion. While lipopolysaccharides comprising the outer membrane of Gram-negative bacteria play a key role in this process, Gram-positive bacteria are deprived of an outer membrane and rely mostly on cell wall glycoproteins such as teichoic acid (Ruhal and Kataria 2021). Furthermore, each bacterium has a specific affinity for a surface depending on its topology, chemical composition, charge, and hydrophobicity, but also depending on environmental factors such as temperature, pH, electrolytes concentration, flow, and presence of antibiotics (Krsmanovic et al. 2021). Adhesion is most effective when electrostatic potentials and hydrophobicity between the bacterium and the surface are opposite and similar, respectively (Filipović et al. 2020).

3.2 Biofilm formation

Following adhesion, bacteria multiply and form numerous microcolonies embedded in multiple layers among an exopolysaccharide matrix composed of EPS (Filipović et al. 2020; Jamal et al. 2018). This extracellular matrix (ECM) provides the mechanical stability of a biofilm and the protection for the community of cells against environment stresses (Wilking et al. 2011). The ECM provides hydration, nutrient storage and protection from external environmental conditions, including mechanical forces, osmolarity fluctuations and antimicrobial treatments. Similar components are found within the matrixes of Gram-negative and Gram-positive bacteria, such as extracellular DNA, polysaccharides, and amyloid-type proteins. These latter proteins are required for biofilm formation but also play roles in biofilm maturation and dispersion (Ruhal and Kataria 2021).

Biofilm growth is initiated by mechanotransduction and chemical signaling within the matrix. The different bacterial microcolonies are separated by aqueous canals in which fluid and molecules circulate (Jamal et al. 2018). Biofilm growth is also influenced by genotypic factors, physicochemical factors, stochastic processes, determinist phenomena, mechanical processes, molecular exchanges and temporal modifications (Krsmanovic et al. 2021). Bis-3′-5′-cyclic dimeric guanosine monophosphate (c-di-GMP) is a key regulator in biofilm formation of Gram-negative bacteria, while its role remains to be established in Gram-positive bacteria (Ruhal and Kataria 2021).

3.3 Biofilm maturation

Maturation of the biofilm involves the formation of pores and channels, which serve as a circulatory system for distributing oxygen, water and nutrients, and evacuating waste, and allow the circulation of molecules produced by bacteria (Quan et al. 2022). Such intercellular signaling system, known as *quorum sensing* (QS), enables inter-bacteria communication via chemotaxis and directly affects their physiological state (Waters and Bassler 2005).

3.4 Biofilm detachment and dispersion

The final stage of biofilm formation is the detachment and dispersion of planktonic cells (Sauer et al. 2022). It is initiated by several mechanisms that allow bacterial release from the biofilm matrix and dispersion into the surrounding environment for further infection. Mechanical stress is one of the primary factors that triggers detachment. The stress can result from shear forces and wearing secondary to fluid flow. When subjected to these stresses, biofilms can become disrupted, leading to the release of individual or clusters of bacteria (Veerachamy et al. 2014). Bacteria can also produce enzymes and tension-active agents, which can induce degradation of or detachment from the ECM (Krsmanovic et al. 2021). This is the case for *P. aeruginosa*, which produces alginate lyases secondary to stress (Jamal et al. 2018). Moreover, bacteria attached to a surface can change condition and become motile again (Krsmanovic et al. 2021). Regulation of biofilm dispersion may differ between Gram-positive and Gram-negative bacteria (Ruhal and Kataria 2021). *A priori*, mechanical stimuli could also influence toxin release, but this open question merits dedicated multidisciplinary and multiscale explorations.

Once parts of biofilms are detached, bacteria are able to disperse throughout the organism. They eventually reach the circulatory system and can cause systemic infections (Rumbaugh and Sauer 2020).

Each stage of the complex biofilm formation is governed and is regulated by mechanobiological factors. The mechanisms by which bacteria detect and respond to mechanical cues come from their environment.

4. Multi-scale mechanobiology of biofilm development

While a healing bone is constantly subjected to mechanical stresses, little is known about the impact of this mechanical environment on biofilm development (Jara et al. 2020; Araújo et al. 2019; Xu et al. 2022). Recent advances in high-resolution imaging techniques and bacterial studies have shed light on bacteria and biofilm mechanobiology. Studies have shown that bacteria are not passive recipients of mechanical cues. They sense mechanical stimuli through different receptors and effectors, which enable them to adapt, deform, and attach to or detach from a surface (Chawla et al. 2020; Araújo et al. 2019). Some mechanical stimuli may even support bacterial development as a defense strategy in a hostile environment (Bottagisio et al. 2020). As the biofilm grows and matures, bacteria are embedded in the self-produced ECM whose composition can change in response to mechanical forces, significantly impacting the overall stability of biofilms.

In the following section, these mechanobiological interactions are explored through a multi-scale prism starting from the bacterial microscopic scale to reach the biofilm mesoscopic scale and finally the macroscopic scale of the fracture site or bone-implant interface. These interactions are illustrated in Figure 3.

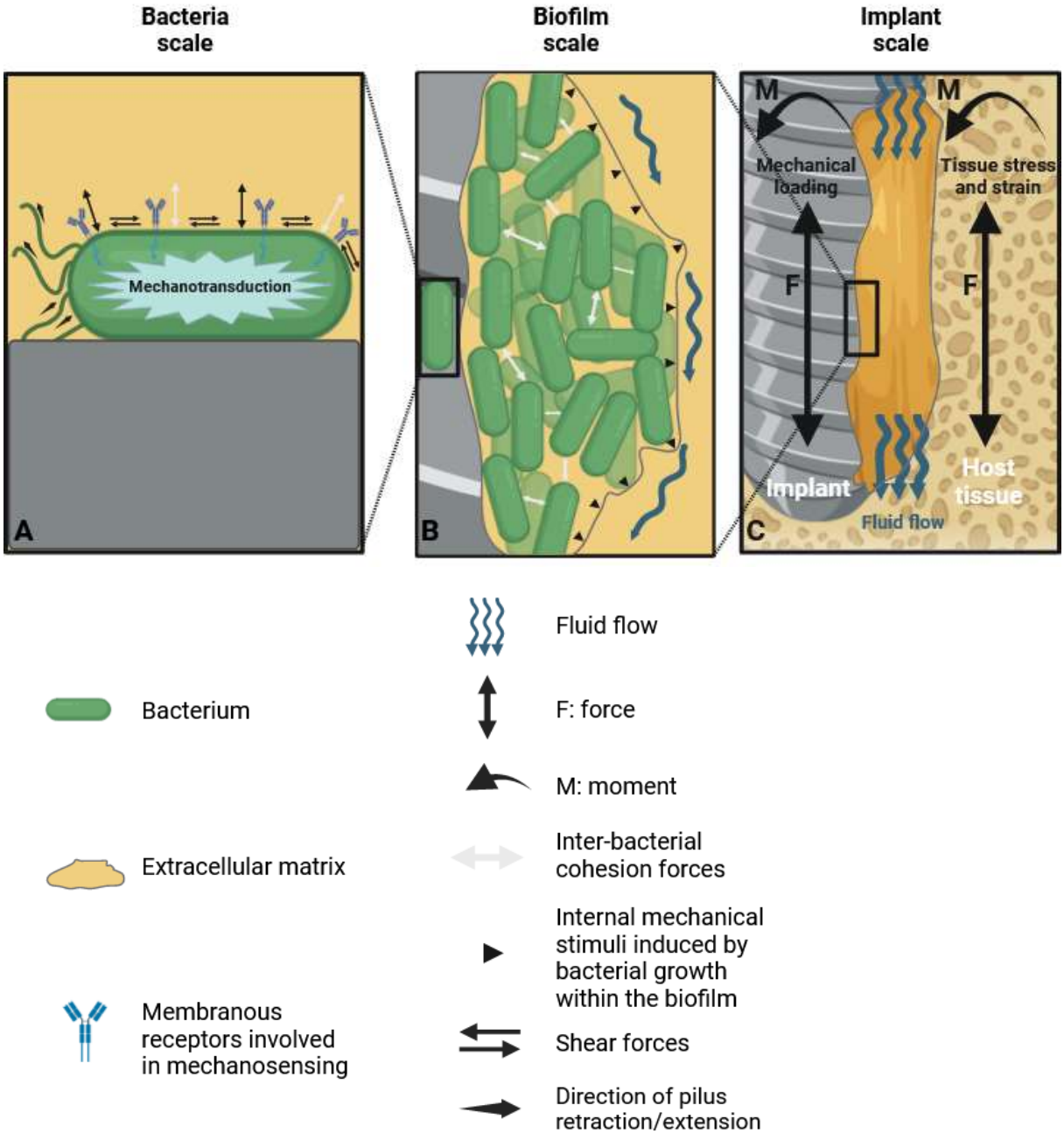

Figure 3: Mechanobiological interactions: from the bacterium to the implant. (A) At the microscopic scale, the isolated bacterium perceives mechanical signals thanks to its membranous receptors, its bacterial envelope and its surface organelles. (B) At the biofilm scale, bacterial growth within the self-produced ECM induces internal mechanical stimuli and increases inter-bacterial cohesion forces. (C) At the macroscopic scale, mechanical loading of the implant and host tissue behavior affects the bone-implant interface.

4.1 Mechanical factors at the microscopic scale of bacteria

Mechanosensitivity, the capacity to sense and respond to mechanical cues, plays a crucial role in the physiological response of bacteria and their survival (Chawla et al. 2020; Dufrêne and Persat 2020; Gordon and Wang 2019). Though studies have identified a direct link between bacterial initial accumulation and motility to the surface properties (Song et al. 2017; Zheng et al. 2021; Gomez et al. 2023), the mechanisms of how bacteria perceive and interact with the substrates are poorly understood. The bacterial cell envelope is a key element of mechanosensitivity, providing not only mechanical stability due to its turgor pressure but also functioning as a sensory interface, allowing bacteria to sense and respond to external mechanical cues such as changes in osmotic pressure and substrate stiffness and topography (Figure 3A) (Song et al. 2017; Zheng et al. 2021; Gomez et al. 2023; Auer and Weibel 2017; Rojas and Huang 2018; Harper and Hernandez 2020; Maier 2021). For example, in *Escherichia Coli,* the NlpE-Cpx transmembranous system activates the virulence factor regulation upon contact between the bacterial envelope and a surface (Otto and Silhavy 2002). Other bacteria respond to mechanical forces through membrane depolarization, which is responsible for a calcium influx, translating mechanical forces into intracellular ionic concentration (Bruni et al. 2017). As a response to the mechanical cues, mechanosensitive channels transduce the mechanical stimuli into cellular responses, regulating ion fluxes and cytoplasmic pressure. Another mechanism is based on cell surface components such as adhesins, which undergo conformational changes when subjected to tension, as seen in *E. Coli* adhesin FimH , thereby reinforcing the bond between the bacterium and the surface (Anderson et al. 2007; Nilsson et al. 2006). This mechanism is known as *catch bond* and is responsible for *a stick and roll* motion of the bacterium on a surface. *S. aureus* can also reinforce its adhesion to a surface when external forces increase (Kerrigan et al. 2008). On the contrary, mechanical forces can destroy a cell-binding site, further proving that mechanosensitivity plays a crucial role in bacterial adhesion (Chabria et al. 2010). The exact mechanisms underlying detection, signaling and responses by membranous receptors are still to be discovered.

Bacterial motility, a fundamental aspect of bacterial behavior, is closely linked to mechanobiology. Some bacteria have extensions, such as flagella or pili, which can serve as mechanosensory systems and enable bacteria to sense the surface and respond according to the structure of the surface, its topography and stiffness (Kreve and Reis 2021; Asp et al. 2023). Flagella-driven propulsion adapts to changes in fluid viscosity and flow by using the coordination of motor proteins within the bacterial cell envelope. The activation system of bacterial flagella is composed of a stator combined to a rotor, which is responsible for rotation and torque. Conformational changes of the stator's components are caused by the proton-motive force, and induce rotation of the rotor and of the flagellum consequently (Dufrêne and Persat 2020). In *E. Coli*, flagella adapt rotation speed and torque according to resistances met by the stator (Chawla et al. 2020; Persat 2017). Adaptation happens mainly through positive feedback: if a force counteracts flagella rotation, for example due to an increase in fluid viscosity, other subunits of the stator are recruited to increase the speed of rotation (Dufrêne and Persat 2020; Persat 2017). When bacteria encounter a surface, the physical interaction with the surface can change the rotation of the flagella. This alteration in flagella rotation allows bacteria to detect the surface and respond by modulating their motility. They may exhibit behaviors such as swimming along the surface, attaching to it, or changing direction to explore the surface features.

Type IV pili are motorized filaments present on the surface of many Gram-positive and Gram-negative bacteria. They are involved in motility and adhesion on surfaces, and they have been shown to have a critical role in bacterium motility. The molecular motor of type IV pilus is composed of different subunits which hydrolyze ATP to polymerize and depolymerize other

subunits (Burrows 2012). When type IV pilus is in contact with a surface, it detects a traction force and retracts, thus attracting the bacterium against the surface. This mechanism is known as *twitching motility* and enables bacteria to move on a surface (Burrows 2012). If the bacterium is subjected to increasing fluid flow and friction forces, the retraction force of the pilus is even greater.

Further research has suggested that bacteria also respond to acoustic cycled waves (Murphy et al. 2016). Specific acoustic waves in the range 800-1600 Hz appear to aggregate bacteria together and promote biofilm formation. Although the underlying mechanisms remain unexplained, concomitance with bacterial population increases might play a role. Indeed, increasing tension in bacteria might activate mechanosensitive channels of the cell membrane with a specific impact upon bacterial wall turgor pressure (Murphy et al. 2016). Biofilms also exhibit frequency-dependent responses. For instance, growth of *P. aeruginosa* and *S. aureus* biofilms are enhanced when exposed to 800 and 1600 Hz cycles for 48h, respectively (Murphy et al. 2016). Conversely, low frequencies might either stimulate or inhibit biofilm growth in *E. Coli* depending on exposure duration (Martirosyan and Ayrapetyan 2015).

4.2 Mechanical factors at the mesoscopic scale of biofilm

While bacteria mechanosensing occurs predominantly on the microscale, biofilms size can range from micrometers, like dental plaques, up to centimeters, such as SSIs, which can be visible to the naked eye. This shift in scale from individual bacteria to biofilms brings new challenges and insights to the mechanobiology.

At the biofilm scale, internal mechanical stimuli induced by bacterial growth can be considered (Figure 3B). The self-produced biofilm matrix not only maintains cohesion between bacterial cells, but also links them to the underlying surface (Costerton, Stewart, and Greenberg 1999). This cohesion is substantial for biofilm survival, as it protects the bacterial community against chemical, biological and mechanical stresses. From a mechanical perspective, the biofilm behaves like a hydrated colloidal gel with rigid bacteria and a viscous matrix (Krsmanovic et al. 2021). This structure grants viscoelastic properties to the biofilm, resulting in both solid-like and liquid-like responses and enables biofilms to withstand mechanical forces such as fluid shear through energy dispersion and mechanical stress distribution and adapting to their mechanical environment (Nguyen et al. 2021). Indeed, mechanical cues can trigger changes in the production of EPS components, thus altering biofilm viscoelasticity through gene expression (Nguyen et al. 2021). For instance, one could hypothesize that bacteria residing within an overly rigid matrix may produce matrix-destroying enzymes to reduce local elasticity so as to pursue bacterial growth. Conversely, bacteria may increase the production of matrix components when they perceive a local increase in elasticity, rendering their environment more rigid. Regardless of the conditions, bacterial cells arrangement within a biofilm influences their mode of interaction and communication, and impacts therefore QS and biofilm growth (Dufrêne and Persat 2020).

Fluid flow and shearing forces play pivotal roles, as they affect biofilm composition. Indeed, biofilms grown under a flow are thicker and denser (Krsmanovic et al. 2021). Moreover, two biofilms originated from the same initial planktonic inoculum exhibit different compositions depending on whether bacterial growth occurs in a laminar or turbulent flow (Dufrêne and Persat 2020). Turbulent flows seem to promote growth of a thin and dense biofilm, whereas laminar flows promote the formation of a more homogeneous, thicker and less dense biofilm (Krsmanovic et al. 2021). Mechanical forces associated with both types of flow can affect the

transport of signaling molecules and nutrients, and are likely to deform or damage the matrix, thus promoting adhesion or dispersion (Dufrêne and Persat 2020).

4.3 Mechanical factors at the macroscopic scale of fracture or implant fixation

Little is known about how mechanical forces influence the risk of infections at the bone implant interface (Figure 3C). At this scale, mechanical stresses and loading patterns significantly affect the dynamics and persistence of infections in and around orthopedic implants and can lead to fracture. *A priori*, clinical practice is considering that instability of the fracture site promotes infection (Fang et al. 2017b), and that conversely, stable fracture sites are less prone to fracture related infection (Foster et al. 2021).

Some experimental studies showed contradictory results depending on bacteria phenotypes and animal species. It has been shown that a femoral osteosynthesis with rigid fixation enabled eradication of inoculated *S. epidermitis* at the fracture site in mice, whereas infection was persisting with a compliant fixation. However, the authors showed that the mouse strain and the type of bacteria affected these results, especially with *S. aureus* resulting in more severe infections (Sabaté Brescó et al. 2017).

Biomechanical analysis and computational modeling have been developed to understand the properties and behavior of biofilms at the bone-implant interface (Acemel, Govantes, and Cuetos 2018; Ferreira, De Oliveira, and Silva 2020). While these models provide valuable insights for optimal fixation configurations and prediction of outcomes, these studies are still relatively new and a need for collaborations between scientists working with numerical models and clinicians is needed.

While bacterial and biofilm responses to mechanical cues are well documented and the subject of many recent studies in interdisciplinary fields, an important gap in knowledge exists on the mechanobiology of infectious sites at the bone-implant interface. A comprehensive understanding of the mechanobiology of biofilms at these different scales is crucial for the development of innovative therapeutic strategies.

5. Therapeutic strategies beyond traditional antibiotics

The complex nature of biofilm-associated infections makes biofilm eradication very challenging, as discussed in section 2.4 of this chapter. In fact, bacteria embedded in biofilms are ten thousand times more tolerant to antibiotics than their planktonic counterparts (Singh et al. 2022). Even if the causes of this tolerance have not clearly been elucidated, some mechanisms have been identified. Among these, one could cite the barrier role played by the ECM, the adaptation of bacterial metabolism through the phenomenon of quiescence… These are illustrated in Figure 4 and summarized in Table 1 (Singh et al. 2022; Dincer, Masume Uslu, and Delik 2020; Hawas, Verderosa, and Totsika 2022).

It should be underlined that MICs are significantly higher for bacteria within a biofilm than for their planktonic counterparts, rendering antibiotic treatments with standard dosages useless. As a result, it is recommended to increase dosage and duration of antibiotic therapy when treating biofilm-associated SSIs, thereby increasing the risk of toxicity and side effects (Y.-K. Wu, Cheng, and Cheng 2019). Therapeutic strategies complementary or alternative to antibiotics are therefore crucial.

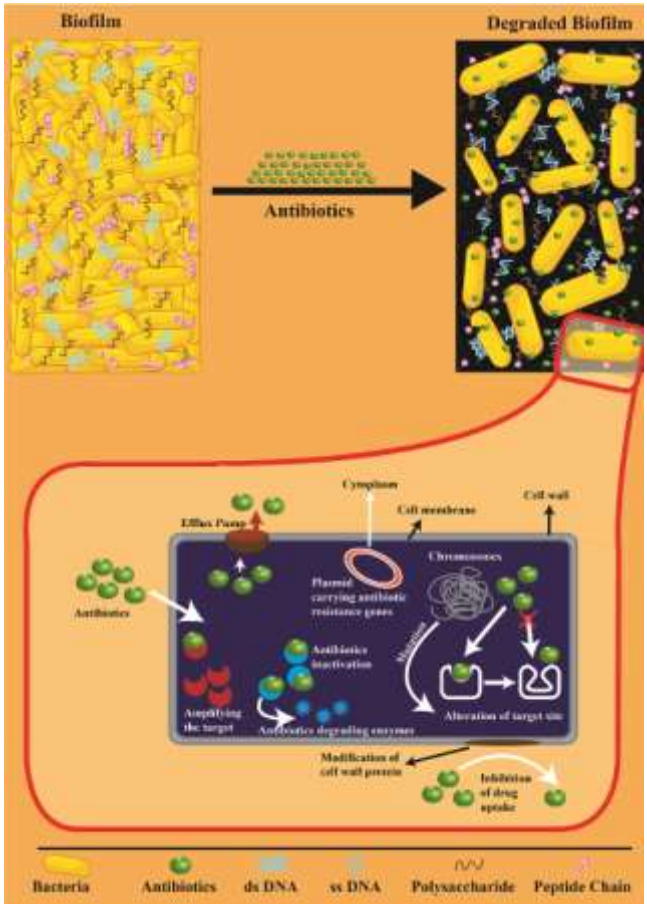

Figure 4: Mechanisms contributing to enhanced biofilm tolerance to antibiotics (from Singh et al. 2022)

Mechanism	Description
Extracellular matrix	Forms a barrier preventing antibiotic penetration within the deeper layers of the biofilm
Quiescence	Phenomenon through which persistent bacterial cells have an extremely low basal metabolism and cell division rate
Accumulation of enzymes within the extracellular matrix	These enzymes are capable of degrading antibiotics
Quorum sensing	Mechanism for bacterial cell-cell communication *via* signaling molecules, which controls biofilm volume, thickness and rugosity
Horizontal transfer of antibiotic resistance genes	Transfer of these genes from one bacterium to the other within a biofilm
Greatest number of efflux pumps expressed by bacteria contained within a biofilm	Allows bacteria to extract more intracellular toxins, including antibiotics
Presence of several concentration gradients within a biofilm	These gradients create aerobic and anaerobic micro-environments which increase tolerance to antiseptics and antibiotics.

Table 1: Underlying mechanisms of bacterial tolerance associated with biofilms (summarized from Singh et al. 2022, Dincer et al. 2020 and Hawas et al. 2022)

The strategic focus for eradicating biofilms encompasses two fronts: (1) inhibition of bacterial adhesion to prevent biofilm formation and (2) promotion of bacterial dispersion to eliminate pre-existing biofilms and eradicate the more easily accessible planktonic bacteria. The prevention of biofilm formation can be achieved through surface modifications to impede bacterial adhesion or biofilm maturation, and implies either physicochemical modifications of surfaces or control of genes implicated in biofilm formation and maturation. Conversely, biofilm dispersion can be induced *via* cell programming or by disrupting matrix constituents. In this section, therapeutic alternatives are discussed according to their underlying mechanisms, i.e. biochemical, biological or biophysical mechanisms.

5.1 Biochemical alternatives

As the SSI environment is predominantly avascular, antibiotics delivered *via* the systemic route often do not reach the targeted infected site with a concentration high enough to be effective. As such, administering antibiotics locally, that is directly at the infection site, enables the reaching of high concentrations while keeping blood concentrations low to undetectable, thus limiting undesirable systemic effects (Patangia et al. 2022). This approach ensures that the antibiotic concentration remains consistently higher than the MIC, which allows eradicating bacteria resistant to systemically-delivered antibiotics (Singh et al. 2022). Local route also reduces the risk of antibiotic resistance (Patangia et al. 2022). However, challenges arise when

the infection site is inaccessible without invasive strategies, such as re-opening of the surgical site.

To overcome this barrier, it is possible to resort to biochemical agents like nanoparticles or specific enzymes that induce bacterial cell death before or in the early stages of biofilm development.

Some nanoparticles have intrinsic antibacterial properties and can be used as vectors for therapeutic agents (Rotello 2023; Bano et al. 2023). Their mechanism of action relies on the creation of electrostatic interactions with the ECM, thus promoting the diffusion of molecules. These interactions also stimulate the dislocation of cell membranes, leading to intra-bacterial components leakage. Furthermore, nanoparticles can induce the production of free radicals and reactive oxygen species, the inactivation of enzymes and the denaturation of proteins (Rotello 2023; Bano et al. 2023). Despite promising *in vitro* results, their translation to clinical practice requires further validation (Rotello 2023).

Lysine or other enzymes acting as cell lysis inducers can kill bacteria in the early stages of biofilm development (Shrestha et al. 2022). *In vitro*, it has been shown that enzymes targeting cell wall peptidoglycans, such as hydrolases, can rupture bacterial cells (Shrestha et al. 2022). Chelators such as ethylenediaminetretraacetic (EDTA), and other biomaterials such as chitosan, are also capable of disrupting bacterial cell walls. These agents were proven to alter effectively *in vitro* the development of *P. aeruginosa* biofilm (Shrestha et al. 2022).

Biochemical agents promoting biofilm dispersion have also been proposed as alternatives to antibiotics. However, when used alone, they lead to the release of bacteria into the circulation system. Dispersal agents are therefore combined with systemic antibiotics to prevent spreading of infection. Promising results have been reported with agents inhibiting QS, with nitric oxide (NO) and with antimicrobial peptides (AMPs) (Hawas, Verderosa, and Totsika 2022).

QS inhibition implies inhibiting the synthesis of auto-inducers, destroying signaling molecules like the c-di-GMP, disrupting mechanisms implicated in signal reception, or inhibiting the reaction chain leading to transduction (Shrestha et al. 2022; Hawas, Verderosa, and Totsika 2022). These mechanisms lead to biofilm dispersion or inhibition. The majority of QS inhibitors are derived from proteins naturally taking part in QS, such as autoinducers, transcription factors and regulators (Auer and Weibel 2017).

NO is a free radical that leads to bacterial biofilm dispersion by decreasing the intracellular concentration of c-di-GMP (Hawas, Verderosa, and Totsika 2022; Visperas et al. 2022). The use of NO is however limited due to its reactivity, its instability and its toxicity at high concentration.

AMPs are multifunctional proteins composed of 12-50 amino acids capable of destroying Gram-positive and Gram-negative bacteria, viruses, and fungi. They act by splitting peptidoglycans, modifying cell membrane permeabilization or potential, neutralizing, or separating lipopolysaccharides, inhibiting cell division and modulating the synthesis and function of adhesion molecules. The bioavailability of antibiotics is increased when they are administered combined to AMPs (Shrestha et al. 2022; Singh et al. 2022; Hawas, Verderosa, and Totsika 2022; Visperas et al. 2022). However, AMPs may be unstable, rendering their use for therapeutic treatments difficult.

5.2 Biological alternatives

Biofilm resistance to antibiotics *in vivo* is in part due to the hypoxic environment at the infection site (Singh et al. 2022; Khan et al. 2021). Hyperbaric oxygen therapy consists in increasing local partial pressure in oxygen and may improve antibiotic efficacy by re-oxygenating poorly oxygenated environments and by establishing an aerobic bacterial metabolism (Jensen et al. 2019). Results are somehow controversial regarding the efficacy of this strategy to improve antibiotic treatment in device-related infections (Bartek Jr. et al. 2018; Jørgensen et al. 2017). Questions also arise as to whether this strategy may promote antibiotic resistance (Jensen et al. 2019).

Another biological alternative relies on the use of phage therapy. Phages are host-specific viruses which infect bacteria and rely only on these for their survival and self-replication (Chang et al. 2022). Many phages have the ability to induce host lysis, thus releasing other phages that will infect neighboring bacterial cells. Some phages are even capable of disrupting biofilm structures (Domingo-Calap and Delgado-Martínez 2018). Bacteriophages have shown encouraging results *in vitro* in combatting orthopedic implant-related infections caused by *S. aureus* (Morris et al. 2019).

Finally, monoclonal and polyclonal antibodies, traditionally used in rheumatology, are being explored for biofilm infections in orthopedic surgeries (Mao et al. 2021; Chung 2023). Their effectiveness in treating biofilm-associated infections has been proven *in vitro* in many animal models, and a vaccine against *S. aureus* is currently under phase III clinical trials (Shrestha et al. 2022). However, only a small number of these antibodies have been proved to be effective in clinical trials (Visperas et al. 2022; Varrone et al. 2014).

5.3 Biophysical and multiphysical alternatives

Physicochemical modification of local adhesion properties of substrate surfaces has been considered a strategy to control device-associated biofilm (Wildemann and Jandt 2021; Getzlaf et al. 2016). Pure surface modifications to modify its topography and decrease the pore size, to increase its stiffness and wettability and to decrease its roughness can render the implant less prone to bacterial adhesion (Wildemann and Jandt 2021). Surfaces can also be rendered anti-adhesive by using passive or active coatings. Passive coatings can imply the use of ultraviolets to irradiate orthopedic implants or the resort to hydroxyapatite, tricalcium phosphate or polymers such as hydrophilic polymethacrylic acid, polyethylene oxide or protein resistant polyethylene glycol (Filipović et al. 2020; Wildemann and Jandt 2021; Getzlaf et al. 2016). As an example, titanium implants were shown to have a bactericidal effect when exposed to UV light due to an increase in reactive oxygen species activity (Gallardo-Moreno et al. 2010). Active coating implies covering implants with broad-spectrum antimicrobials such as N, N dodecyl, methyl-polyethylenimine (Schaer et al. 2012), chitosan (Chua et al. 2008), *Gendine* (Bahna et al. 2007), which were all proven to be effective *in vitro* to prevent *S. aureus* biofilm formation, or with hydrogels capable of delivering multiple antibiotics to the implant site (Drago et al. 2014). Studies published so far on surface modifications show promising results *in vitro* (Wildemann and Jandt 2021). However, clinical efficiency remains to be proven.

Active physical stimuli might be attractive to envisage clinical applications, and propagation of ultrasonic waves seems to be a good candidate. Low-frequency ultrasound might render bacteria more susceptible to antibiotics, as demonstrated with *E. Coli* and gentamicin (Peterson and Pitt 2000; Carmen et al. 2004). Even if magnitude and frequency might show

contradictory influences on biofilm responses, it appears that waves could modify diffusive properties of the ECM, increase antibiotic concentration, and lowers the risk of gene mutation.

Finally, recent developments in multi-physical treatments include cold atmospheric plasma therapy and bacterial photodynamic inactivation, both of which induce bactericidal properties and constitute promising treatment options (Ribeiro et al. 2022; Alqutaibi et al. 2023).

Numerous strategies complementary or alternative to antibiotics have been explored. However, the viability of their use in clinical settings remains uncertain for many of them. Other complex and as yet unexplored biophysical mechanisms may play a role, such as specific mechanobiological responses due to strain or stress relaxation and creep or cyclic fatigue associated with physiological thresholds.

Chapter II:
Design of an experimental setup to study the influence of a mechanical stimulus on biofilm growth

1. Introduction

A healing bone is constantly subjected to mechanical stresses, either inherent to the healing process itself, or due to external forces applied to it consequently to load bearing for instance. A loaded bone is mainly subjected to three stresses – shear, compression and tension – which result in bending and torsion.

When considering fracture fixation, bone plates are among the most common internal fixation implants used (Kim et al. 2020). An osteosynthesis plate must withstand three main types of loading: axial compression, bending and torsion. Bending forces cause the highest stress, because plates are placed eccentric to the neutral axis of the bone, unlike other implants such as nails which are placed near the neutral axis of the bone (Deprey et al. 2022).

While a healing bone and an osteosynthesis plate are constantly subjected to mechanical stresses, little is known about the impact of this mechanical environment on biofilm development (Jara et al. 2020; Araújo et al. 2019; Xu et al. 2022). As discussed in chapter I, bacteria and biofilms respond to mechanical cues. Nevertheless, the impact of an external mechanical stimulus, especially bending, on biofilm development has not been studied so far. In fact, it is not known whether bending stimulates or inhibits biofilm formation. Exploration of this phenomenon could allow understanding how a biofilm forms on an osteosynthesis plate under mechanical stimuli, and how it behaves once it has formed.

In this chapter, we have developed an experimental setup that enables application of a bending moment during the attachment and growth of a biofilm. We shall first present the experimental setup that includes a mechanical and a microfluidic device, and the challenges related to its conception. We then present how the mechanical device was designed, by describing its kinematics and its different components. Next, we focus on the microfluidic device and provide details on microchip fabrication, on manufacturing of the bending substrate and on the assembly of both components to create the microfluidic device. Finally, we present the mechanical response of the microfluidic device, which was explored using numerical modeling.

2. Experimental setup and associated challenges

The experimental workbench designed to expose a bacterial biofilm to a bending moment included a microfluidic device and a mechanical device. The microfluidic device comprised of two microchips bonded to a flexible substrate. Each microchip contained a fluidic microchannel in which bacteria were subsequently inoculated and left to grow until biofilms formed. Fluid and nutrients necessary for biofilm growth were delivered through the microfluidic device using a controlled syringe pump and were collected in an output reservoir (Figure 5).

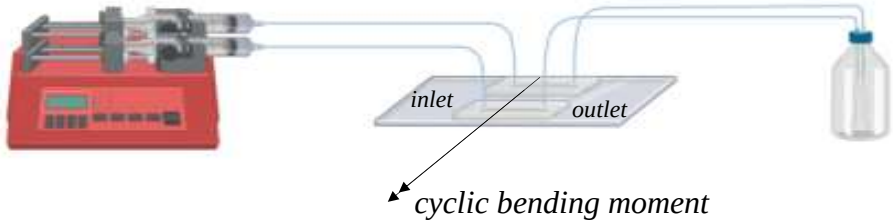

Figure 5: General description of the experimental setup. PDMS microchips were bonded to a PETG coverslip to form the microfluidic device

We chose to use polydimethylsiloxane (PDMS) to create the microchips. In fact, PDMS is often used for fabricating microfluidic chips given its material properties such as elasticity, optical transparency, biocompatibility, gas permeability and low autofluorescence (Shakeri, Khan, and Didar 2021). PDMS is also known to facilitate cell adhesion (Pattanayak et al. 2021), and therefore constituted an ideal substrate for biofilm growth (Ramos et al. 2023). Fluid and nutrients were delivered into the microchannel through a specific inlet punch.

Glass is the substrate most commonly used when creating microfluidic devices (Borók, Laboda, and Bonyár 2021), but the substrate had to be flexible for the purpose of our study so as to submit the chips to bending forces and to study the effects of this mechanical stimulus on biofilm growth. Polyethylene terephthalate (PET) is one of favored substrates when the planned application requires flexibility; it is optically transparent, strong and lightweight, has chemical inertness, good gas permeability and low cost (Borók, Laboda, and Bonyár 2021). In this study, we developed a method to bind the PDMS microchips to polyethylene terephthalate glycol (PETG) coverslips, which proved to be challenging since bonding of two differentiated polymeric species is especially arduous, as detailed in section 4.3 of this chapter.

The flexible coverslip was subjected to a cyclic bending moment generated by a homemade mechanical device that induced lateral deflection and mechanical strain inside the microchips (

Figure 6). The cyclic lateral force $F(t)$ in the transverse plane (O, y_0, z_0) induced lateral and symmetrical deflection $v(x)$ in the longitudinal plane (O, x_0, y_0). As the PETG coverslip was in pinned-pinned boundary conditions, the symmetry plane involved (O, y_0, z_0) for geometry, material distribution pattern, boundary conditions and loading conditions. Given the low elastic modulus of PDMS compared to PETG, the mechanical response, and in particular the lateral deflection, was close to that of a sole PETG coverslip tested in three-point bending, with a

maximum bending moment located at the symmetry plane and with negligible shear effect due to significant slenderness, i.e. ~ 70 mm/2 mm = 35.

Nevertheless, the PDMS microchip and the microchannel in the vicinity of the coverslip interface may show local mechanical strain and stress gradients due to local material properties gradient. This point will be later discussed in section 5 of this chapter.

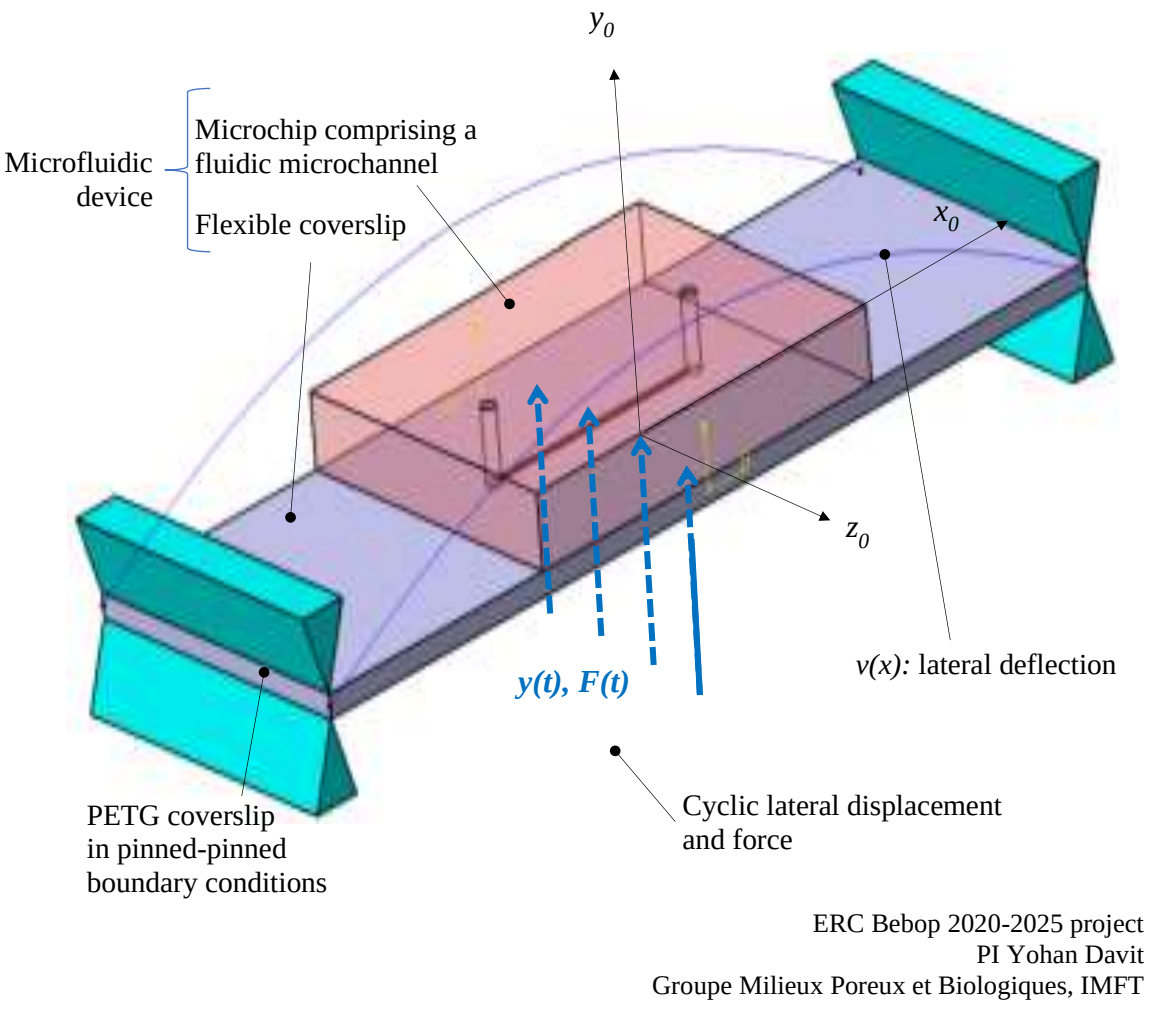

Figure 6: Schematic description of the experimental workbench: PDMS microchip bonded to a PETG coverslip with a cyclic lateral force *F(t)* that induces a bending moment and symmetrical deflection *v(x)*.

3. Design of the mechanical device

The design of the mechanical device was based on the use of a motion transformation system to impose a bending moment to the flexible substrate of the microfluidic device. The system consisted in associating an engine shaft to a cam system, and was composed of three components (Figure 7): a rotating shaft **1**, a cam disk **2** and a rolling ring **3**. Ball bearings were interposed between cam disk **2** and rolling ring **3**.

The Young modulus of a PDMS microchip and a PETG coverslip are 2 MPa and 2 GPa, respectively, and their densities are 970 kg/m^3 and 1400 kg/m^3, respectively. Thus, imposed displacement $y(t)$ and induced lateral force $F(t)$ were targeted between 0 Hz and 2 Hz, in order to avoid resonance excitation for both components of the microfluidic device.

3.1 Kinematics of the mechanical device

A schematic representation of the kinematics of the mechanical device is given in Figure 7. Reference frame of the base was set at (O_0, x_0, y_0, z_0). A rotating shaft **1**, associated with reference frame (O_1, x_1, y_1, z_1), was connected with a pivot joint at O_0; its rotation was described by $\theta_1(t)$. A cam disk **2**, associated with reference frame (O_2, x_2, y_2, z_2), was connected to rotating shaft **1** with a pivot joint at O_1; its position relative to rotating shaft **1** was set by adjusting θ_2. A rolling ring **3** centered on O_2 established a linear contact with a flexible coverslip **4** supporting the microchips at point M_3. It enabled having only rolling without sliding on the flexible coverslip **4**. Figure 8 shows the geometrical settings and the successive reference frames.

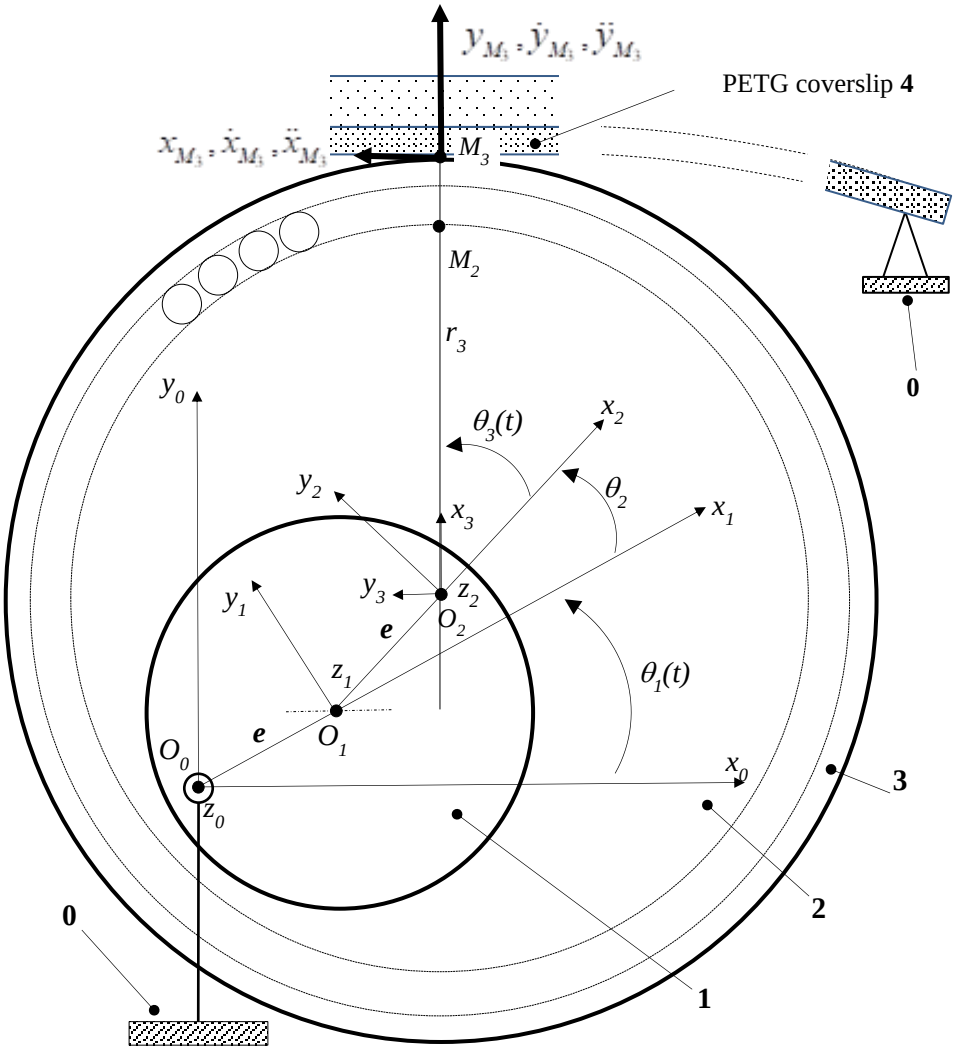

Figure 7: Schematic representation of the kinematics of the mechanical device. Rotating shaft **1** is in pivot joint $\theta_1(t)$ with base **0** at point O_0. Cam disk **2** is in pivot joint θ_2 with rotating shaft **1** at point O_1, and rolling ring **3** is in pivot joint $\theta_3(t)$ with cam disk **2** at point O_2. Rolling ring **3** and flexible coverslip **4** are in contact at point M_3

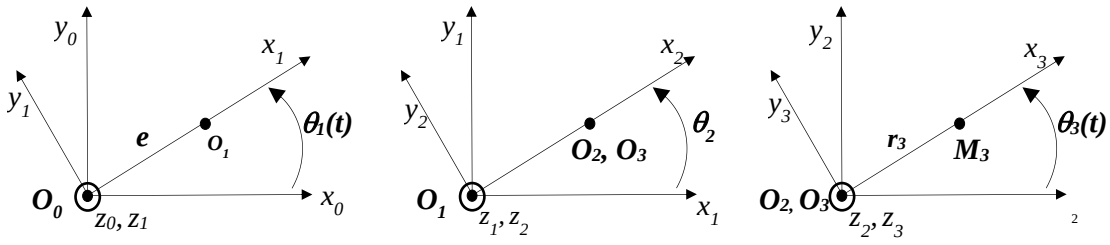

Figure 8: Geometrical settings and reference frames showing time varying parameters $\theta_1(t)$ and $\theta_3(t)$. Modifiable parameters are: θ_2, eccentric e and the radius of ring 3 r_3

By conceiving the mechanical device as exposed, the flexible coverslip not only described a vertical displacement, but also a horizontal displacement, which was the consequence of the kinematics by adjustable cam. This point is discussed in section 6.

The kinematical equations describing the motion of the mechanical device are detailed in Appendix A. The horizontal and vertical displacement fields (equations (2a) and (2b) respectively in Appendix A) and the vertical acceleration (equation (4b) in Appendix A) of M_3 when the angle $\theta_2 = 0$ and when the constant angular frequency of rotating shaft $\dot{\theta}_1 = \Omega_1$ presented harmonic variations as shown in Figure 9. The harmonic patterns were of a 2π-period, and both vertical displacement and acceleration were of opposite sign.

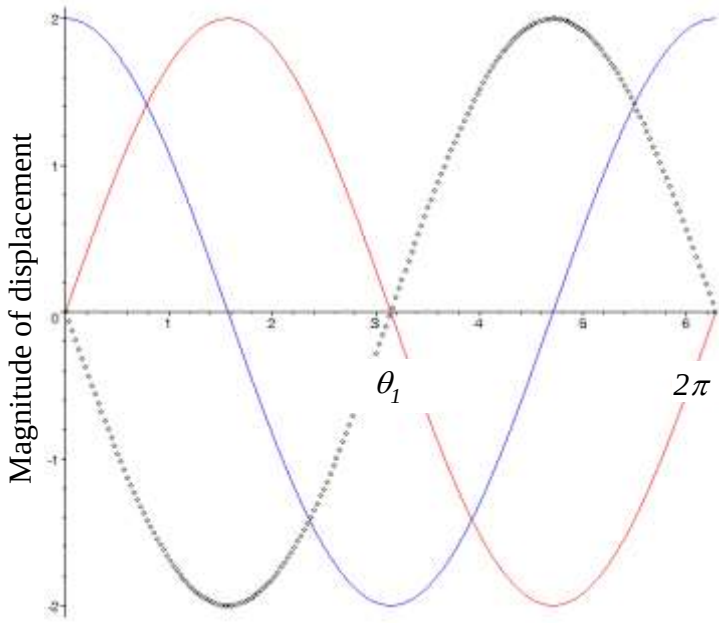

Figure 9: Kinematics of M_3 for $\theta_2 = 0$ and $\dot{\theta}_1 = \Omega_1$. The normalized horizontal displacement of M_3, i.e. x_{M3}/e, is plotted in blue, the normalized vertical displacement of M_3, i.e. $(y_{M3}-r_3)/e$, is plotted in red, and the normalized vertical acceleration of M_3, i.e. $\ddot{y}_{M3}/e{\Omega_1}^2$, is plotted using black points.

The magnitude of both the horizontal and vertical displacements of the flexible coverslip **4** could be changed by modifying angle θ_2, as shown by equations (2) in Appendix A. Indeed, when θ_2 varied in the range [0; π], lateral bending varied in the range [2e sin θ_1; 0] while horizontal magnitude varied in the range [2e cos θ_1; 0]. The magnitude of the normalized vertical displacement of M_3, i.e. $(y_{M3}-r_3)/e$, when cam disk angle θ_2 varied from 0 to $\pi/2$ is illustrated in Figure 10. Disruption of the transverse displacement cycles can be obtained by modifying the initial location of the coverslip **4** relatively to cam disk **2**. As an illustration, the black points plotted in Figure 10 shows nil transverse displacement due to contact loss for θ_1 varying between π and 2π for an initial location of 2e.

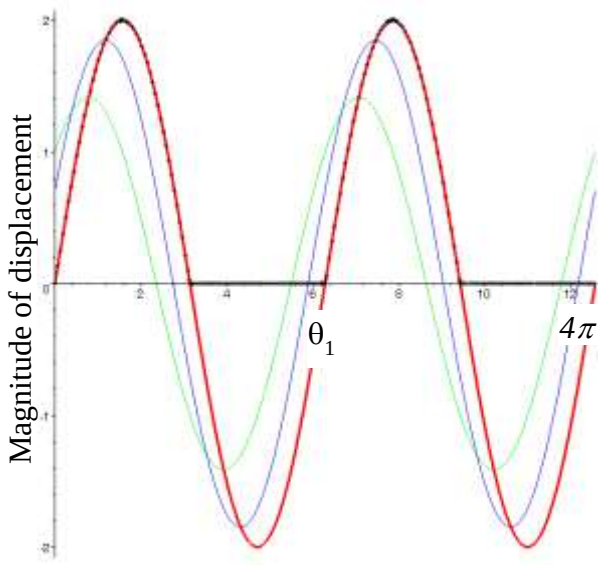

Figure 10: Magnitude of the normalized vertical displacement of M_3, i.e. $(y_{M3}-r_3)/e)$, when cam disk angle θ_2 varies from 0 to $\pi/2$. Red line, blue line and green line are associated to $\theta_2 = 0$, $\theta_2 = \pi/4$ and $\theta_2 = \pi/2$, respectively. Nil transverse displacement of the microfluidic device can be obtained for θ_1 varying between π and 2π, as shown by the black points.

3.2 Fabrication and assembly of the different components

The motion transformation system is schematically represented Figure 11A, with the following values for θ_1, θ_2 and θ_3: $\theta_1 = \pi/2$, $\theta_2 = 0$ and $\theta_3 = 0$. The distances between O_0 - O_1 and O_1 - O_2 were identical and fixed to e. The angle θ_2 between cam disk **2** and rotating shaft **1** could be adjusted thanks to a cylindrical pin which could be positioned at five discrete and predetermined locations, *i.e.* 0, $\pi/4$, $\pi/2$, $3\pi/4$ and π. Cam disk **2** was associated to ball bearings (HPC®) also in contact with rolling ring **3.** The main technological components of the mechanical device were created thanks to additive manufacturing process (Ultimaker).

Figure 11B describes how the flexible coverslip **4** supporting the microchip was fixed relatively to the shaft-cam device. The coverslip was clamped into a dedicated pivot joint to represent pinned-pinned boundary conditions. Only one kinematic joint is shown on Figure 11B. Two symmetrical bearing springs associated to a vertical sliding joint were used to adjust the initial distance between the coverslip **4** and rolling ring **3**. The controlled location of the coverslip **4** was then locked by 2 mm screws not represented in Figure 11B.

The motion transformation system was actuated by an encoder gear motor associated with electronic control and acquisition boards (Arduino®). Housing is shown in Figure 11C and the assembled device is shown in Figure 11D. Details on mounting of the different electro-mechanical components are provided in Appendix B. The controlled angular frequency ranged between 0 Hz and 2 Hz with an accuracy of 0.02 Hz, and lateral bending deflection could vary between 0 mm and 3 mm with a mean reproducibility of 0.1 mm. Vertical displacement of the PETG coverslip once the motor was turned on is shown in Figure 11E and is in good agreement with the kinematical equation (2b) provided in Appendix A.

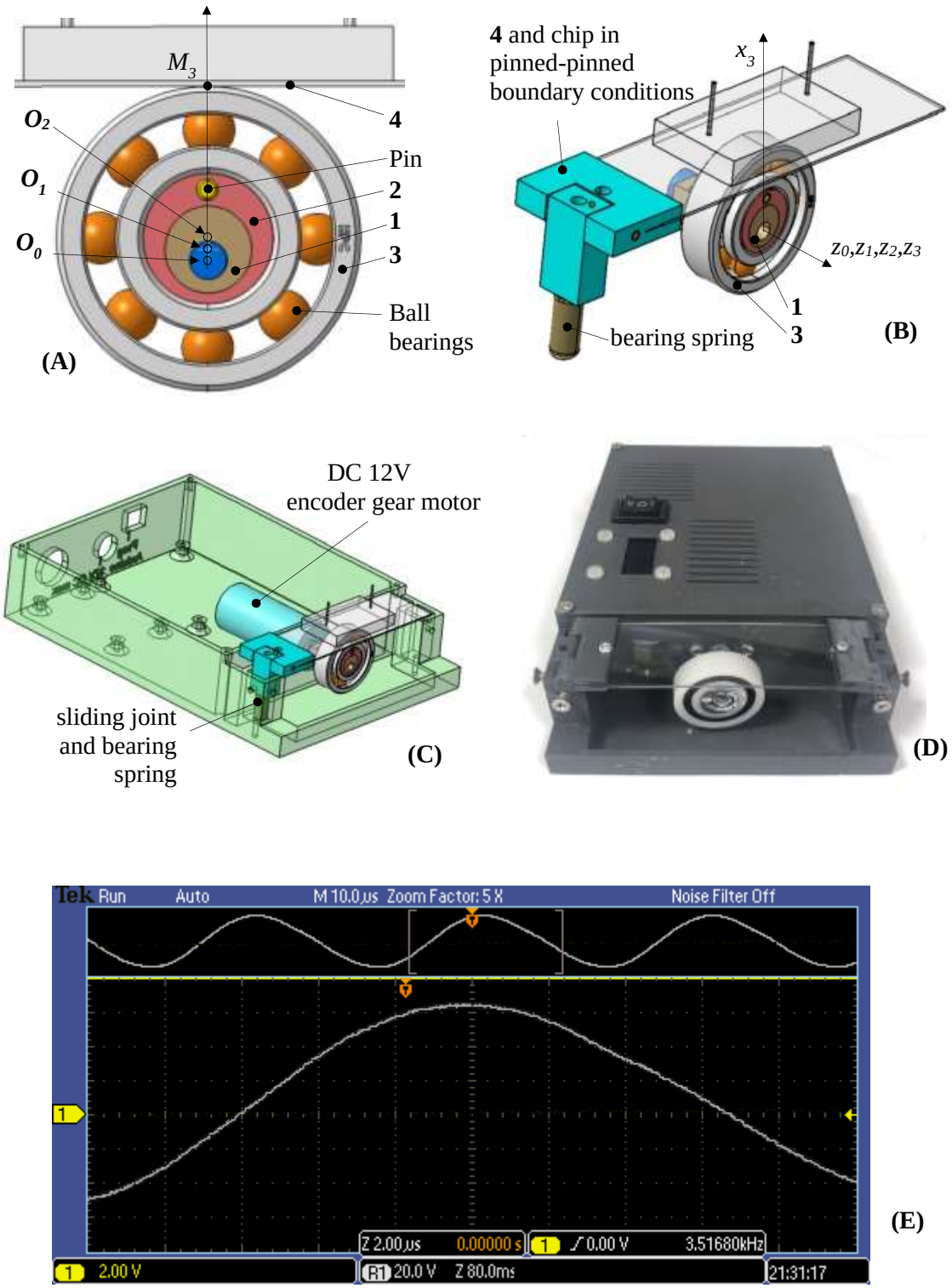

Figure 11: Technological design of the mechanical device. (A) Schematic representation of the motion transformation system, composed of a rotating shaft **1**, a cam disk **2**, and a rolling ring **3**. The flexible coverslip **4** was in contact with rolling ring **3** at point M_3; (B) Details of the pinned-pinned boundary conditions of the PETG flexible coverslip **4** and the PDMS chip; (C) Housing description and electro-mechanical components mountings; (D) Assembled mechanical device with PETG coverslip locked into the pivot joints; (E) Experimental signal describing the vertical motion of the PETG coverslip

4. Elaboration process of the microfluidic device

4.1 Microchip fabrication

In our study, the PDMS microchips were fabricated using Sylgard^{TM} 184 by mixing the silicone elastomer base with the corresponding curing agent in a ratio 1:10 which was then degassed. Straight channels (19.56 mm long and with a 100 µm x 100 µm square cross-section) were created in the PDMS chip by molding the former degassed elastomer mixture on a silicon wafer so as to obtain final chips 2 mm thick (Figure 12A-B). The silicon wafer was fabricated using photolithography methods and dry film negative photoresist (EMS-Nagase DF10100). A final degassing was achieved for another 30 minutes to remove all bubbles, before the mold containing the PDMS was cured at 80°C for 1h30.

Unmolding was performed cautiously once the mold was at room temperature. The different chips were individualized using a scalpel blade. The final microchips were 30 mm long, 10 mm large and 2 mm thick (Figure 12C). Inlets and outlets were finally punched at each end of the microchannels with a 1.5 mm punch cutter to provide access to the channel. The processes of cutting and punching were performed with the engraved microchannels located side up.

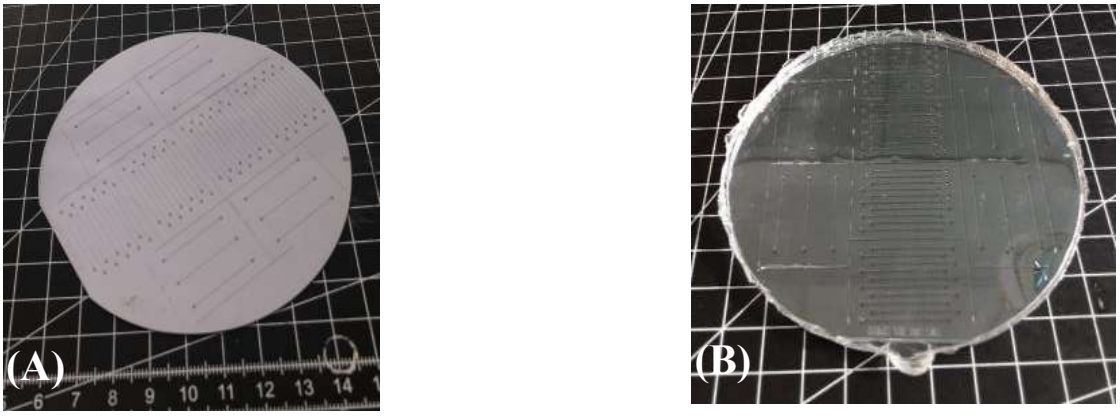

ERC Bebop 2020-2025 project, PI Yohan Davit, Groupe Milieux Poreux et Biologiques, IMFT

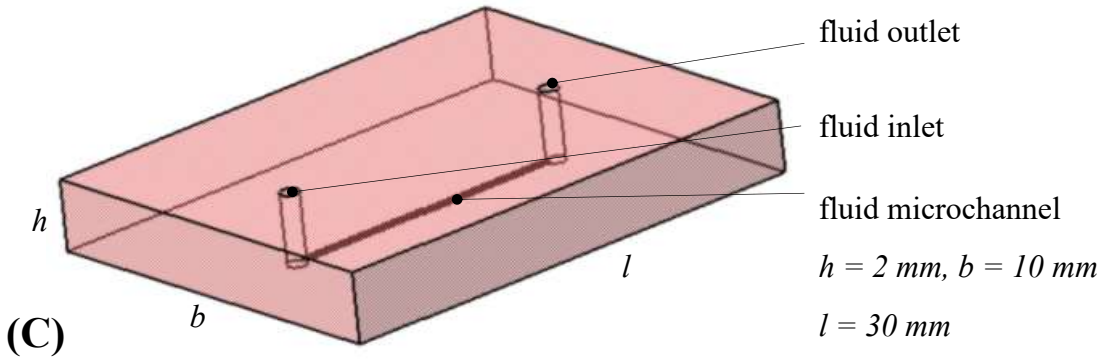

Figure 12: Fabrication of a PDMS microchip. (A) Silicon wafer used to create the microchannels; (B) Molding of PDMS mixture on silicon wafer; (C) Schematic representation of the microchips obtained. The fluidic microchannel was 19.56 mm long with a 100 µm × 100 µm cross-section. Fluid inlet/outlet measured 1.5 mm diameter.

4.2 Manufacturing of the bending substrate

As discussed in section 2 of this chapter, PET is the substrate most commonly used when the planned application requires flexibility. In this study, we used polyethylene terephthalate glycol (PETG) sheets (HIPEX® G) 1 mm thick. The sheets were cut using a laser cutting machine (Speedy 360 Flexx, Trotec) so as to obtain PETG coverslips measuring 75 mm long, 25 mm large and 1 mm thick.

Holes were finally drilled at both ends of the coverslip to accommodate the 2 mm screw used to lock the coverslip into the pivot joint of the mechanical device (Figure 11B-D).

4.3 Assembly of the microfluidic device components

4.3.1 Principles for microchip bonding

The next step in the preparation of the microfluidic device was to choose an effective method to bond the PDMS chips to the PETG coverslip.

Bonding methods can be categorized into direct and indirect approaches (Giri and Tsao 2022). While direct bonding does not require using additional material or reagent layer in the bonding interface, indirect bonding implies using materials such as chemical reagents, epoxy or adhesive tape to assist the bonding. Different PDMS-PET bonding techniques combining surface activation, surface functionalization and/or adhesive-based gluing have been reported in the literature (W. Wu et al. 2015; Tang and Lee 2010; Sivakumar and Lee 2020; Agostini, Greco, and Cecchini 2019; Zhang and Lee 2015; Lee and Chung 2009) (Appendix C).

Surface activation is categorized as a direct bonding approach. Its aim is to remove contaminants and to increase the surface energy by forming polar functional groups for covalent bonding (Shakeri, Khan, and Didar 2021; Borók, Laboda, and Bonyár 2021). It can be performed either using corona discharge treatment or oxygen plasma treatment.

The use of oxygen plasma requires working in a clean room facility and placing the exposed bonding surfaces in a low-vacuum environment in the presence of oxygen gas. On the contrary, corona discharge can be performed at room temperature and standard pressure, thus reducing the cost and the complexity of the procedure. Corona discharge is obtained through a hand-held corona device that generates a high voltage potential between the electrodes at the tip of it, thus ionizing the air (Haubert, Drier, and Beebe 2006). When treating PDMS with a corona discharge for instance, the terminal methyl groups ($-CH_3$) are replaced by silanol groups, which can form covalent siloxane bonds (Si-O-Si) with a similar silanol group on another activated silicon-based surface.

Bonding of PDMS to thermoplastics further requires surface functionalization, also called chemical gluing, because reactive covalent groups are not generated when a polymer is activated with corona or oxygen plasma (Borók, Laboda, and Bonyár 2021). Surface functionalization is categorized as an indirect bonding approach.

The thermoplastic substrate needs first to be activated either with corona or oxygen plasma to break the carbon backbones of the thermoplastic substrate, and it must then be covered with a coupling agent. An organosilane, such as (3-aminopropyl) triethoxysilane (APTES), (3-mercaptopropyl) trimethoxysilane (MPTMS), (3-glycidyloxypropyl) triethoxysilane (GPTES), (3-glycidyloxypropyl) trimethoxysilane (GPTMS), and (3-triethoxysilyl) propylsuccinic anhydride (TESPSA), is commonly used. The silanol groups of the activated PDMS can directly

form bonds with the amino groups (-NH_2) of APTES or the thiol groups (-SH) of MPTMS functionalized polymers.

Adhesive-based gluing is another indirect bonding method. It consists in applying a small amount of adhesive material, such as epoxy or a silicon-based adhesive, between the two surfaces to bond (Borók, Laboda, and Bonyár 2021). It is often used in combination with chemical gluing methods to improve the quality of the bond.

To choose the proper bonding process for the required application, several factors have to be taken into consideration, especially the mechanical and optical properties of the bonding interface. For the purpose of our study, the resulting PDMS/thermoplastic bond had to be strong enough to prevent leakage while a flow circulated through the microchip microchannel and while the microfluidic device was submitted to a bending moment. Moreover, the bonding interface had to be optically transmissive to allow observation of bacteria under a microscope.

Bonding strength is another important factor to consider. Different methods are used to check the quality of the prepared bond, such as manual peeling, tensile strength measurements, shear strength measurement, peel test (Borók, Laboda, and Bonyár 2021). Manual peeling is a simple, easy and cheap qualitative test. It consists in forcibly removing by hand the PDMS chip from the substrate. If the PDMS chip cannot be easily removed, or if it breaks instead of detaching from the substrate, the formation of chemical bonds can be assumed, and the result of the manual peeling test is considered positive. Manual peeling was performed for each microfluidic device assembled to check bond formation.

4.3.2 Application

Several bonding protocols were tested as summarized in Table 2. In all protocols, surface preparation was similar, with both the PDMS chip and the PETG coverslip being cleaned with ethanol 70% and deionized water (DIW), and further dried with compressed air. Surface activation was performed with a corona plasma wand (ElectroTechnic BD-20AC Corona surface treater), and surface functionalization involved depositing APTES (Sigma-Aldrich 440140) on the surface (PDMS or PETG) during 20 minutes at room temperature. The protocols differed by the surface treated (PDMS and/or PETG) and the time duration of corona discharge (either 30s or 60s). In some cases, adhesive-based gluing with a light cure adhesive (Loctite® AA3494, Henkel) was further added to the bonding process *via* different methods.

The quality of the bond obtained with each protocol was tested by manual peeling and microchannel permeability was checked (Appendix D, part A). When an adhesive was used, its distribution at the PETG coverslip/PDMS chip interface was also subjectively evaluated.

Only two protocols successfully passed both the manual peeling test and the microchannel permeability test: protocols 1 and 11. In fact, protocol 1 turned out to be effective for several microchips. However, it could no longer be retained after several weeks, as many PDMS chips could be peeled off manually from the PETG coverslip, either immediately or after several hours under a mechanical stimulus. The use of an adhesive in the following tested protocols added challenge regarding the maintenance of channel permeability. In many protocols tested, the adhesive was found to seal either the inlet/outlet of the microchannel, or the channel path itself.

Two microfluidic devices fabricated using the bonding protocols 1 and 11 were subsequently tested for leakage over three days, one in static, the other in dynamic conditions (see Appendix D, part B). No leak was observed between the PDMS chips and the PETG coverslip after 60 hours of flow whether the coverslip had been submitted or not to a mechanical stimulus. Manual peeling of the chips from the coverslip could not be achieved after 60 hours for both conditions.

	Surface preparation		**Adhesive-based gluing**	**Treated area**		**Observations**
	PDMS	**PETG**	**Loctite® AA3494**	**PDMS**	**PETG**	
1	Ethanol 70% DIW Compressed air	Ethanol 70% DIW Compressed air	None	Surface activation (30s)	Surface activation (30s) Surface functionalization	Positive peeling test Homogeneous bonding Positive microchannel permeability test
2	Ethanol 70% DIW Compressed air	Ethanol 70% DIW Compressed air	None	Surface activation (60s)	Surface activation (30s) Surface functionalization	Negative peeling test
3	Ethanol 70% DIW Compressed air	Ethanol 70% DIW Compressed air	None	Surface activation (30s) Surface functionalization	Surface activation (30s) Surface functionalization	Negative peeling test
4	Ethanol 70% DIW Compressed air	Ethanol 70% DIW Compressed air	Spin-coating on separate glass coverslip (2000 rpm, 1 min)	Surface activation (30s) Surface functionalization Adhesive-based gluing (5s contact with glass coverslip)	None	Negative peeling test Heterogenous adhesive distribution Heterogenous bonding
5	Ethanol 70% DIW Compressed air	Ethanol 70% DIW Compressed air	Spin-coating on chip (2000 rpm, 1 min)	Surface activation (30s) Surface functionalization Adhesive-based gluing	None	Negative peeling test Heterogenous adhesive distribution Heterogenous bonding
6	Ethanol 70% DIW Compressed air	Ethanol 70% DIW Compressed air	Spin-coating on chip (500 rpm, 2 min)	Surface activation (30s) Surface functionalization Adhesive-based gluing	None	Negative peeling test Homogenous adhesive distribution Heterogenous bonding

DIW: deionized water

Table 2 (1/2): Protocols tested for bonding a PDMS microchip to a PETG coverslip

	Surface preparation		Adhesive-based gluing	Treated area		Observations
	PDMS	**PETG**	**Loctite® AA3494**	**PDMS**	**PETG**	
7	Ethanol 70% DIW Compressed air	Ethanol 70% DIW Compressed air	Deposited on chip	Surface activation (30s) Surface functionalization Adhesive-based gluing	None	Positive peeling test Homogenous adhesive distribution Homogenous bonding Negative microchannel permeability test
8	Ethanol 70% DIW Compressed air	Ethanol 70% DIW Compressed air	Deposited on chip sealing inlet/outlet	Surface activation (30s) Surface functionalization Adhesive-based gluing	None	Positive peeling test Homogenous adhesive distribution Homogenous bonding Negative microchannel permeability test
9	Ethanol 70% DIW Compressed air	Ethanol 70% DIW Compressed air	Deposited on chip bypassing inlet/outlet	Surface activation (30s) Surface functionalization Adhesive-based gluing	None	Positive peeling test Homogenous adhesive distribution Homogenous bonding Negative microchannel permeability test
10	Ethanol 70% DIW Compressed air	Ethanol 70% DIW Compressed air	Trickle deposited on chip edges	Surface activation (30s) Surface functionalization Adhesive-based gluing	Surface activation (30s)	Negative peeling test Homogenous adhesive distribution Homogenous bonding
11	Ethanol 70% DIW Compressed air	Ethanol 70% DIW Compressed air	Trickle deposited on chip edges	Surface activation (30s) Adhesive-based gluing	Surface activation (30s) Surface functionalization	Positive peeling test Homogenous adhesive distribution Homogenous bonding Positive microchannel permeability test

DIW: deionized water

Table 2 (2/2): Protocols tested for bonding a PDMS microchip to a PETG coverslip

5. Exploration of the mechanical behavior using numerical modeling

The mechanical response of a microfluidic device comprising one microchip bonded to a PETG coverslip was evaluated by using a finite element numerical model based upon the displacement method (Abaques®). Due to the symmetry planes *(O, x, z)* and *(O, y, z)*, and considering the horizontal displacement negligible, the numerical model only covered quarter of the structure, as shown in Figure 13A. In the end, the meshed coverslip was 37 mm long, 12.5 mm large and 1 mm thick, and the meshed microchip was 15 mm long, 12.5 mm large and 2 mm thick and involved quarter of a microchannel (half longitudinally, half transversely). Displacement continuity at the interface was respected.

Meshing was constituted of twenty nodes quadratic elements (H20), with three translational degrees of freedom per node element. Meshing was of about 6×10^6 degrees of freedom. The material was homogeneous and isotropic, with a couple (elastic modulus E; Poisson ratio υ) fixed to (2×10^9 Pa; 0.3) and (1×10^6 Pa; 0.45) for PETG and PDMS, respectively (Ariati et al. 2021; Valvez, Silva, and Reis 2022). Transverse displacement was fixed at $x = L/2$ to mimic pinned-pinned boundary conditions, symmetrical conditions were applied to nodes located in the symmetry planes and an imposed displacement w_0 was applied at $x = 0$ to model the line contact between rolling ring **3** and flexible coverslip **4**.

A geometrical non-linear computation was implemented and achieved using a conventional Newton-Raphson algorithm. Transverse displacements, i.e. $w(x)$, were predominant because of the structure constitution, and of the boundary and loading conditions. Displacement field is shown in Figure 13C. The responses, namely $F(w)$, computed with and without a PDMS microchip, were normalized using an imposed displacement w_0 and the maximum resulting force F_0 obtained for PETG coverslip. As shown in Figure 13D, no non-linear effects were depicted even for superimposition of the chip and the coverslip. Imposed displacement up to $w_0 = 2$ mm was still valid in the linear domain to reach $F_0 = 3.3$ N. An increase of the bending linear stiffness between the PETG coverslip and the assembly [PETG coverslip-PDMS microchip], namely k_{PET} and $k_{PETG+PDMS}$, was found and was limited to 10 % as shown in Figure 13D.

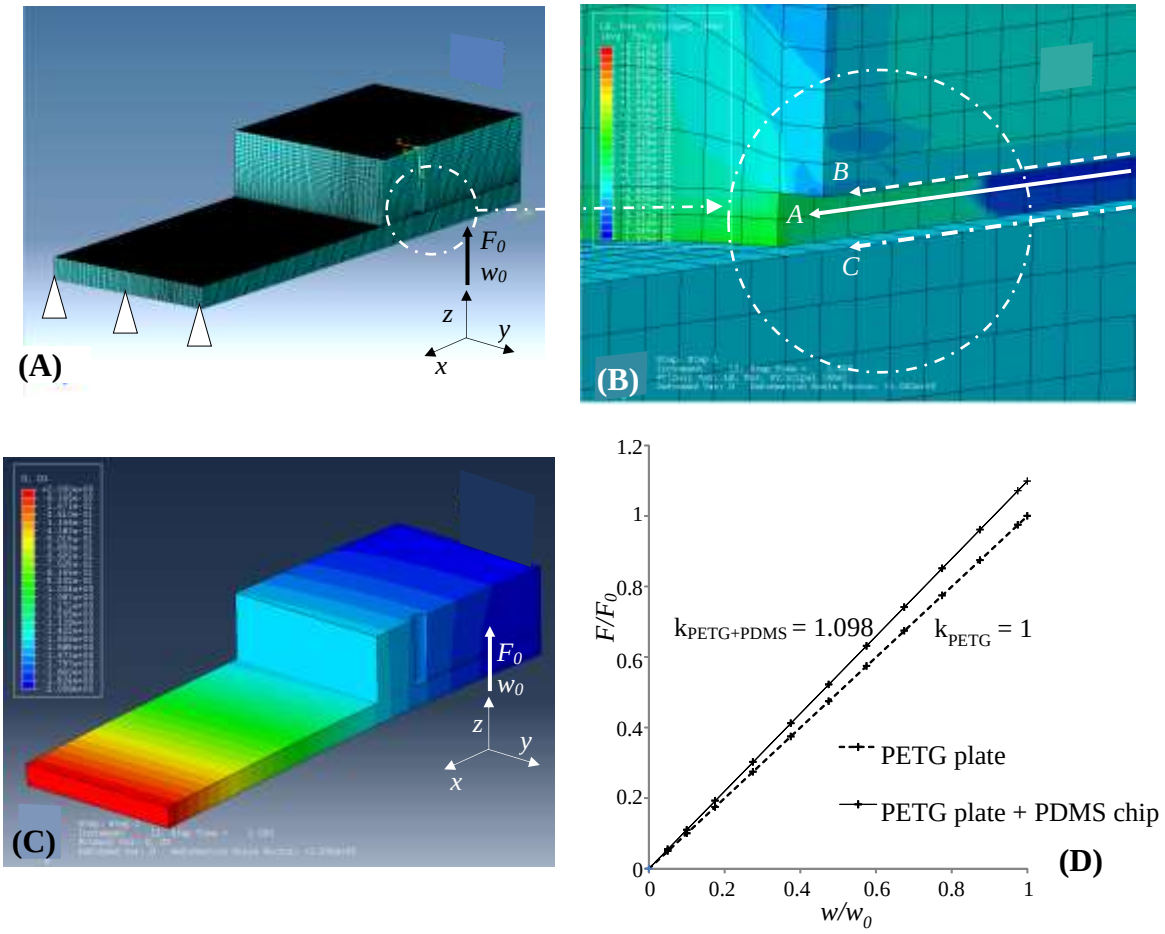

Figure 13: Numerical modeling (finite element method) of the microfluidic device involving PETG coverslip and PDMS chip. (A) 3D meshing of a quarter of the microfluidic device; (B) Details of the quadrilateral microchannel showing lateral wall *A*, upper wall *B* and lower wall *C*; (C) Displacement field under imposed displacement w_0 of line contact between rolling ring **3** and flexible coverslip **4** and located at $x = 0$; (D) Structural response of the PETG coverslip without the PDMS microchip (- -) and with the PDMS microchip (—). A 10% increase was observed between $k_{PETG+PDMS}$ and k_{PETG} bending linear stiffnesses.

The next investigation concerned strain distribution patterns along the microchannel walls. When considering half of the cross-section of the quadrilateral microchannel, the lateral wall *A*, the upper wall *B* and the lower wall *C* remained, as depicted in Figure 13B. Walls *A* and *B* were associated to the PDMS microchip, while wall *C* was the PETG coverslip upper surface. The explored path was located in the middle of each wall and normalized by half of the channel length (x_0 = 10 mm), thus avoiding local perturbation due to the inlet and outlet holes. Strain magnitudes were normalized using wall *C* values as reference.

Strain tensor components involving *y*-components were negligible because of the structural symmetry properties. Only normal strain ε_{xx} and shear strain ε_{xz} were investigated in detail. Figure 14A shows that the maximum variation of the normalized normal strain was limited to 15 %. In return, shear strain showed significant variations (Figure 14B). Indeed, shear strain on the upper wall *B*, namely $\varepsilon_{xz}B$, was one magnitude order higher compared to that on bottom wall *C*, with significant evolution along the path. In addition, shear strain on lateral wall *A*,

namely $\varepsilon_{xz}A$, was significantly increased (up to two magnitude order) and more constant along the path. Magnitudes for x_0, $\varepsilon_{xx}C$ and $\varepsilon_{xz}C$ were 2 mm, [21×10^{-4}, 29×10^{-4}] and [0.06×10^{-4}, 2.2×10^{-4}].

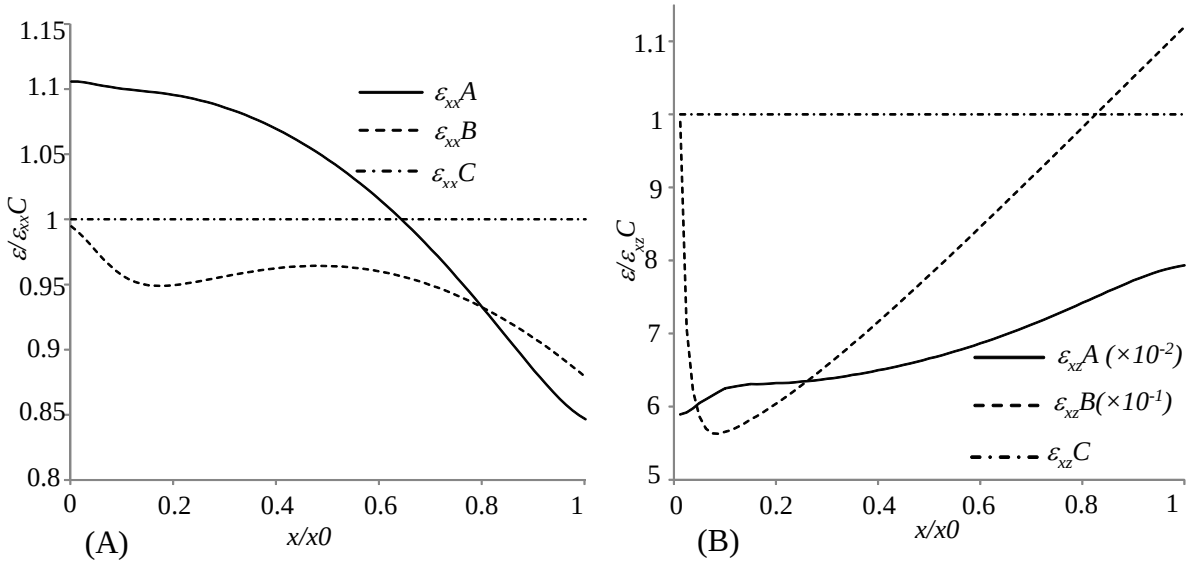

Figure 14: Distribution patterns of strains along walls *A*, *B* and *C* of the microchannel. The path is normalized using micro-channel length x_0 with the origin located at the symmetry plane *(O, y, z)*. Strain magnitudes are normalized using *C* values as reference. (A) Normal strain ε_{xx} ; (B) Shear strain ε_{xz}. Compared to *C*, shear strains are higher of one order of magnitude for *B* and two orders of magnitude for *A*.

6. Discussion and conclusion

The central aim of our study is to explore the effects of mechanical stimuli on biofilm growth, and in this chapter, we have designed the experimental workbench to do so. To our knowledge, this is the first experimental setup that allows exploring the effects of cyclic mechanical stresses on biofilm development. The core of the microfluidic device was a PDMS microchip bonded to a flexible PETG coverslip. Each microchip involved a quadrangular microfluidic channel acting as a support for bacterial growth and biofilm formation, while the coverslip was able to be transversely loaded thanks to a dedicated mechanical device.

The architecture of the mechanical device was first designed. It was decided to work at imposed displacement by designing an eccentric system controllable in frequency and amplitude. The kinematic equations governing the motion of the mechanical device are given in Appendix A. The mechanical device conceived imposed not only a vertical displacement to the flexible coverslip, but also a horizontal displacement, which was the consequence of the kinematics controlled by an adjustable cam. A mechanism inducing only a vertical displacement could have been designed, but would have necessitated introducing additional couplings and thus additional items to annul the x component. This was beyond the scope of our study, as our project was mainly based on the design of a simple system to explore the short-term impact of a mechanical loading while minimizing technological risks. However, this x component induced with our mechanical device implies a change in the point of application of the mechanical force, which represents a mechanical parameter that could be used in future studies. Manufacturing of the mechanical device used significant opportunities offered by 3D printing, and kinematic monitoring relied on an open-source electronics platform hardware and software.

A preliminary evaluation of the structural response of the microfluidic device was then undertaken by using 3D finite element modeling. Even if superimposition of the chip on the coverslip represented a significant modification of the structural geometry compared to that of the plate alone, it showed limited role in the global response. Indeed, the modulus ratio between the chip and the coverslip, namely 2×10^3, considerably reduced the impact of the chip on the overall response of the microfluidic device despite its geometric extent.

This modeling step also allowed predicting the strain tensors along the fluidic microchannel. Indeed, the channel walls showed strain fields that could be transmitted to the bacterial population and consequently modify the biological responses. Our model only comprised 2 elements, and thus 5 nodes, in the thickness of the channel, as shown in Figure 13B. Meshing of the channel could have been denser, and the interface between the PDMS microchannel and the biofilm could also have been added, but our model gave a general overview of the different strain fields expected. Overall, the results showed that normal strain fields ε_{xx} were one to two orders of magnitude higher to shear fields ε_{xz}. This was explained by the predominance given to the bending load when designing the experimental device. However, a significant increase in shear stress was observed along the side walls of the channel. This was the consequence of a properties' gradient at the interface between the PDMS chip and the PETG coverslip.

The greatest challenge was related to the bonding protocol used to create the microfluidic device. Most studies report bonding of a PDMS chip to silicon-based materials such as glass *via* a rather reproducible process of surface activation (Borók, Laboda, and Bonyár 2021). In our study, the substrate had to be flexible. PDMS-polymer bonding is more difficult because

reactive covalent groups are not generated when a polymer such as thermoplastics is activated with corona or oxygen plasma (Appendix C). A custom-made surface functionalization is therefore required (Borók, Laboda, and Bonyár 2021).

One could argue that the manual peeling test used to check the quality of the bond was not discriminant enough, and that more objective tests, such as characterizing the bond by its tensile strength (Borók, Laboda, and Bonyár 2021), would have been more appropriate. Nevertheless, the aim was to choose a protocol that would lead to a leak-free bond between the chips and the coverslip over at least 48 hours. It has been observed that when surfaces are activated, they become hydrophilic, and regain hydrophobicity quickly under ambient conditions (Hillborg and Gedde 1998). Mechanical stimuli can also accelerate this recovery process (Hillborg and Gedde 1998). This explains why a leakage test over sixty hours, either in static or in dynamic conditions, was performed prior to retaining the tested bonding protocol. It should be noticed that for the leakage test in the dynamic condition, the cycling frequency was set to 1 Hz to be close to that of the walking gait, and the coverslip was loaded at its maximum displacement magnitude to induce the most unfavorable conditions in terms of strain and stress in the vicinity of microfluidic device.

Our experiments were therefore managed in two main series. In the first series, bonding was effective when using surface activation with corona discharge combined to surface functionalization with APTES. However, the second bonding series showed deficiencies in the bonding protocol since all chips could be peeled off manually from the coverslip. After scanning a significant number of parameters, it appeared that the environmental parameters, and especially the ambient humidity level, may have played a significant role. Indeed, the time period of the first series was winter, when room temperature was of 26 °C and humidity level was of 30%, whereas the second series took place in spring with a 25.5°C room temperature and 65% humidity level. Our observation was corroborated by other studies raising limitations in their bonding protocol due to uncontrolled humidity levels during the bonding process. Indeed, it has been shown that humidity could negatively impact adhesion by significantly reducing surface reactivity and hydrophilicity due to augmented hydroxyl groups on surfaces (Alam, Howlader, and Deen 2014). Pursuing our experiments in a clean room was mentioned but too costly in the framework of our preliminary study. Finally, a solution was found by adding an adhesive in the bonding protocol to obtain a satisfying manufacturing process.

In this chapter, we have achieved the development of an experimental setup comprising a microfluidic device dedicated to the study of bacterial growth and biofilm formation, and that could be submitted to a transverse load variable in magnitude and frequency thanks to a mechanical device. To our knowledge, this was the first experimental setup designed that allows exploring the effects of a kinematical controlled stimulus on biofilm dynamic response.

Chapter III:
Influence of bending on biofilm growth – preliminary study

1. Introduction

Biofilms are ubiquitous in our environment, and most predominantly form in aqueous habitats. The effect of shear stress on biofilm growth has been the most studied given the role flow plays in biofilm formation (Krsmanovic et al. 2021; Jara et al. 2020; Fonseca and Sousa 2007; Ai et al. 2016). When comparing biofilm development in a dynamic model to its formation in a static model by respectively submitting or not bacterial cultures of *Cutibacterium acnes* to a given flow, Varin-Simon et al. (2021) showed that the percentage of live bacteria within the biofilm was higher in the dynamic model than in the static one (Varin-Simon et al. 2021). To our best knowledge, no studies exploring the effects of bending on biofilm development have been published so far.

In this chapter, we present the first results obtained with the experimental setup described in chapter II. To quantify biofilm development, microchips were inoculated with bacteria containing a fluorescent protein-expressing plasmid. The microfluidic devices thus inoculated were either submitted to a bending moment thanks to the mechanical system described in chapter II (dynamic condition) or not (static control). Imaging with epifluorescence microscopy was performed to compare fluorescence between static and dynamic conditions.

The experimental methodology was based on two test campaigns, namely Experiment 1 and Experiment 2. Experiment 1 was designed as a prototype, while Experiment 2 enabled improvements in the procedure and results exploration.

2. Materials and Methods

2.1 Preparation of the microfluidic device

Polydimethylsiloxane (PDMS, Sylgard™ 184) microchips of 30 x 10 x 2 mm and PETG (HIPEX® G) coverslips of 75 x 25 x 1 mm were prepared as described in chapter II. Microfluidic devices were created by bonding two PDMS microchips on one PETG coverslip using the two bonding protocols presented in Chapter II. Using two microchips allowed increasing observations while keeping symmetry properties as shown in Figure 15. Details of the experimental methodology are summarized in Table 3.

2.1.1 Experiment 1

For the first set of experiments, the bonding protocol combined surface activation and surface functionalization (protocol 1, Table 2). The PETG coverslip was first cleaned with ethanol 70% using a Kimtech ™ wipe, and was dried with compressed air. Surface activation was performed under the recirculating hood by exposing the PETG coverslip to a corona discharge for 30 seconds. Several drops of APTES were then spread uniformly on the PETG coverslip by pipette (surface functionalization). Two PDMS chips were immersed in ethanol 70% for 2 minutes. They were then rinsed abundantly with DIW and dried with compressed air. After 20 minutes of PETG coverslip-APTES contact, the coverslip was abundantly rinsed with DIW, air-dried, and placed in a 3D-printed guide to bond the chip at the middle of the coverslip as shown in Figure 15. The use of this specific guide allowed respecting symmetrical properties of the assembled microchips and PETG coverslip in both longitudinal and lateral directions as detailed in section 2 of chapter II and in Figure 6. Under the recirculating hood, one PDMS microchip was exposed to a corona discharge for 30 seconds making sure the subsequently activated side was the one comprising the microchannel. The PDMS microchip was placed at one edge of the PETG coverslip. Propagation of a bonding front was visualized once both surfaces were in contact. A slight digital pressure on one edge of the microchip was sometimes necessary for the bonding front to form. The second PDMS microchip was treated similarly before being bonded at the same level as the first PDMS microchip, on the contralateral side of the coverslip. The microfluidic device was left untouched for 2 hours.

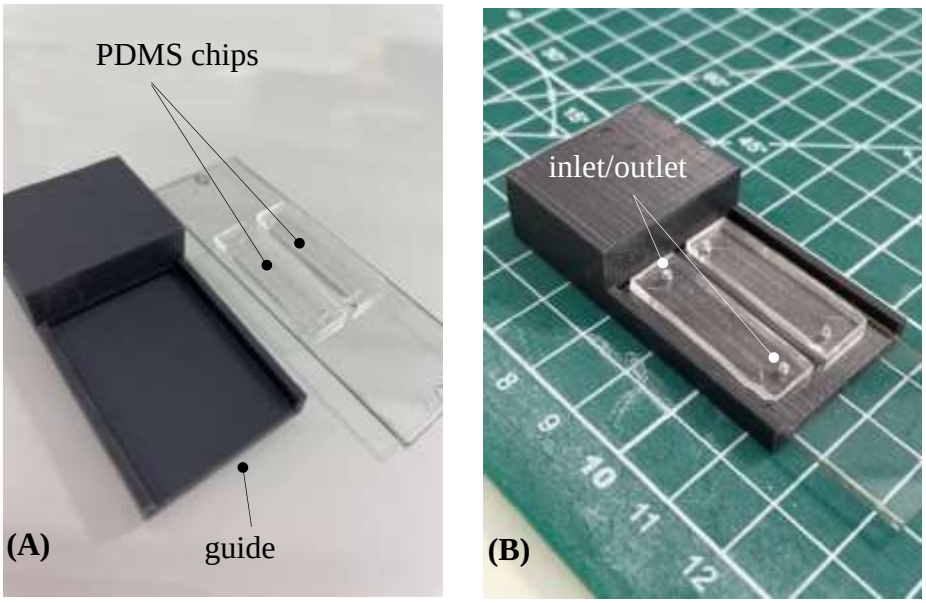

Figure 15: Positioning of the microfluidic device components for bonding. (A) 3D-printed guide with two PDMS microchips and one PETG coverslip; (B) Relative location of the microfluidic device components once bonded with lateral and longitudinal stops.

2.1.2 Experiment 2

For Experiment 2, the following bonding protocol (protocol 11, Table 2) was retained: the PETG coverslip was activated and functionalized as in Experiment 1 (corona treatment for 30 seconds and APTES). Two PDMS chips were immersed in ethanol 70% for 2 minutes, and were then rinsed abundantly with DIW and dried with compressed air. After 20 minutes of PETG coverslip-APTES contact, the plate was abundantly rinsed with DIW, air-dried, and placed in the 3D-printed guide. Under the recirculating hood, the side comprising the engraved channel of one PDMS chip was treated with corona discharge for 30 seconds. A thin trickle of adhesive was applied on the four edges of the PDMS chip. Bonding was achieved by placing the PDMS chip at one edge of the PETG coverslip, and by slightly pressing on the chip from the center to the periphery. This first allowed bonding between the PETG coverslip and the PDMS chip at the level of the microchannel, and then reinforcing the bond with the adhesive at the edge. The second PDMS chip was treated similarly, i.e. 30 seconds corona discharge followed by a thin trickle of adhesive at the four edges, and was bonded at the same level as the first PDMS chip, on the contralateral side of the coverslip (Figure 15). The microfluidic device conceived was then placed under UVs during 1h30 to let the adhesive cure.

Prior to experiment, all microfluidic devices were tested for effective bonding with a manual peeling test and a microchannel permeability test (Appendix D, part A). When both PDMS microchips were effectively bonded and permeable, the microfluidic device was tested either in dynamic or in static condition.

2.2 Culture media and strain preparation

Sterile culture media was prepared by mixing 18.7 g of brain heart infusion (BHI) broth from Sigma-Aldrich® with 400 mL of sterile DIW. The BHI solution was autoclaved at 121°C,

and 100 mL of sterile ampicillin solution concentrated at 1.5 mg/mL was added once it had cooled down.

Biofilm development of *Pseudomonas aeruginosa* strain ATCC 15692 GFP was used in this study. This strain of *P. aeruginosa* is very well studied in the literature and is very stable, which makes it a perfect model system. To make sure no contamination of the original strain occurred, a strict aseptic protocol was respected for the following steps. This included sterilization of all instruments by autoclaving them at 121°C, cleaning of all working surfaces with ethanol (C_2H_6O, 70%) prior to any manipulation, and working under a recirculating hood. Cultures were reconstructed from a -80°C stock and cultured overnight in 25 mL of sterile culture media at 32°C and 70 rpm.

Bacterial density of the reconstituted culture was estimated by measuring the optical density at 600 nm (OD_{600}) with a spectrophotometer (Eppendorf BioPhotometer®) using sterile culture media as control. Dilution was performed until obtaining an OD_{600} of 1 in Experiment 1, and of 0.2 in Experiment 2 as detailed in Table 3. These concentrations ensured bacterial attachment to the microchannel walls during the inoculation phase.

			Experiment 1	**Experiment 2**
Microfluidic device preparation	Surface preparation	PDMS	C_2H_6O, DIW, compressed air	C_2H_6O, DIW, compressed air
		PETG	C_2H_6O, DIW, compressed air	C_2H_6O, DIW, compressed air
	Surface activation	Type	Plasma (Corona)	Plasma (Corona)
		t (s)	30	30
	Surface functionalization	Type	APTES	APTES
		T (°C)	RT	RT
		t (min)	20	20
	Adhesive gluing		-	Chip edges
	Treated surface	PDMS	Activation	Activation, **adhesive**
		PETG	Activation, functionalization	Activation, functionalization
Experimental conditions	OD_{600} of bacterial culture		1	**0.2**
	Flow rate (µl/min)		20	**0.2**
	Duration (h)		40	**24, 48**
	Dynamic cycle (Hz)		1	1
	Dynamic magnitude (mm)		2	2
	Temperature (mean °C)		26	25.5
	Humidity level (mean %)		30	**65**

C_2H_6O: ethanol; APTES: (3-aminopropyl)triethoxysilane ; DIW : deionized water ; PDMS : polydimethylsiloxane; RT: room temperature; PETG: polyethylene terephthalate glycol; T: temperature; t: time

Table 3: Protocols for microfluidic devices preparation and experimental conditions in Experiment 1 and Experiment 2. Parameters differing between both experiments are underlined in bold

2.3 Inoculation of the microchip

Before bacterial inoculation, the channel of each PDMS chip was cleaned with ethanol (C_2H_6O, 70%) and rinsed with sterile culture media under the recirculating hood to diminish the risk of contamination. Air was finally injected into the channel to empty it from any liquid. The diluted bacterial culture was flowed into the microchannel of the PDMS microchip through the outlet punch using a sterile syringe connected to a flexible plastic tube (Tygon®, diameter 0.5 mm) (see Appendix D). To ensure the whole channel remained inoculated during the following hour, another sterile flexible plastic tube (Tygon®) 30 mm long was inserted into the inlet punch, and injection of the bacterial culture was pursued until the inlet tube was full. After inoculation, the microfluidic device was left untouched under the recirculating hood for 1 hour to allow bacterial adhesion to the channel walls.

2.4 Fluidic experimental setup

The fluidic circuit for biofilm growth consisted of a sterile culture media delivery system, the microfluidic device, either placed on a flat surface for the static condition or fixed into the dedicated mechanical device for the dynamic condition, and a waste reservoir (Figure 16).

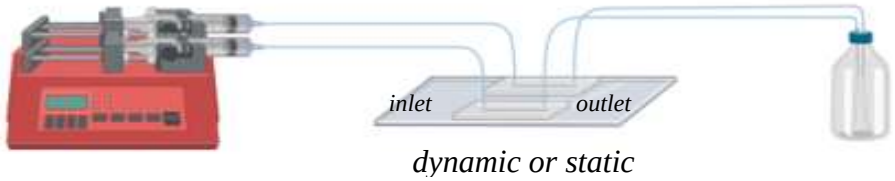

Figure 16: Schematic description of the fluidic experimental setup. Microfluidic devices were either placed on a flat surface (static condition) or fixed into the mechanical device (dynamic condition)

The experimental setup for the dynamic condition is shown in Figure 17.

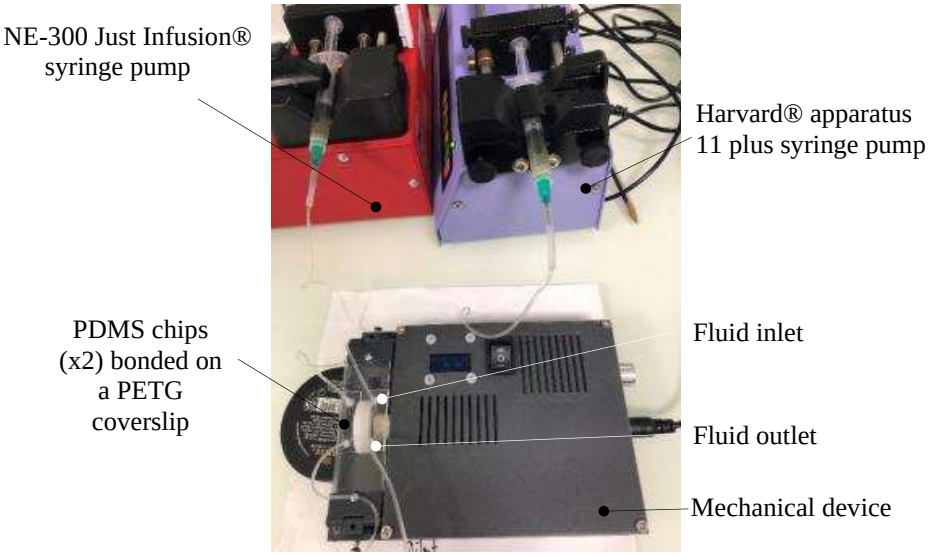

Figure 17: Microfluidic device tested dynamically

Degassed sterile culture media was pumped into the microchannels via syringes pumps (Harvard® PHD 2000, Harvard® apparatus 11 plus or NE-300 Just Infusion™ Syringe Pump) as shown in Figure 17. Adhesive sealant (Loctite SI5366, Henkel®) was finally applied at the junction between the tubes and the inlet and outlet punches of the microchip. Flow rates of the syringe pumps were set to 20 µL/min for Experiment 1 and to 0.2 µL/min for Experiment 2 as described in Table 3.

Once the PDMS microchips bonded to the PETG coverslip were connected to the microfluidic circuit, the coverslip was either placed on a flat surface for the static experiment, or fixed into the dedicated pivot joints of the mechanical device for the dynamic condition, as described in chapter II. For all dynamic experiments, cycling frequency was fixed to 1 Hz with a maximum vertical displacement of 2 mm.

To summarize, experimental conditions distinguishing Experiment 2 from Experiment 1 were the bonding protocol of the microchips on the coverslip, the duration of biofilm growth, the initial bacterial density inoculated, the fluid flow rate and the ambient uncontrolled humidity level (Table 3).

2.5 Imaging protocol

Biofilms were imaged using a camera (sCMOS pco.edge 4.2 bi) connected to an inverted epifluorescence microscope (Ti2-E, Nikon) with a 10x objective (NA = 0.3), as shown in Figure 18. Images were taken in bright field (BF) and in green fluorescence (GF). For fluorescence images, a light source (Lumencor Sola light engine SM at 10%) combined with a green fluorescent protein (GFP) filter (Nikon filter cube GFP-3035D) excited the GFP produced by the bacteria (GFPmut3). Here, brightfield imaging was used as a control to detect the presence of biofilms. Fluorescence imaging not only detects the presence of biofilms but it also provides a level of quantification of bacterial density. Indeed, the greater the intensity, the greater the number of bacteria.

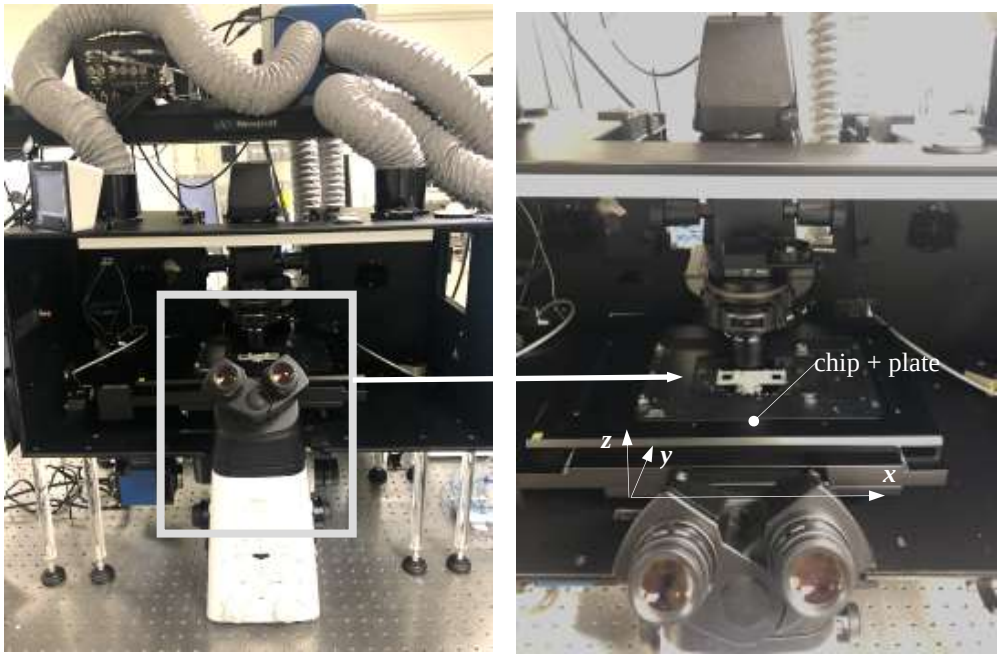

Figure 18: High-resolution camera connected to an inverted epifluorescence microscope (Ti2 Eclipse, Nikon) used for biofilm imaging

Images were recorded at multiple points of the microfluidic channels in Experiment 1, and the full channel was recorded using stitching in Experiment 2. All images were acquired at the midplane of the microchannel.

3. Results

3.1 Experiment 1

In Experiment 1, biofilms were imaged after having let bacteria develop for 40 hours. Results were available for one microchip tested in static condition, and three microchips tested in dynamic condition. Microscopic 10x images resulted in regions of interest (ROIs) of 889 × 889 µm. The channel length was 19.56 mm. Recorded images were post-processed using Fiji (Schindelin et al. 2012) by subtracting the background noise and by correcting the unevenness with a rolling ball of 50. Images were realigned when needed and cropped using a single ROI.

Six ROIs of the microchannel were microscopically explored in the static condition and four ROIs were explored in the dynamic condition (Figure 19A and Figure 20A). ROIS R_3, R_4 and R_5 in the static experiment coincided with R_3 location in the dynamic experiment.

Figure 19B-C and Figure 20B-C show the images obtained in the static and in the dynamic conditions, respectively. Biofilm presence was depicted by darker regions in BF imaging (black and white imaging - Figure 19B and Figure 20B) and by brighter green regions in fluorescence imaging (Figure 19C and Figure 20C).

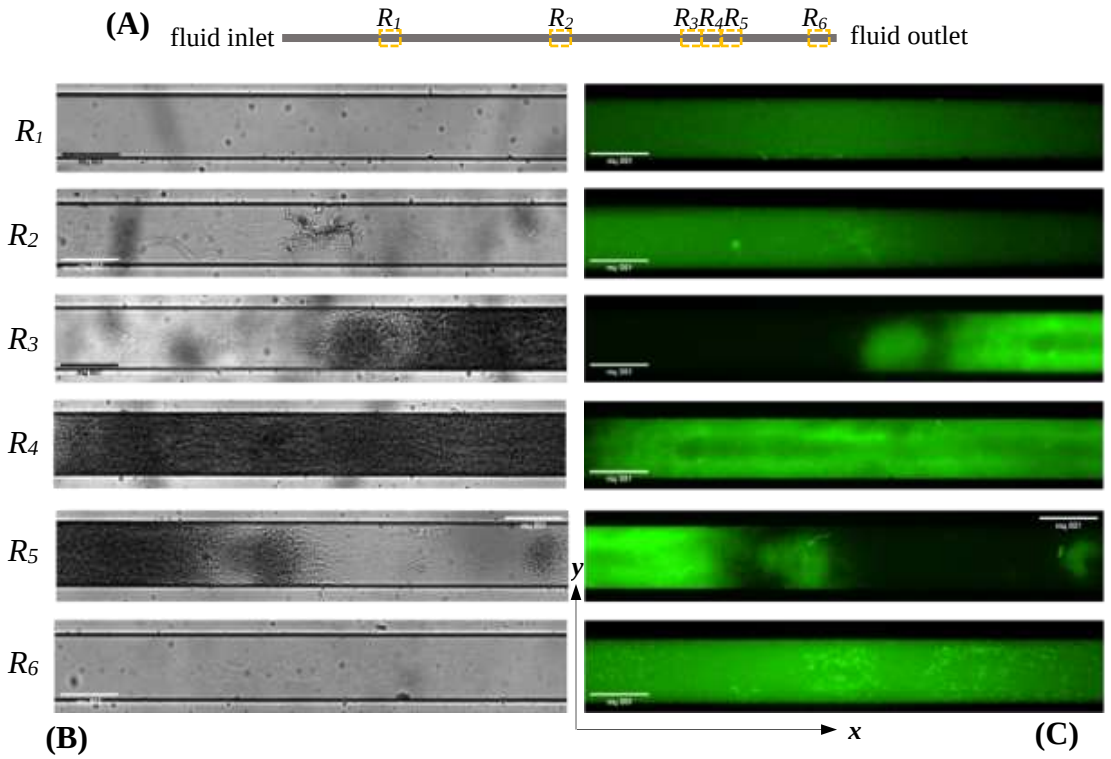

Figure 19: Biofilm imaging in static condition after 40h growth. (A) Location of ROIs; (B) Bright field imaging; (C) Green fluorescence imaging. The scale bar was 100 µm

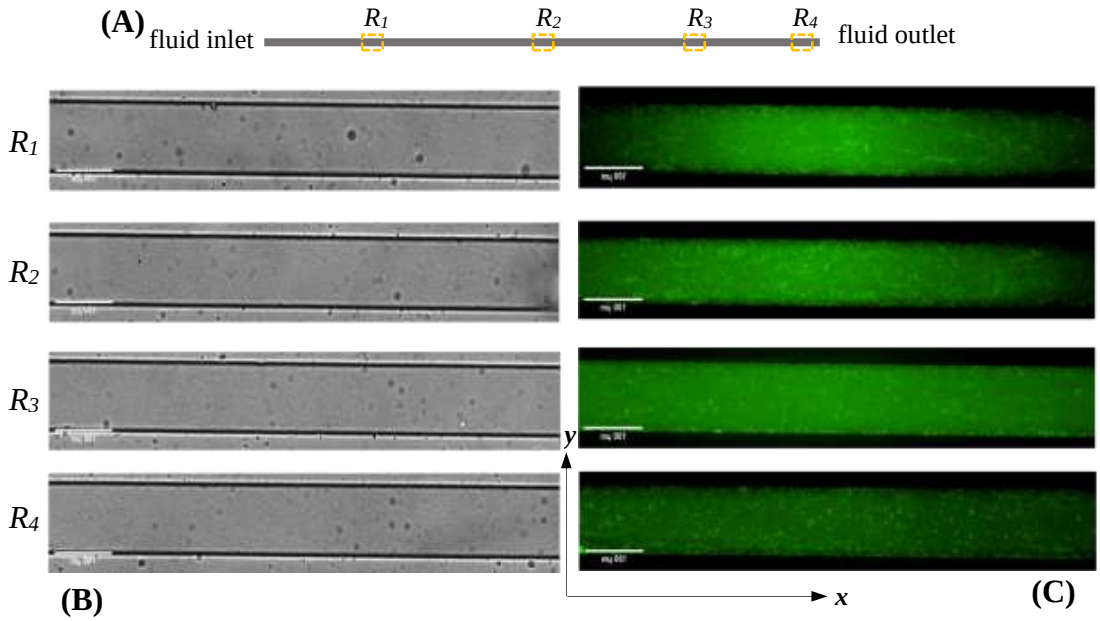

Figure 20: Biofilm imaging in dynamic condition after 40h growth. (A) Location of ROIs; (B) Bright field imaging; (C) Green fluorescence imaging. The scale bar was 100 µm

Mean fluorescence intensity I_m was analyzed on each ROI (excluding the borders outside the ROIs) by measuring the intensity of the whole area of the ROI including the background intensity I_{bg}. Figure 21 shows normalized intensity I_s relative to background intensity I_{bg}, namely $I_s = (I_m - I_{bg})/I_{bg}$.

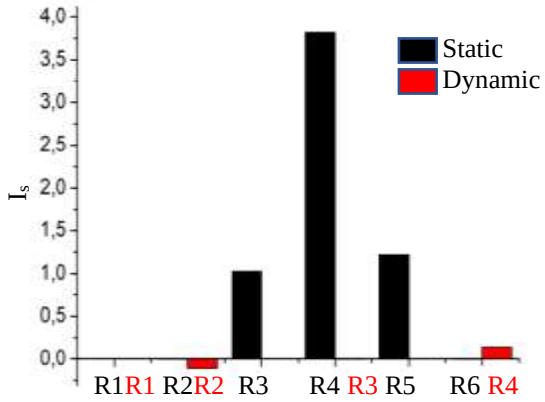

Figure 21: Distribution of biofilm fluorescence signal (normalized intensity I_s) along the microchannel (ROI) in static and dynamic conditions

Results show that applying a dynamic bending moment to the substrate for 40 hours limited bacterial biofilm growth, especially at the center of the channel.

Experiment 1 was used as a proof of concept. For the next experiment, we imaged biofilm growth over the whole channel and for two different time points: 24h and 48h.

3.2 Experiment 2

In Experiment 2, biofilms were imaged after 24h and 48h growth. Results in static condition were available for three chips at 24h and one chip at 48h, while results in dynamic condition were available for two chips at 24h and for one chip at 48 h.

Images in green fluorescence for the static and the dynamic conditions after 24h growth are shown in Figure 22A. Brighter green fluorescence indicates biofilm presence.

Fluorescence maps in the (*O*, *x*, *y*) plane of the microchannel are plotted in Figure 22B. The color scale represents fluorescence intensity normalized by the maximum value of fluorescence: blue indicates no fluorescence, and the warmer the color, the more intense the fluorescence.

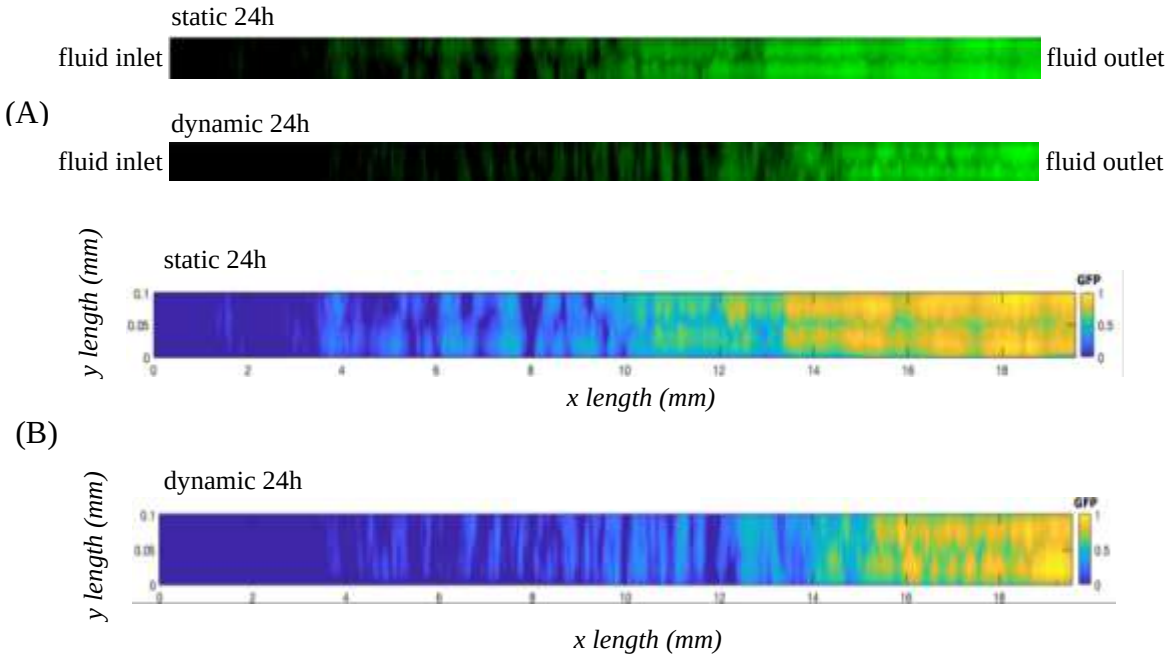

Figure 22: Imaging of biofilm after 24h growth in static and dynamic conditions. (A) Green fluorescence; (B) Fluorescence intensity. The longitudinal microchannel path follows the *x*-length (0 - 19.56 mm) and the transversal length follows the *y*-length (0 - 100 μm). Color scale represents green fluorescence intensity, from no fluorescence (0, blue) to intense fluorescence (1, yellow).

Images in green fluorescence and fluorescence intensity after 48h growth are shown in Figure 23A and Figure 23B, respectively.

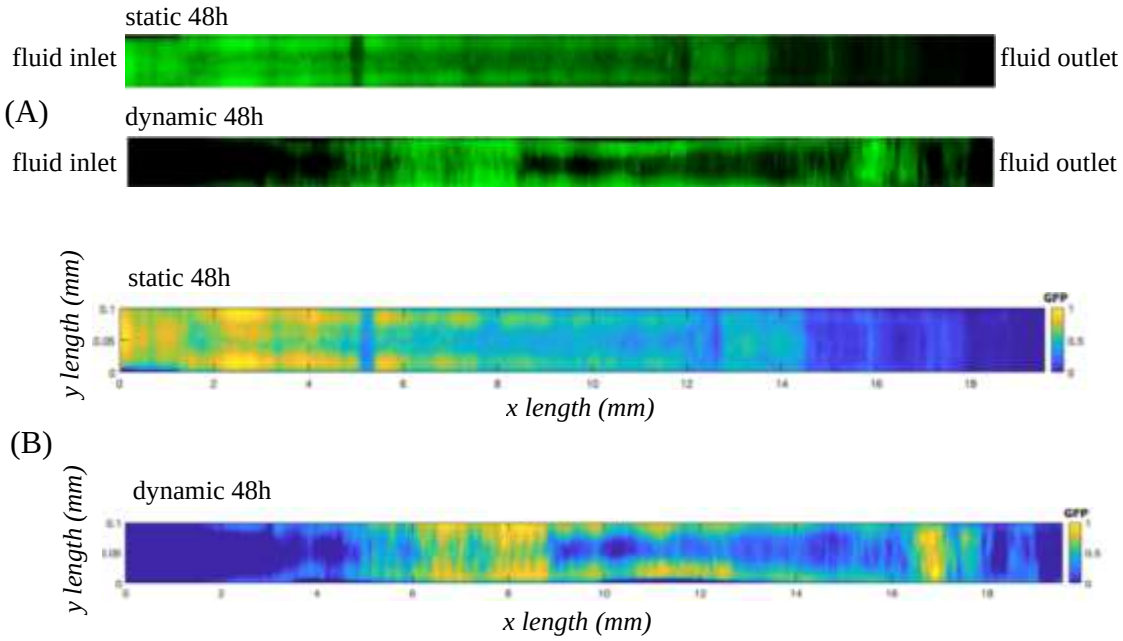

Figure 23: Imaging of biofilm after 48h growth in static and dynamic conditions. (A) Green fluorescence; (B) Fluorescence intensity. The longitudinal microchannel path follows the *x*-length (0 - 19.56 mm) and the transversal length follows the *y*-length (0 - 100 μm). Color scale represents green fluorescence intensity from no fluorescence (0, blue) to intense fluorescence (1, yellow).

To go further in the analysis, an open-source software, Ilastik (Berg et al. 2019), was used to segment the biofilms. Acquired images (Figure 24A) were first processed to subtract the background and correct the unevenness in Fiji. The Ilastik segmentation involved an interactive pixel classification, where a subset of pixels representing the biofilm were manually labelled. These labels then trained a machine learning algorithm, namely the Random Forest algorithm, and provided a probability map that separated the images into biofilm and background (Figure 24B-C). The features selected here for the classification were the edge detection, texture, and color intensity. Post-segmentation, the object classification workflow was used in Ilastik to classify the biofilms using the following thresholds: smooth 0.6/0.6, threshold 0.5 and size filter between 10 and 10^7 to ensure all biofilms were taken into account. After the machine learning was trained using the user-annotated data (Figure 24D-E), several features of the objects were exported in a .cvs format, including the size of the object, the position, as well as the total intensity. These data were finally processed using Matlab.

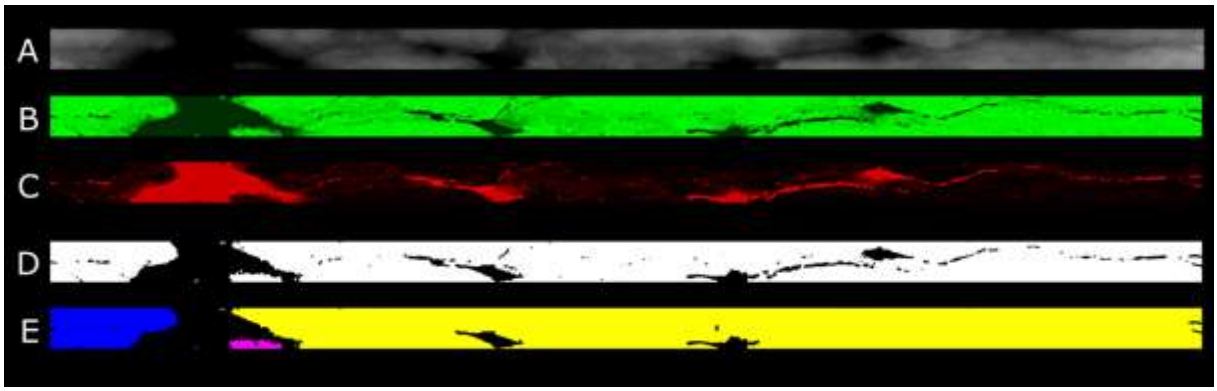

Figure 24: Image processing of Experiment 2 using Fiji and Ilastik. (A) Brighfield image of one section of a channel in static condition at 24h. This section shows biofilm in grey with pores in black; (B) Probability map of the biofilm in green, and (C) pores in red done in the pixel classification workflow of Ilastik. (D-E) Object classification of the biofilm using the object classification workflow in Ilastik. In (E), the different biofilms are presented in different colors.

Using the information from segmentation, biofilm surface fraction S_b was calculated from the ratio between the surface occupied by biofilms and that of the microchannel (Figure 25A). Biofilm mean fluorescence intensity I_b normalized by its maximum value is shown in Figure 25B. Finally, the location of the maximum amount of biofilm x_b normalized by the microchannel length is shown in Figure 25C, with 0: inlet and 1: outlet.

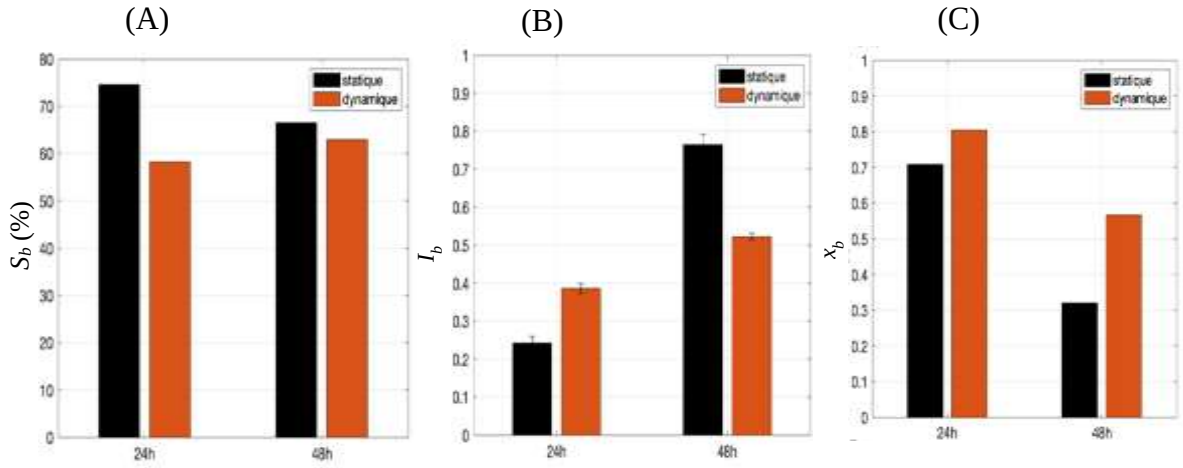

Figure 25: Histograms of biofilm properties according to time growth and mechanical stimuli. (A) Biofilm surface fraction S_b; (B) Normalized fluorescence intensity I_b; (C) Normalized location of maximum amount of biofilm x_b (0: inlet, 1: outlet)

For further quantitative analysis, the coupling between biofilm size (in pixel^2) and fluorescence intensity was studied and is summarized in Figure 26. It concerned both 24h and 48h growth and the number *n* of measured objects which corresponded to one bacterial microcolony inside the microchannels.

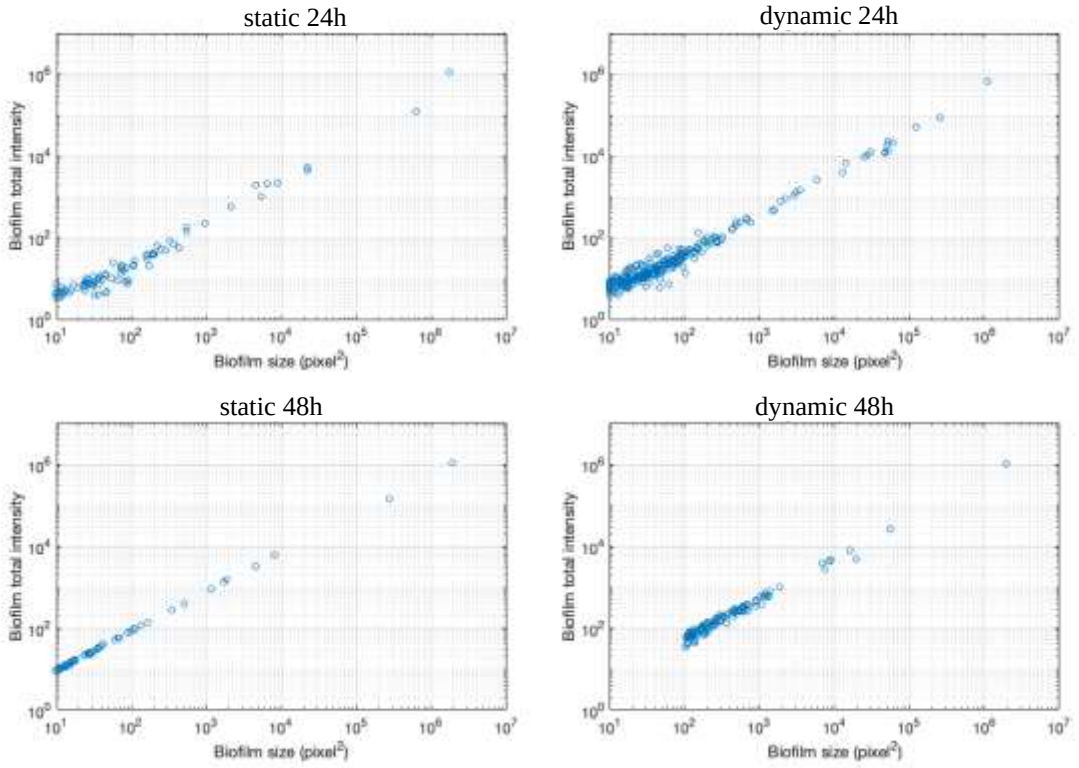

Figure 26: Total fluorescence intensity of each biofilm as a function of the biofilm size for each condition. The number of biofilms classified by Ilastik is:
- for the static condition: N=29 at 24h, and N=14 at 48h;
- for the dynamic condition: N=63 at 24h and N=107 at 48h.

4. Discussion and conclusion

This discussion focuses on three main topics: biofilm formation and location, biofilm size and fluorescence intensity, and interactions between biofilm formation and local mechanical stimuli.

As a preliminary remark, it could be noticed that in our experiments, there was a fairly direct link between bacterial numbers and biofilm formation since there were virtually no more isolated bacteria after 24h culture.

From a mechanical point of view, the dynamic assays compared favorably with what happens *in vivo* in numerous points. As already discussed in chapter II, the cycling frequency of the mechanical device was set to 1 Hz to be close to that of the walking gait, and the device was loaded at its maximum displacement magnitude to induce the most unfavorable conditions in terms of strain and stress in the vicinity of microfluidic device. However, it is possible that a 2-mm displacement does effectively occur in the case of implant failure or in comminutive fractures for which the different bone fragments are mobile relative to each other. Even though flow is more likely to be turbulent and multidirectional *in vivo*, we chose to study biofilm development under a laminar and unidirectional flow given the possibility of biofilm development under these conditions, as proven by our research group.

Biofilm formation and location

In **Experiment 1**, darker zones were visualized in bright field microscopy and further confirmed by bright green fluorescence mainly in ROIs $R_3R_4R_5$ of the static control microchannel, as depicted in Figure 19B and Figure 19C. Conversely, significant biofilm formation was not observed for the dynamic condition, since isolated bacteria were found in all regions of interest as shown in Figure 20B and Figure 20C. This could suggest that biofilm detachment might have occurred consequently to mechanical loading. In **Experiment 2**, brighter green regions were found in all imaged microchannels as shown in Figure 22A and Figure 23A. This demonstrated that biofilms were able to form with our experimental setup, whether the bacterial culture was tested in static or in dynamic conditions.

However, culture duration seemed to influence the distribution of green fluorescence along the microchannel. Indeed, brighter signals were visualized near the microchannel outlet after 24h growth for both the static and the dynamic conditions as shown in Figure 22A. After 48h growth, a fluorescence gradient in the longitudinal direction, i.e. the channel *x*-axis, spread from the microchannel inlet up to its mid-length in the static condition, whereas more constant profiles were found in the dynamic condition as shown in Figure 23A. The warm color distribution patterns along the *x*-axis confirmed this result, as shown in Figure 22B and Figure 23B.

In addition, the number of biofilms formed was influenced by mechanical stimuli, i.e. static or dynamic conditions. Under static condition, biofilms concentrated near the outlet at 24h ($x_b \approx 0.7$) and near the inlet at 48h growth ($x_b \approx 0.3$), as shown in Figure 25C. Under dynamic conditions, more biofilms formed near the outlet ($x_b \approx 0.8$) at 24h, but the initial outlet concentration site migrated towards the middle of the channel at 48h ($x_b \approx 0.55$).

No significant gradient of biofilm distribution was found in the transverse direction of the microchannel, i.e. the *y*-axis, as shown in Figure 22B and Figure 23B. However, a more intense

fluorescence was visualized on the walls of the channel, particularly in its mid-length zone at 48h growth.

Biofilms concentration at the microchannel outlet in both static and dynamic conditions at 24h coincided with the site of bacteria inoculation, that is through the chip outlet punch. Bacteria adhered to the first surface they met, i.e. the local outlet walls, and then found favorable conditions to proliferate and form biofilm. During the next 24h and under no mechanical stress, biofilms formed according to nutrient gradients, which explains their concentration at the microchannel inlet at 48h. Bacterial detachment followed by adhesion and biofilm formation can therefore explain the observed growth pattern for the static condition.

Mechanical cyclic loading induced more evenly distributed biofilm formation along the microchannel, especially after 48h growth. Biofilm migration from the outlet to the inlet was still present. However, dynamic excitation might have prevented subsequent bacterial adhesion and biofilm development at the channel inlet.

Biofilm size and fluorescence intensity

At 24h growth, biofilms occupied a greater surface in the static microchannel than in the dynamic microchannel, as shown by the surface fraction plotted Figure 25A. Thus, the static condition was more amenable to biofilm formation than the dynamic condition. However, convergence appeared with time since similar surface fractions were found at 48h growth (Figure 25A).

Analysis of mean green fluorescence intensity provided useful information. Indeed, two biofilms occupying the same surface area may not fluoresce with the same intensity, as they may not contain the same number of bacteria expressing the GFP. **Experiment 1** showed an intensity loss at 40h between the static and the dynamic conditions (Figure 19C and Figure 20C). This was confirmed by the difference in the normalized fluorescence intensity between each ROI, as this criterion depicted fluorescence of biological components only. In Figure 21, a significant difference between biofilm fluorescence and isolate bacteria fluorescence was observed.

Experiment 2 confirmed this trend. Indeed, when quantifying mean green fluorescence intensity normalized by maximum fluorescence intensity, fluorescence was less intense in the static than in the dynamic channels at 24h, but the opposite result was found at 48h growth as shown in Figure 25B.

Most importantly, biofilm surface fraction decreased between 24h and 48h growth in the static microchannels, while normalized biofilm fluorescence intensity more than tripled between these two time points, as illustrated by Figure 25A-B. Under static condition, biofilms formed were small with limited green fluorescence, whereas they remained small but brighter green at 48h as shown in Figure 26. Under dynamic conditions, normalized biofilm fluorescence was globally identical between 24h and 48h as shown in Figure 25B. This corroborated the results of Figure 26. Indeed, biofilms mean fluorescence intensity in dynamic conditions stayed identical, but their size increased.

Finally, mechanical cyclic stimuli might therefore have an impact on biofilm composition over time. Biofilms developing under dynamic condition seemed to increase in size but to lose

fluorescence intensity compared to biofilms developing in static condition. We could suggest that mechanical strain and stress might inhibit bacterial concentration within the biofilm and stimulate extracellular matrix production, which could be translated by loss of fluorescence intensity and increase in biofilm size, respectively.

Biofilm formation and mechanical stimuli

In our work, the mechanical stimuli induced to the bacterial population and the biofilm formed within the microfluidic device could be considered as the superimposition of two different stimulus: one resulting from fluid flow ("fluid stress") and the other resulting from stretching generated by the mechanical device ("solid stress"). Assuming a homogeneous growth of biofilm on the microchannel parietal surfaces, an evaluation at the first order of parietal shear stress can be established by using an analytical solution of laminar flow into a quadrangular cross-section (Shah and London 1978; Delplace 2018; Benbelkacem 2024; Bruus 1997).

For the two flow rates q used in our experimental sessions, i.e. q = 0.2 µL/min and q = 20 µL/min, the Reynolds number varies from a very low value of 0.03 (Stokes flow) to a low value of 33 (laminar flow). Shear stress σ_{xz} due to fluid flow had a minimal value of 2×10^{-3} Pa for the lowest flow rate, and reached 0.2×10^{3} Pa for the maximum flow rate with 90% of the microchannel sealed by biofilm. Details are given in Appendix E.

Prediction of the microfluidic device mechanical response has been detailed in section 5 of chapter II. At the first order, the mean normal strain ε_{xx} was almost identical on each parietal zone of the microchannel and equal to 24×10^{-4}. The unidirectional stress-strain relationship, namely $\sigma_{xx} = E_i \cdot \varepsilon_{xx}$ with E_i being the elastic modulus of the PETG coverslip or the PDMS chip, gave normal stress σ_{xx} at the bottom wall *C*, the upper wall B and the lateral wall *A* of the microchannel. Results were 5×10^{6} Pa, 2.4×10^{3} Pa and 2.6×10^{3} Pa, respectively.

The mean shear strain ε_{xz} was more site-dependent. Results for the bottom wall, the upper wall and the lateral wall were 1.3×10^{-4}, 1.2×10^{-3}, 9.4×10^{-3}, respectively. The unidirectional stress-strain relationship, namely $\sigma_{xz} = G_i \cdot \varepsilon_{xx}$ with shear modulus $G_i = E_i/2(1+\nu_i)$ and Poisson ratio ν_i, gave shear stresses of 0.1×10^{-3} Pa, 0.4×10^{3} Pa and 3.3×10^{3} Pa, respectively.

These main results are summarized in Figure 27.

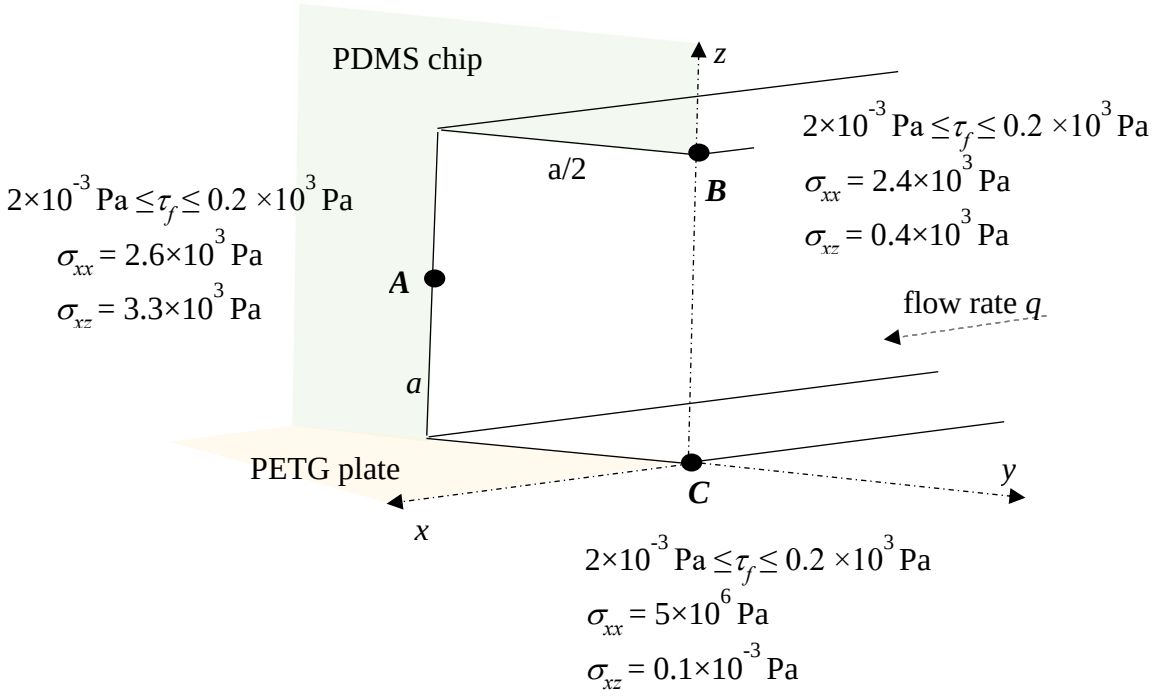

Figure 27: Mean fluid and solid stress expressed in local reference frames of the microchannel walls, i.e. bottom wall *C*, upper wall *B* and lateral wall *A*. Fluid shear stress, solid shear stress and solid normal stress are τ_f, σ_{xz} and σ_{xx}, respectively.

When a comparative study of stress magnitude was carried out, it appeared that at the bottom wall *C*, the solid normal stress, i.e. the one on the PETG coverslip, was predominant, and that the solid shear stress was much lower than the fluid shear stress. Concerning the lateral wall *A*, the solid normal stress was no longer predominant given the increased solid shear stress, and both components were an order of magnitude greater at least than fluid shear stress. For the upper wall *B*, the solid shear stress and the fluid shear stress tended towards the same value, particularly at 90% biofilm growth. The solid normal stress remained higher. The mechanical properties of the growing biofilm layers were not taken into account in this preliminary study. Indeed, it was assumed that very low mechanical properties, namely about 100 Pa for shear modulus (Benbelkacem 2024), did not modify strain energy distribution in the channel cross-section at the first order.

Could channel walls show strain fields and stress fields capable of influencing bacteria population responses? Our preliminary experimental results completed by fluid and solid predictive mechanical models showed that a combination of fluid and solid stimuli have to be examined to explore the mechanobiological response of the bacterial population.

Our combined methodology was corroborated by recent studies showing that the bacterial micro-environment is susceptible to be influenced by their surface attachment and substrate strain. Indeed, recent advances in high-resolution imaging techniques and bacterial studies have shed light on bacteria and biofilm mechanobiology (Jara et al. 2020; Araújo et al. 2019; Chawla et al. 2020; Xu et al. 2022). These studies have shown that bacteria sense mechanical stimuli through different receptors and effectors, which enable them to adapt, deform, and attach to or detach from a surface. Some mechanical stimuli may even support biofilm

development as a defense strategy in a hostile environment (Bottagisio et al. 2020). As the biofilm grows and matures, bacteria are embedded in the self-produced extracellular matrix which composition can change in response to mechanical forces, significantly impacting the overall stability of biofilms. These mechanobiological interactions thus occur at different scales: bacteria, biofilm and substrate.

Limitations

Our study involved several limitations, especially regarding our experimental methodology and the theoretical modeling.

Concerning the experimental procedures, our study has to be considered as a preliminary study given the reduced number of included samples. Numerous microchips were inoculated and tested, but several microfluidic devices leaked after starting our experiments, either when tested in static condition or in dynamic condition. The initial bacterial density inoculated into the microchip could have promoted these leaks. Indeed, the more the bacteria initially inoculated, the more numerous and the quicker biofilms would form, thus leading to a sudden increase of pressure inside the microchannel, resulting in increased stress on the microchip-coverslip bond. Therefore, the optical density of the bacterial culture inoculated was divided by five between our two main experimental studies, namely Experiment 1 and Experiment 2. The fluid flow rate was also reduced by two orders of magnitude, as it was observed in a companion study that the lag phase and the exponential growth phase of biofilm development were respectively longer and shorter with such a modified flow rate (Benbelkacem 2024). We considered that obtaining results for only one chip tested in static condition was enough in Experiment 1, as our results compared favorably with those of the research group working exclusively in static conditions.

The second depicted limitation regarding our experimental methodology was the control over the environmental parameters, especially temperature and humidity levels. It should be noted that leakage was mainly observed between the tenth and the twenty-fourth hour of growth. Although the temperature remained almost unchanged between Experiment 1 and Experiment 2, humidity levels doubled between these two sets. This probably had an impact on the robustness of bonding between the microchip and the bending plate, as discussed in Chapter II. This limitation could have been overcome by carrying out experiments in a thermally and hydrometrically regulated room, but this costly facility was not available for our study. Furthermore, our experiments were conducted at room temperature (25-26°C), which is much lower than body temperature (37°C). This could have impacted bacterial growth and biofilm development relatively as to what happens *in vivo*. Working at 37°C would have necessitated the use of temperature-controlled chambers. However, we chose not to use these chambers and to stay at room temperature in order to compare our dynamic results with the static results obtained by colleagues of our research group.

It should also be noticed that bending of the coverslip induced a non-uniform loading, which was more important at the middle of the coverslip, and which could have impacted our results. Furthermore, the vertical and horizontal displacements induced by the mechanical device to the flexible coverslip could have induced coverslip distortion, and thus local heating at the level of the microfluidic device. Measurement of this change in local temperature could be interesting, as it has been shown in a companion study that the rate of biofilm growth was very temperature-dependent, with different thresholds identified.

The results of our project are valid for the bacterial strain tested, namely *Pseudomonas aeruginosa* strain ATCC 15692 GFP. We chose this species because of its capability to form biofilms in static conditions, which was described in the literature and implemented by our research group in previous and companion studies. This choice gave static controls and limited failing risks for our dynamic study. Observing results, it seems that our protocol and facilities

can be used for other bacterial strain in future studies. However, bacteria can lose their fluorescence when subjected to stress such as hypoxia, nutrient lack and possibly mechanical stress but the role of stress on fluorescence response is still an open question.

Finally, the results were obtained for a single cycle frequency with significant magnitude and steady state laminar fluid flow. Reproducing a physiological cycle such as walking, and forcing dynamic responses as opposed to static control guided these choices. Regardless of the conditions, bacterial cells arrangement within a biofilm influences their mode of interaction and communication, and impacts therefore *quorum sensing* and biofilm growth (Dufrêne and Persat 2020). Shear fluid flow might affect biofilm composition from initial planktonic inoculum to thicker and denser biofilm. Mechanical forces can affect transport of signaling molecules and nutrients, and are likely to deform or damage the matrix, thus promoting adhesion or dispersion.

Concerning the upstream design of our methodology, we implemented kinematic, structural and microfluidic modeling which showed that our experimental device was versatile enough to explore more complex kinematic and fluid loading cycles in terms of duration and magnitude patterns.

Even if the kinematic approach was complete, a theoretical exploration of both solid and fluid stimuli was proposed at the first order. Regarding the predictive response of the coverslip and the microchip, only the maximum response in lateral bending was envisaged with no mass effects nor dissipative energy, even if a non-linear algorithm was implemented. The lateral acceleration imposed upon structural and fluid components was obtained from equation (4b) as detailed in Appendix A and maximum magnitude was 1.6×10^{-2} g. This very low level of acceleration, combined with very slow flow, rules out the impact of solid-fluid dynamic effects. Nevertheless, exploring time-dependent parameters of the microfluidic device substrate and biofilm could give access to time dephasing of the mechanical stimulus. Indeed, a time shift between solid and fluid strains and stresses could impact the mechanobiological response. This latter aspect could support improved modeling of biofilm growth and associated mechanical properties to predict the inhomogeneous distributions and detachments observed experimentally.

In this chapter, our preliminary results have shown that dynamic mechanical stimuli can influence biofilm development.

It appeared that cyclic mechanical stimuli induced a shift in the location where biofilms formed over time. Indeed, after twenty-four hours, biofilms mainly formed near the microchannel outlets where bacterial inoculation within the microchannel was performed, whether in static or dynamic conditions. However, at forty-eight hours, growth profiles diverged: static conditions led to biofilm development near the fluid inlet whereas dynamic conditions provoked more randomly distributed patterns of biofilm formation along the microchannel length.

Not only did cyclic mechanical stimuli play a role on the localization of biofilm growth, but they also had an impact on biofilm size and fluorescence intensity. Biofilms formed under static conditions showed tripled fluorescence intensity between twenty-four and forty-eight hours, while their size stayed quite similar. An opposite effect was observed for biofilms developing in microchannels under dynamic conditions. Indeed, mean biofilm fluorescence intensity remained unchanged between twenty-four hours and forty-eight hours while biofilm size increased. These preliminary results suggested that cyclic loading could modify biofilm structure notably by reducing bacterial concentration.

General conclusion and perspectives

Bacterial biofilms are a major problem in orthopedic surgery, and complicate the eradication of postoperative infections. They are associated with consequent functional outcomes, revision surgery and prolonged hospital stays. Even though antibiotics are commonly administered as first-line treatment after diagnosis of postoperative orthopedic SSI, their sole use is inefficient in the struggle against biofilms. Moreover, massive use of antibiotics has led to the emergence of numerous multidrug-resistant organisms, which compromise treatment efficiency.

Alternatives to conventional antibiotic therapy are progressively taking shape. Empirical approaches when treating biofilm-associated SSIs can be reduced by understanding the underlying mechanisms involved in biofilm development. In this context, the role of mechanical stimulus in biofilm growth seems clinically relevant, since a healing bone tissue is continuously subjected to mechanical loads. Normal strain and stress due to bending but also tangential strain and stress due to torsion and shear play a significant role at the bone-implant interface in fracture healing secondary to plate osteosynthesis. It is also observed that time-varying loading profiles condition biological responses. In addition, many aspects of biofilm formation are governed by mechanical factors (Blondel et al. 2024).

The central hypothesis of our research was that cyclic strain and stress might influence bacterial responses and biofilm formation. We designed a dedicated methodology mainly based upon an experimental approach to evaluate the reliability of this hypothesis within a microfluidic device, the static response being used as control. Biofilm development of *Pseudomonas aeruginosa* strain ATCC 15692 GFP was studied in this work.

In the first bibliographic chapter, the clinical aspects of surgical site infection in bone tissue were presented in both animals and humans, and bacterial biofilm formation mechanisms were described. The multiscale aspect of biofilm mechanobiology was then discussed from the bacterial microscopic scale to the biofilm mesoscopic scale up to the fracture or implant macroscopic scale (Blondel et al. 2024). Ultimately, clinical research strategies in complement or alternative to antibiotics were presented. This first chapter underlined the fact that the impact of mechanical stimuli upon biofilm formation was still poorly documented whereas these play significant roles clinically, notably in fracture healing.

The second chapter was devoted to describing the experimental methodology conceived to explore how mechanical stimuli could impact biofilm growth, and to provide details regarding the associated devices. A single microchannel was embedded within a PDMS microchip, which was then bonded to a flexible PETG coverslip. The microfluidic device formed was then loaded in lateral flexion. An imposed displacement and frequency control system was designed and the microfluidic device conceived enabled bacterial biofilm growth while being mechanically loaded. Specific challenges had to be overcome, particularly regarding bonding of the microchip to the PETG coverslip under cyclic mechanical loading. Modeling of the mechanical behavior of the microfluidic device with preliminary considerations for both structural and stokes fluid flow responses has been proposed. Finally, we have suggested a rather versatile experimental setup to study biofilm dynamic response under different kinematical and fluidic conditions.

Chapter three was dedicated to the application of the previously exposed methodology and experimental device to explore biofilm development under cyclic loading. Three issues were examined, namely, biofilm formation and location, biofilm size and fluorescence intensity and biofilm formation and mechanical stimuli. The main result was that cyclic mechanical stimuli induced a shift in biofilm growth over time compared to static conditions. It appeared that

dynamic conditions provoked more random patterns in the distribution of biofilm location formation. Biofilms formed under dynamic conditions also increased in size over time, while fluorescence intensity was only weakly modified. These observations suggested that cyclic loading could modify biofilm structure notably by reducing bacterial concentration. Finally, these preliminary results tended to validate our underlying hypothesis based upon a differentiated mechanobiological response of biofilm under dynamic stimuli.

To go further, it will be important to validate the reliability of the results found in our study. Indeed, our research brought bricks to explore the mechanobiological response of biofilms and suggested an experimental workbench to do so, but this merits consolidation. In addition, we proposed preliminary models to investigate the interrelations between mechanical stimuli, either structural or induced by fluid flow, and biofilm evolution but scenarios of intrinsic mechanisms have not yet been proposed. As a consequence, two complementary perspectives might be suggested.

The first track would be to consolidate our experimental data by applying variable spatio-temporal mechanical stimuli to depict response thresholds, types and patterns of biofilm development. Versatility of the proposed experimental set-up allows this point to be reached.

Our methodology concerned a specific strain of *Pseudomonas aeruginosa*, which is not the most commonly incriminated bacterium in postoperative orthopedic infection. Inoculation with other bacterial strain such as *Staphylococcus aureus* could be envisaged in presence or not of targeted antibiotics. In fact, the developed microfluidic device and experimental setup could allow spatio-temporal control of antibiotics delivery, and the impact of cyclic mechanical loading on the action of antibiotics could be quantified. By mimicking *in vivo* situation, the use of our experimental setup with monitored mechanobiological factors could help reducing some therapeutical empirical aspects.

Modeling of the theoretical and numerical mechanobiological response is the second perspective track. This would allow multiscale events inaccessible experimentally to be explored, and beyond, to propose fundamental laws governing biofilm development. A generic framework could be reactive transport in deformable porous media.

Appendix A: Kinematical equations governing the motion of the mechanical device

Reference frame of the base was set at (O_0, x_0, y_0, z_0). A rotating shaft **1**, associated with reference frame (O_1, x_1, y_1, z_1), was connected with a pivot joint at O_0; its rotation was described by $\theta_1(t)$. A cam disk **2**, associated with reference frame (O_2, x_2, y_2, z_2), was connected to rotating shaft **1** with a pivot joint at O_1; its position relative to rotating shaft **1** was set by adjusting θ_2. A rolling ring **3** centered on O_2 established a linear contact with a flexible coverslip **4** supporting the microchips at point M_3.

Location of M_3 is described in the reference frame R_0 (O_0, x_0, y_0, z_0) as follows:

$$\overrightarrow{O_0M_3} = \overrightarrow{O_0O_1} + \overrightarrow{O_1O_2} + \overrightarrow{O_2M_3} = \begin{pmatrix} x_{M_3} \\ y_{M_3} \\ 0 \end{pmatrix}_{R0} = \begin{pmatrix} e \\ 0 \\ 0 \end{pmatrix}_{R1} + \begin{pmatrix} e \\ 0 \\ 0 \end{pmatrix}_{R2} + \begin{pmatrix} r_3 \\ 0 \\ 0 \end{pmatrix}_{R3} = \begin{pmatrix} e[cos\,\theta_1 + cos(\theta_1 + \theta_2)] + r_3\,cos(\theta_1 + \theta_2 + \theta_3) \\ e[sin\,\theta_1 + sin(\theta_1 + \theta_2)] + r_3\,sin(\theta_1 + \theta_2 + \theta_3) \\ 0 \end{pmatrix}_{R0} \quad (1)$$

With a property that fixes x_3 vertical during motion, equation (1) is simplified into relations (2a) and (2b) with $\theta_3 = \frac{\pi}{2} - (\theta_1 + \theta_2)$.

$$x_{M_3} = e[cos\,\theta_1 + cos(\theta_1 + \theta_2)] \quad (2a)$$

$$y_{M_3} = r_3 + e[sin\,\theta_1 + sin(\theta_1 + \theta_2)] \quad (2b)$$

Derivatives with respect to time give M_3 kinematic as follows. Velocity components are expressed by equations (3a) and (3b) while acceleration components are given by equations (4a) and (4b).

$$\dot{x}_{M_3} = -e\dot{\theta}_1[sin\,\theta_1 + sin(\theta_1 + \theta_2)] \quad (3a)$$

$$\dot{y}_{M_3} = e\dot{\theta}_1[cos\,\theta_1 + cos(\theta_1 + \theta_2)] \quad (3b)$$

$$\ddot{x}_{M_3} = -e\ddot{\theta}_1[sin\,\theta_1 + sin(\theta_1 + \theta_2)] - e\dot{\theta}_1{}^2[cos\,\theta_1 + cos(\theta_1 + \theta_2)] \quad (4a)$$

$$\ddot{y}_{M_3} = e\ddot{\theta}_1[cos\,\theta_1 + cos(\theta_1 + \theta_2)] - e\dot{\theta}_1{}^2[sin\,\theta_1 + sin(\theta_1 + \theta_2)] \quad (4b)$$

Additionally, the angular velocity of ring **3** is expressed by the following equation (5), and is opposite to shaft rotation. It shows that the rolling elements associated with cam disk **2** permit a particular contact condition without sliding on flexible plate **4**.

$$\overrightarrow{\Omega_3^2} = \overrightarrow{\Omega_3^0} + \overrightarrow{\Omega_0^1} + \overrightarrow{\Omega_1^2} = -\overrightarrow{\Omega_0^1} = -\dot{\theta}_1 \cdot \vec{z}_0 \quad (5)$$

Finally, the kinematic problem is fully determined since equation (3) gives the motion of ring **3**. Motions of rotating shaft **1** and cam disk **2** are straightforwardly obtained as follows:

$$\overrightarrow{V_1^0}O_1 = 0 \text{ and } \overrightarrow{\Omega_1^0} = \dot{\theta}_1 \cdot \vec{z}_0 \quad (6)$$

$$\overrightarrow{V_2^0}O_2 = -e\dot{\theta}_1[sin\,\theta_1 + sin(\theta_1 + \theta_2)]\vec{x}_0 + e\dot{\theta}_1[cos\,\theta_1 + cos(\theta_1 + \theta_2)]\vec{y}_0 \text{and } \overrightarrow{\Omega_2^0} = \overrightarrow{\Omega_2^1} + \overrightarrow{\Omega_1^0} = \dot{\theta}_1 \cdot \vec{z}_0 \quad (7)$$

Appendix B: Details on mounting of the different electromechanical components

The different electromechanical components of the mechanical device are shown in Figure 28. The actuator was an electric motor (12V DC, 200 rpm rated speed, 1:34 reduction ratio, 12 pulses encoder) piloted by a speed controller associated with an extension board (Arduino Nano®). Temperature and humidity sensors (AHT20) were associated to the device. Rotation frequency (0-2.5 Hz), temperature and humidity level were shown on a window display (ssd1306 0.96" I2c oled).

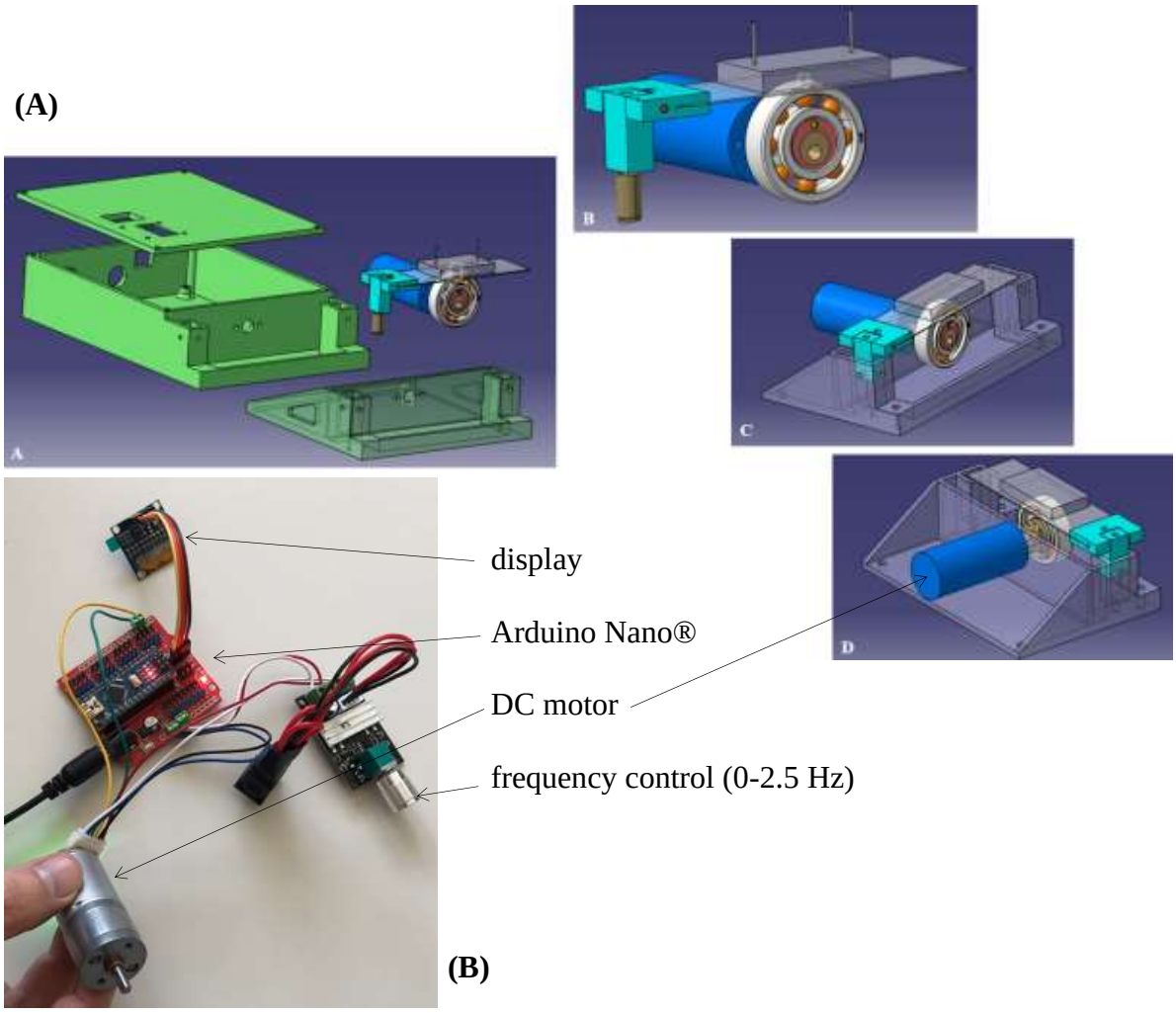

Figure 28: Technological design of the mechanical device: (A) Housing description and electromechanical components mountings; (B) Electromechanical device involving an Arduino® controller, sensors and a frequency control knob (0-2.5 Hz)

Appendix C: Bonding techniques

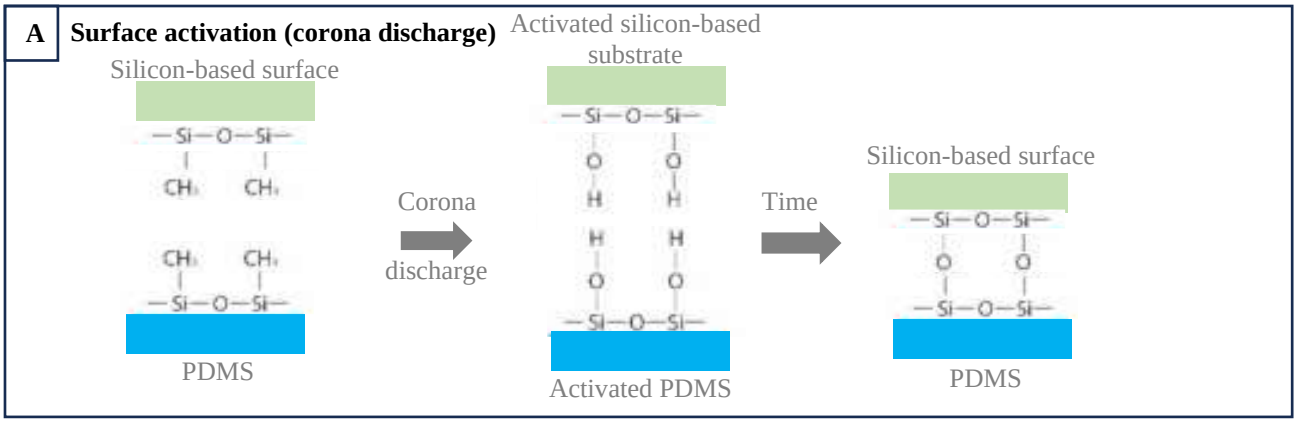

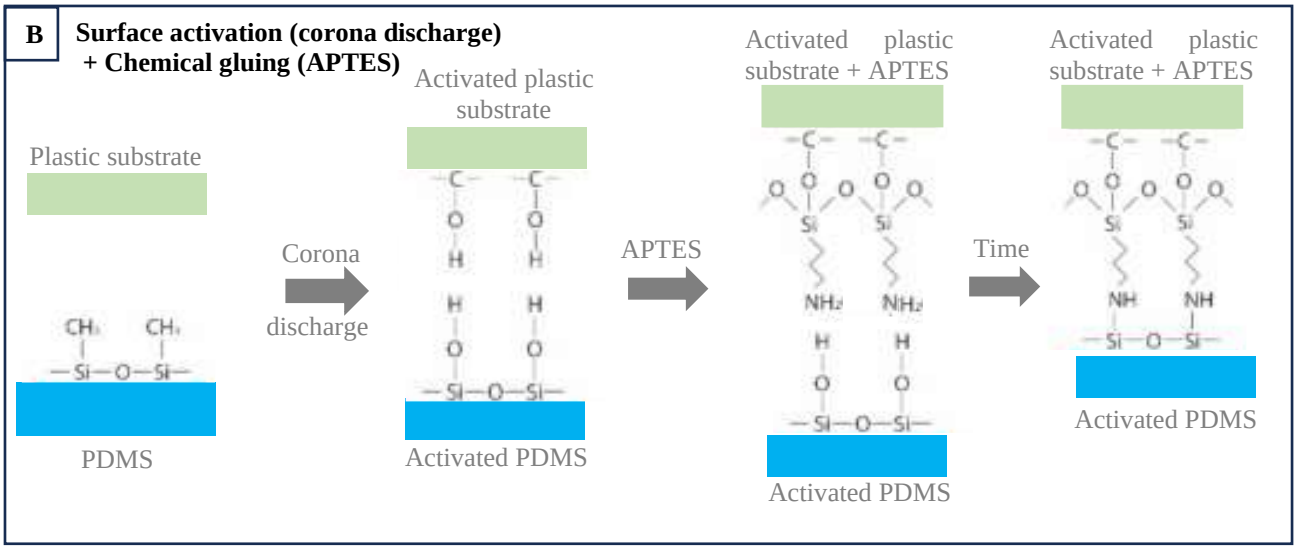

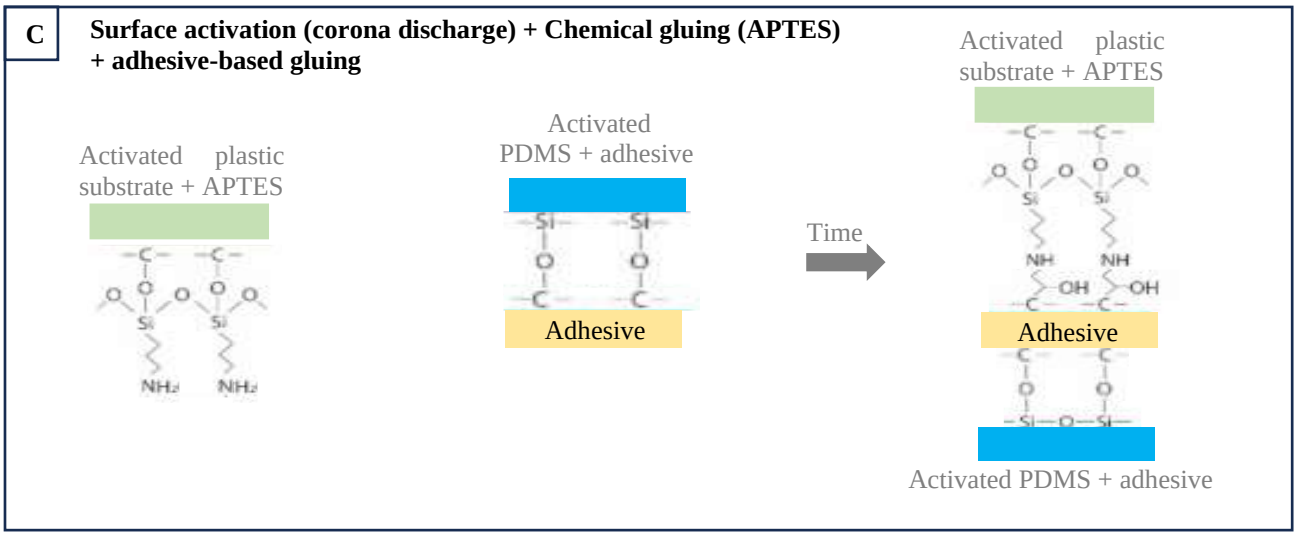

Appendix D: Permeability testing of the microfluidic device

Part A: If the manual peeling test was positive, each microfluidic device was tested for microchannel permeability and leakage. This was performed by injecting deionized water through the inlet or the outlet punch of the microchip using a syringe connected to a flexible plastic tubing (Tygon®) of internal diameter 0.5 mm thanks to the connection system presented Figure 29. If the water injected through the inlet/outlet exited through the outlet/inlet and if no leaks were noted between the chip and the coverslip, the microchannel was considered permeable and the PDMS chip-PETG coverslip bonding effective.

Figure 29: Connection system:18G blunt-end Luer lock syringe needle (Darwin fz13) connected to a "Novosil" silicone tube of internal diameter 1 mm (Fisher Scientific®). This system allowed connecting a syringe to a flexible plastic tubing (Tygon®) of internal diameter 0.5 mm, which fitted perfectly inside the inlet/outlet punch

Part B: Finally, to confirm the leakproof nature of the bonded microfluidic device over time and when submitted to a mechanical stimulus, a fluid flow was applied inside two microfluidic devices over 3 days. A 60 mL syringe was filled with deionized water, and connected to a 30cm long flexible plastic tubing (Tygon®) of internal diameter 0.5 mm using the connection system of Figure 29. Water was injected to fill the plastic tube, prior to gently inserting the other end of it into the inlet punch of the PDMS chip. The tip of another 30 cm long flexible plastic tubing (Tygon®) was similarly inserted into the outlet punch of the chip, while the other end was placed in a waste reservoir. The 60 mL syringe was placed into a Harvard® PHD 2000 syringe pump to inject deionized water throughout the circuit at a controlled rate of 10µL/min. One microfluidic device was placed on a flat surface (static condition). The other was fixed with screws into the pivot joints of the mechanical device conceived (dynamic condition). Rotational speed was set to 1 Hz, and vertical displacement of the coverslip was maximum.

Appendix E: Some considerations about microfluidic flow

With laminar flow, the adimensioned Reynolds number is defined by equation (A1) (Shah and London 1978; Delplace 2018). The shear stress on the liquid/solid surface of the microchannel is expressed by equation (A2) (Benbelkacem 2024; Bruus 1997).

$$Re = k\frac{\rho}{\mu}C \cdot q \tag{A1}$$

$$\tau = \frac{a\Delta p}{4L} = \frac{A}{4}\frac{\mu q}{a^3} \tag{A2}$$

with ρ, μ : fluid density and dynamic viscosity

L, Δp, q: channel length, inlet-outlet differential pressure and fluid flow rate

For a square cross-section $a \times a$, involved parameters are expressed as follows:

$A = \frac{12}{1-\sum_{n,odd}^{\infty}\frac{1}{n^5}\frac{192}{x^5}tanh\left(\frac{n\pi}{2}\right)} \approx 2.51$ with $n = 1,3$ $k = 1/2$ and $C = 2/a$

Assuming a homogeneous growth of biofilm on a microchannel parietal surface, we obtained an evaluation at the first order of parietal shear stress for two flow rates q used in our experimental sessions, i.e. q = 0.2 µl/min and q = 20 µl/min. Results were as follows:

$\tau = 2$ mPa $-$ 210 mPa at initial state, i.e. without biofilm

$\tau = 2$ Pa $-$ 210 Pa with 90 % microchannel sealed by biofilm

Reynolds number varied from very low value of 0.03 (Stokes flow) to low value of 33 (laminar flow).

The lateral acceleration of PETG bending coverslip and PDMS chip is expressed by equation (4b) in Appendix A as follows:

$$\ddot{y}_{M_3} = e\ddot{\theta}_1[cos\,\theta_1 + cos(\theta_1 + \theta_2)] - e\dot{\theta}_1{}^2[sin\,\theta_1 + sin(\theta_1 + \theta_2)] \tag{A3}$$

In steady state motion at 1 Hz, we have $\ddot{\theta}_1 = 0, \dot{\theta}_1 = 2\pi f_1$ with $f_1 = 1$Hz. For $\theta_2 = 0$ the maximum lateral acceleration is expressed by equation (A4).

$$\left|\ddot{y}_{M_3}\right| = 8e\pi^2\,sin\,\theta_1 \tag{A4}$$

In our experiment, e was fixed to 2 mm, thus acceleration peak was obtained for $\theta_1 = \pi/2$ and equal to ~ 0.16 m/s^2 ~ 1.6×10^{-2} g.

References

Acemel, Rafael D., Fernando Govantes, and Alejandro Cuetos. 2018. ‘Computer Simulation Study of Early Bacterial Biofilm Development’. *Scientific Reports* 8 (1): 5340.

Agostini, Matteo, Gina Greco, and Marco Cecchini. 2019. ‘Polydimethylsiloxane (PDMS) Irreversible Bonding to Untreated Plastics and Metals for Microfluidics Applications’. *APL Materials* 7 (8): 081108.

Ai, Hainan, Jingwei Xu, Wei Huang, Qiang He, Bingjie Ni, and Yinliang Wang. 2016. ‘Mechanism and Kinetics of Biofilm Growth Process Influenced by Shear Stress in Sewers’. *Water Science and Technology: A Journal of the International Association on Water Pollution Research* 73 (7): 1572–82.

Alam, A U, M M R Howlader, and M J Deen. 2014. ‘The Effects of Oxygen Plasma and Humidity on Surface Roughness, Water Contact Angle and Hardness of Silicon, Silicon Dioxide and Glass’. *Journal of Micromechanics and Microengineering* 24 (3): 035010.

Alqutaibi, Ahmed Yaseen, Abdulbari Aljohani, Abdullah Alduri, Abdulmajid Masoudi, Anas M. Alsaedi, Hesham Mohammed Al-Sharani, Ahmed E. Farghal, et al. 2023. ‘The Effectiveness of Cold Atmospheric Plasma (CAP) on Bacterial Reduction in Dental Implants: A Systematic Review’. *Biomolecules* 13 (10): 1528.

Anderson, Brett N., Albert M. Ding, Lina M. Nilsson, Kaoru Kusuma, Veronika Tchesnokova, Viola Vogel, Evgeni V. Sokurenko, and Wendy E. Thomas. 2007. ‘Weak Rolling Adhesion Enhances Bacterial Surface Colonization’. *Journal of Bacteriology* 189 (5): 1794–1802.

Araújo, Glauber R. de S., Nathan B. Viana, Fran Gómez, Bruno Pontes, and Susana Frases. 2019. ‘The Mechanical Properties of Microbial Surfaces and Biofilms’. *Cell Surface (Amsterdam, Netherlands)* 5 (December):100028.

Ariati, Ronaldo, Flaminio Sales, Andrews Souza, Rui A. Lima, and João Ribeiro. 2021. ‘Polydimethylsiloxane Composites Characterization and Its Applications: A Review’. *Polymers* 13 (23): 4258.

Asp, Merrill E., Minh-Tri Ho Thanh, Subarna Dutta, Jessica A. Comstock, Roy D. Welch, and Alison E. Patteson. 2023. ‘Mechanobiology as a Tool for Addressing the Genotype-to-Phenotype Problem in Microbiology’. *Biophysics Reviews* 4 (2): 021304.

Auer, George K., and Douglas B. Weibel. 2017. ‘Bacterial Cell Mechanics’. *Biochemistry* 56 (29): 3710–24.

Badia, J.M., A.L. Casey, N. Petrosillo, P.M. Hudson, S.A. Mitchell, and C. Crosby. 2017. ‘Impact of Surgical Site Infection on Healthcare Costs and Patient Outcomes: A Systematic Review in Six European Countries’. *Journal of Hospital Infection* 96 (1): 1–15.

Bahna, Paul, Tanya Dvorak, Hend Hanna, Alan W. Yasko, Ray Hachem, and Issam Raad. 2007. ‘Orthopaedic Metal Devices Coated with a Novel Antiseptic Dye for the Prevention of Bacterial Infections’. *International Journal of Antimicrobial Agents* 29 (5): 593–96.

Bano, Sara, Noor Hassan, Muhammad Rafiq, Farwa Hassan, Maliha Rehman, Naveed Iqbal, Hazrat Ali, Fariha Hasan, and Ying-Qian Kang. 2023. ‘Biofilms as Battlefield Armor for Bacteria against Antibiotics: Challenges and Combating Strategies’. *Microorganisms* 11 (10): 2595.

Bartek Jr., Jiri, Simon Skyrman, Michael Nekludov, Tiit Mathiesen, Folke Lind, and Gaston Schechtmann. 2018. 'Hyperbaric Oxygen Therapy as Adjuvant Treatment for Hardware-Related Infections in Neuromodulation'. *Stereotactic and Functional Neurosurgery* 96 (2): 100–107.

Benbelkacem, M. 2024. 'Couplings between Mass Transport, Growth and Flow-Induced Removal Control the Spatio-Temporal Dynamics of Pseudomonas Aeruginosa Biofilms in Microchannel Flows.' PhD Thesis, Toulouse: Toulouse University.

Berg, Stuart, Dominik Kutra, Thorben Kroeger, Christoph N. Straehle, Bernhard X. Kausler, Carsten Haubold, Martin Schiegg, et al. 2019. 'Ilastik: Interactive Machine Learning for (Bio)Image Analysis'. *Nature Methods* 16 (12): 1226–32.

Blondel, Margaux, Camille Machet, Britt Wildemann, Yara Abidine, and Pascal Swider. 2024. 'Mechanobiology of Bacterial Biofilms: Implications for Orthopedic Infection'. *Journal of Orthopaedic Research: Official Publication of the Orthopaedic Research Society*, March.

Borók, Alexandra, Kristóf Laboda, and Attila Bonyár. 2021. 'PDMS Bonding Technologies for Microfluidic Applications: A Review'. *Biosensors* 11 (8): 292.

Bottagisio, Marta, Pietro Barbacini, Alessandro Bidossi, Enrica Torretta, Elinor deLancey-Pulcini, Cecilia Gelfi, Garth A. James, Arianna B. Lovati, and Daniele Capitanio. 2020. 'Phenotypic Modulation of Biofilm Formation in a Staphylococcus Epidermidis Orthopedic Clinical Isolate Grown Under Different Mechanical Stimuli: Contribution From a Combined Proteomic Study'. *Frontiers in Microbiology* 11:565914.

Bowler, Philip, Christine Murphy, and Randall Wolcott. 2020. 'Biofilm Exacerbates Antibiotic Resistance: Is This a Current Oversight in Antimicrobial Stewardship?' *Antimicrobial Resistance and Infection Control* 9 (1): 162.

Bruni, Giancarlo N., R. Andrew Weekley, Benjamin J. T. Dodd, and Joel M. Kralj. 2017. 'Voltage-Gated Calcium Flux Mediates *Escherichia Coli* Mechanosensation'. *Proceedings of the National Academy of Sciences* 114 (35): 9445–50.

Bruus, Henrik. 1997. *Theoretical Microfluidics*. Oxford University PressOxford.

Burrows, Lori L. 2012. '*Pseudomonas Aeruginosa* Twitching Motility: Type IV Pili in Action'. *Annual Review of Microbiology* 66 (1): 493–520.

Calderwood, Michael S., Deverick J. Anderson, Dale W. Bratzler, E. Patchen Dellinger, Sylvia Garcia-Houchins, Lisa L. Maragakis, Ann-Christine Nyquist, et al. 2023. 'Strategies to Prevent Surgical Site Infections in Acute-Care Hospitals: 2022 Update'. *Infection Control & Hospital Epidemiology* 44 (5): 695–720.

Carmen, John C., Christopher M. Runyan, Rachel A. Robison, Jared L. Nelson, Benjamin L. Beckstead, William G. Pitt, and G. Bruce Schaalje. 2004. 'Ultrasonic-Enhanced Gentamicin Transport through Colony Biofilms of Pseudomonas Aeruginosa and Escherichia Coli'. *Journal of Infection and Chemotherapy* 10 (4): 193–99.

Chabria, Mamta, Samuel Hertig, Michael L. Smith, and Viola Vogel. 2010. 'Stretching Fibronectin Fibres Disrupts Binding of Bacterial Adhesins by Physically Destroying an Epitope'. *Nature Communications* 1 (1): 135.

Chang, Cheng, Xinbo Yu, Wennan Guo, Chaoyi Guo, Xiaokui Guo, Qingtian Li, and Yongzhang Zhu. 2022. 'Bacteriophage-Mediated Control of Biofilm: A Promising New Dawn for the Future'. *Frontiers in Microbiology* 13 (April):825828.

Chawla, Ravi, Rachit Gupta, Tanmay P. Lele, and Pushkar P. Lele. 2020. ‘A Skeptic’s Guide to Bacterial Mechanosensing’. *Journal of Molecular Biology* 432 (2): 523–33.

Cheung, Gordon Y. C., Justin S. Bae, and Michael Otto. 2021. ‘Pathogenicity and Virulence of Staphylococcus Aureus’. *Virulence* 12 (1): 547–69.

Chua, Poh-Hui, Koon-Gee Neoh, En-Tang Kang, and Wilson Wang. 2008. ‘Surface Functionalization of Titanium with Hyaluronic Acid/Chitosan Polyelectrolyte Multilayers and RGD for Promoting Osteoblast Functions and Inhibiting Bacterial Adhesion’. *Biomaterials* 29 (10): 1412–21.

Chung, Pooi Yin. 2023. ‘Immunotherapies for the Prevention and Treatment of *Staphylococcus Aureus* Infections: Updates and Challenges’. *Pathogens and Disease* 81 (January):ftad016.

Connaughton, Alexander, Abby Childs, Stefan Dylewski, and Vani J. Sabesan. 2014. ‘Biofilm Disrupting Technology for Orthopedic Implants: What’s on the Horizon?’ *Frontiers in Medicine* 1 (August):22.

Cordero, José, Luis Munuera, and Maria Dolores Folgueira. 1996. ‘Influence of Bacterial Strains on Bone Infection’. *Journal of Orthopaedic Research* 14 (4): 663–67.

Costerton, J. W., Philip S. Stewart, and E. P. Greenberg. 1999. ‘Bacterial Biofilms: A Common Cause of Persistent Infections’. *Science* 284 (5418): 1318–22.

Delplace, Franck. 2018. ‘Fluids Flow Stability in Ducts of Arbitrary Cross-Section’. *J Mod Appl Physics* 2 (2): 10–15.

Deprey, Julie, Margaux Blondel, Charles Saban, Michel Massenzio, Olivier Gauthier, Pierre Moissonnier, Eric Viguier, and Thibaut Cachon. 2022. ‘Mechanical Evaluation of a Novel Angle-Stable Interlocking Nail in a Gap Fracture Model’. *Veterinary Surgery: VS* 51 (8): 1247–56.

Depypere, Melissa, Jonathan Sliepen, Jolien Onsea, Yves Debaveye, Geertje A. M. Govaert, Frank F. A. IJpma, Werner Zimmerli, and Willem-Jan Metsemakers. 2022. ‘The Microbiological Etiology of Fracture-Related Infection’. *Frontiers in Cellular and Infection Microbiology* 12 (July):934485.

Dincer, Sadık, Fatima Masume Uslu, and Anil Delik. 2020. ‘Antibiotic Resistance in Biofilm’. In *Bacterial Biofilms*, edited by Sadik Dincer, Melis Sümengen Özdenefe, and Afet Arkut. IntechOpen.

Domingo-Calap, Pilar, and Jennifer Delgado-Martínez. 2018. ‘Bacteriophages: Protagonists of a Post-Antibiotic Era’. *Antibiotics* 7 (3): 66.

Drago, Lorenzo, Willemijn Boot, Kostantinos Dimas, Kostantinos Malizos, Gertrud M. Hänsch, Jos Stuyck, Debby Gawlitta, and Carlo L. Romanò. 2014. ‘Does Implant Coating With Antibacterial-Loaded Hydrogel Reduce Bacterial Colonization and Biofilm Formation in Vitro?’ *Clinical Orthopaedics & Related Research* 472 (11): 3311–23.

Dufrêne, Yves F., and Alexandre Persat. 2020. ‘Mechanomicrobiology: How Bacteria Sense and Respond to Forces’. *Nature Reviews Microbiology* 18 (4): 227–40.

Dumont, Sophie, and Manu Prakash. 2014. ‘Emergent Mechanics of Biological Structures’. *Molecular Biology of the Cell* 25 (22): 3461–65.

Fang, Christian, Tak-Man Wong, Tak-Wing Lau, Kelvin KW To, Samson SY Wong, and Frankie Leung. 2017a. 'Infection after Fracture Osteosynthesis – Part I: Pathogenesis, Diagnosis and Classification'. *Journal of Orthopaedic Surgery* 25 (1): 230949901769271.

Fang, Christian, Tak-Man Wong, Tak-Wing Lau, Kelvin Kw To, Samson Sy Wong, and Frankie Leung. 2017b. 'Infection after Fracture Osteosynthesis – Part I: Pathogenesis, Diagnosis and Classification'. *Journal of Orthopaedic Surgery* 25 (1): 230949901769271.

Ferreira, J. A., Paula De Oliveira, and Pascoal M. Silva. 2020. 'Computational Simulation of Bacterial Infections in Surgical Procedures: An Exploratory Study'. In *Differential and Difference Equations with Applications*, edited by Sandra Pinelas, John R. Graef, Stefan Hilger, Peter Kloeden, and Christos Schinas, 333:413–25. Springer Proceedings in Mathematics & Statistics. Cham: Springer International Publishing.

Filipović, Urška, Raja Gošnak Dahmane, Slaheddine Ghannouchi, Anamarija Zore, and Klemen Bohinc. 2020. 'Bacterial Adhesion on Orthopedic Implants'. *Advances in Colloid and Interface Science* 283 (September):102228.

Fonseca, A. P., and J. C. Sousa. 2007. 'Effect of Shear Stress on Growth, Adhesion and Biofilm Formation of Pseudomonas Aeruginosa with Antibiotic-Induced Morphological Changes'. *International Journal of Antimicrobial Agents* 30 (3): 236–41.

Foster, Andrew L., T. Fintan Moriarty, Charalampos Zalavras, Mario Morgenstern, Anjali Jaiprakash, Ross Crawford, Marc-Antoine Burch, et al. 2021. 'The Influence of Biomechanical Stability on Bone Healing and Fracture-Related Infection: The Legacy of Stephan Perren.' *Injury* 52 (1): 43–52.

Friedrich, B., and P. Klaue. 1977. 'Mechanical Stability and Post-Traumatic Osteitis: An Experimental Evaluation of the Relation between Infection of Bone and Internal Fixation'. *Injury* 9 (1): 23–29.

Funk, Shawn S., and Lawson A.B. Copley. 2017. 'Acute Hematogenous Osteomyelitis in Children'. *Orthopedic Clinics of North America* 48 (2): 199–208.

Gallardo-Moreno, Amparo M., Miguel A. Pacha-Olivenza, María-Coronada Fernández-Calderón, Ciro Pérez-Giraldo, José M. Bruque, and María-Luisa González-Martín. 2010. 'Bactericidal Behaviour of Ti6Al4V Surfaces after Exposure to UV-C Light'. *Biomaterials* 31 (19): 5159–68.

Getzlaf, Matthew A., Eric A. Lewallen, Hilal M. Kremers, Dakota L. Jones, Carolina A. Bonin, Amel Dudakovic, Roman Thaler, Robert C. Cohen, David G. Lewallen, and Andre J. Van Wijnen. 2016. 'Multi-disciplinary Antimicrobial Strategies for Improving Orthopaedic Implants to Prevent Prosthetic Joint Infections in Hip and Knee'. *Journal of Orthopaedic Research* 34 (2): 177–86.

Gieling, Fabian, Sarah Peters, Christoph Erichsen, R. Geoff Richards, Stephan Zeiter, and T. Fintan Moriarty. 2019. 'Bacterial Osteomyelitis in Veterinary Orthopaedics: Pathophysiology, Clinical Presentation and Advances in Treatment across Multiple Species'. *Veterinary Journal* 250 (August):44–54.

Giri, Kiran, and Chia-Wen Tsao. 2022. 'Recent Advances in Thermoplastic Microfluidic Bonding'. *Micromachines* 13 (3): 486.

Gitajn, Ida, Paul Werth, Robert V. O'Toole, Mandarin Joshi, David Jevsevar, Brent Wise, Ajinya Rane, et al. 2022. 'Microbial Interspecies Associations in Fracture-Related Infection'. *Journal of Orthopaedic Trauma* 36 (6): 309–16.

Gomez, Sofia, Lionel Bureau, Karin John, Elise-Noëlle Chêne, Delphine Débarre, and Sigolene Lecuyer. 2023. 'Substrate Stiffness Impacts Early Biofilm Formation by Modulating Pseudomonas Aeruginosa Twitching Motility'. *eLife* 12 (May):e81112.

González-Martín, Margarita, Vanessa Silva, Patricia Poeta, Juan Alberto Corbera, and María Teresa Tejedor-Junco. 2022. 'Microbiological Aspects of Osteomyelitis in Veterinary Medicine: Drawing Parallels to the Infection in Human Medicine'. *Veterinary Quarterly* 42 (1): 1–11.

Gopal, S., S. Majumder, A. G. Batchelor, S. L. Knight, P. De Boer, and R. M. Smith. 2000. 'Fix and Flap: The Radical Orthopaedic and Plastic Treatment of Severe Open Fractures of the Tibia'. *The Journal of Bone and Joint Surgery. British Volume* 82 (7): 959–66.

Gordon, Vernita D., and Liyun Wang. 2019. 'Bacterial Mechanosensing: The Force Will Be with You, Always'. *Journal of Cell Science* 132 (7): jcs227694.

Harper, Christine E., and Christopher J. Hernandez. 2020. 'Cell Biomechanics and Mechanobiology in Bacteria: Challenges and Opportunities'. *APL Bioengineering* 4 (2): 021501.

Haubert, Kathryn, Tracy Drier, and David Beebe. 2006. 'PDMS Bonding by Means of a Portable, Low-Cost Corona System'. *Lab on a Chip* 6 (12): 1548.

Hawas, Sophia, Anthony D. Verderosa, and Makrina Totsika. 2022. 'Combination Therapies for Biofilm Inhibition and Eradication: A Comparative Review of Laboratory and Preclinical Studies'. *Frontiers in Cellular and Infection Microbiology* 12 (February):850030.

Hillborg, H., and U.W. Gedde. 1998. 'Hydrophobicity Recovery of Polydimethylsiloxane after Exposure to Corona Discharges'. *Polymer* 39 (10): 1991–98.

Jamal, Muhsin, Wisal Ahmad, Saadia Andleeb, Fazal Jalil, Muhammad Imran, Muhammad Asif Nawaz, Tahir Hussain, Muhammad Ali, Muhammad Rafiq, and Muhammad Atif Kamil. 2018. 'Bacterial Biofilm and Associated Infections'. *Journal of the Chinese Medical Association* 81 (1): 7–11.

Jara, Josué, Francisco Alarcón, Ajay K. Monnappa, José Ignacio Santos, Valentino Bianco, Pin Nie, Massimo Pica Ciamarra, et al. 2020. 'Self-Adaptation of Pseudomonas Fluorescens Biofilms to Hydrodynamic Stress'. *Frontiers in Microbiology* 11:588884.

Jennings, Jessica Amber, Jacobus J. Arts, Ezzuddin Abuhussein, Volker Alt, Nicholas Ashton, Susanne Baertl, Sanjib Bhattacharyya, et al. 2023. '2023 International Consensus Meeting on Musculoskeletal Infection: Summary from the Treatment Workgroup and Consensus on Treatment in Preclinical Models'. *Journal of Orthopaedic Research: Official Publication of the Orthopaedic Research Society*, December.

Jensen, P.Ø., S.A. Møller, C.J. Lerche, C. Moser, T. Bjarnsholt, O. Ciofu, D. Faurholt-Jepsen, N. Høiby, and M. Kolpen. 2019. 'Improving Antibiotic Treatment of Bacterial Biofilm by Hyperbaric Oxygen Therapy: Not Just Hot Air'. *Biofilm* 1 (December):100008.

Jørgensen, Nis, Kasper Hansen, Caroline Andreasen, Michael Pedersen, Kurt Fuursted, Rikke Meyer, and Eskild Petersen. 2017. 'Hyperbaric Oxygen Therapy Is Ineffective as an Adjuvant to Daptomycin with Rifampicin Treatment in a Murine Model of Staphylococcus Aureus in Implant-Associated Osteomyelitis'. *Microorganisms* 5 (2): 21.

Kennedy, Darragh G., Aoife M. O'Mahony, Eamonn P. Culligan, Caitriona M. O'Driscoll, and Katie B. Ryan. 2022. 'Strategies to Mitigate and Treat Orthopaedic Device-Associated Infections'. *Antibiotics* 11 (12): 1822.

Kerrigan, Steven W., Niamh Clarke, Anthony Loughman, Gerardene Meade, Timothy J. Foster, and Dermot Cox. 2008. 'Molecular Basis for *Staphylococcus Aureus* –Mediated Platelet Aggregate Formation Under Arterial Shear In Vitro'. *Arteriosclerosis, Thrombosis, and Vascular Biology* 28 (2): 335–40.

Khan, Javairia, Sumbal Mudassar Tarar, Iram Gul, Uzam Nawaz, and Muhammad Arshad. 2021. 'Challenges of Antibiotic Resistance Biofilms and Potential Combating Strategies: A Review'. *3 Biotech* 11 (4): 169.

Kim, Tiffany, Carmine Wang See, Xiaochun Li, and Donghui Zhu. 2020. 'Orthopedic Implants and Devices for Bone Fractures and Defects: Past, Present and Perspective'. *Engineered Regeneration* 1:6–18.

Kreve, Simone, and Andréa C. Dos Reis. 2021. 'Bacterial Adhesion to Biomaterials: What Regulates This Attachment? A Review'. *Japanese Dental Science Review* 57 (November):85–96.

Krsmanovic, Milos, Dipankar Biswas, Hessein Ali, Aloke Kumar, Ranajay Ghosh, and Andrew K. Dickerson. 2021. 'Hydrodynamics and Surface Properties Influence Biofilm Proliferation'. *Advances in Colloid and Interface Science* 288 (February):102336.

Lee, Nae Yoon, and Bong Hyun Chung. 2009. 'Novel Poly(Dimethylsiloxane) Bonding Strategy via Room Temperature "Chemical Gluing"'. *Langmuir* 25 (6): 3861–66.

Maier, Berenike. 2021. 'How Physical Interactions Shape Bacterial Biofilms'. *Annual Review of Biophysics* 50 (1): 401–17.

Mao, Yanjie, Florent Valour, Nhu T. Q. Nguyen, Thien M. N. Doan, Holly Koelkebeck, Christopher Richardson, Lily I. Cheng, Bret R. Sellman, Christine Tkaczyk, and Binh An Diep. 2021. 'Multimechanistic Monoclonal Antibody Combination Targeting Key Staphylococcus Aureus Virulence Determinants in a Rabbit Model of Prosthetic Joint Infection'. *Antimicrobial Agents and Chemotherapy* 65 (7): e01832-20.

Martirosyan, Varsik, and Sinerik Ayrapetyan. 2015. 'Comparative Study of Time-Dependent Effects of 4 and 8 Hz Mechanical Vibration at Infrasound Frequency on *E. Coli* K-12 Cells Proliferation'. *Electromagnetic Biology and Medicine* 34 (4): 293–97.

Mathews, J. A., J. Ward, T. W. Chapman, U. M. Khan, and M. B. Kelly. 2015. 'Single-Stage Orthoplastic Reconstruction of Gustilo-Anderson Grade III Open Tibial Fractures Greatly Reduces Infection Rates'. *Injury* 46 (11): 2263–66.

McNally, Martin, Geertje Govaert, Maria Dudareva, Mario Morgenstern, and Willem-Jan Metsemakers. 2020. 'Definition and Diagnosis of Fracture-Related Infection'. *EFORT Open Reviews* 5 (10): 614–19..

Metsemakers, W. J., R. Kuehl, T. F. Moriarty, R. G. Richards, M. H. J. Verhofstad, O. Borens, S. Kates, and M. Morgenstern. 2018. 'Infection after Fracture Fixation: Current Surgical and Microbiological Concepts'. *Injury* 49 (3): 511–22.

Morgenstern, Mario, Christoph Erichsen, Matthias Militz, Zhao Xie, Jiachen Peng, James Stannard, Willem-Jan Metsemakers, et al. 2021. 'The AO Trauma CPP Bone Infection Registry: Epidemiology and Outcomes of Staphylococcus Aureus Bone Infection'. *Journal of Orthopaedic Research: Official Publication of the Orthopaedic Research Society* 39 (1): 136–46.

Moriarty, T. Fintan, Willem-Jan Metsemakers, Mario Morgenstern, Marloes I. Hofstee, Alejandro Vallejo Diaz, James E. Cassat, Britt Wildemann, Melissa Depypere, Edward M. Schwarz, and R. Geoff Richards. 2022. 'Fracture-Related Infection'. *Nature Reviews Disease Primers* 8 (1): 67.

Morris, Jodie, Natasha Kelly, Lisa Elliott, Andrea Grant, Matthew Wilkinson, Kaushik Hazratwala, and Peter McEwen. 2019. 'Evaluation of Bacteriophage Anti-Biofilm Activity for Potential Control of Orthopedic Implant-Related Infections Caused by *Staphylococcus Aureus*'. *Surgical Infections* 20 (1): 16–24.

Motififard, Mehdi, Mehdi Teimouri, Kiana Shirani, Saeed Hatami, and Mahila Yadegari. 2021. 'Prevalence of Bacterial Surgical Site Infection in Traumatic Patients Undergoing Orthopedic Surgeries: A Cross-Sectional Study'. *International Journal of Burns and Trauma* 11 (3): 191–96.

Murphy, Mark F., Thomas Edwards, Glyn Hobbs, Joanna Shepherd, and Frederic Bezombes. 2016. 'Acoustic Vibration Can Enhance Bacterial Biofilm Formation'. *Journal of Bioscience and Bioengineering* 122 (6): 765–70.

Nguyen, Hoa, Abraham Ybarra, Hakan Başağaoğlu, and Orrin Shindell. 2021. 'Biofilm Viscoelasticity and Nutrient Source Location Control Biofilm Growth Rate, Migration Rate, and Morphology in Shear Flow'. *Scientific Reports* 11 (1): 16118.

Nilsson, Lina M., Wendy E. Thomas, Evgeni V. Sokurenko, and Viola Vogel. 2006. 'Elevated Shear Stress Protects *Escherichia Coli* Cells Adhering to Surfaces via Catch Bonds from Detachment by Soluble Inhibitors'. *Applied and Environmental Microbiology* 72 (4): 3005–10.

Okae, Yu, Kohei Nishitani, Akio Sakamoto, Toshiyuki Kawai, Takuya Tomizawa, Motoo Saito, Yutaka Kuroda, and Shuichi Matsuda. 2022. 'Estimation of Minimum Biofilm Eradication Concentration (MBEC) on In Vivo Biofilm on Orthopedic Implants in a Rodent Femoral Infection Model'. *Frontiers in Cellular and Infection Microbiology* 12 (July):896978.

Otto, Karen, and Thomas J. Silhavy. 2002. 'Surface Sensing and Adhesion of *Escherichia Coli* Controlled by the Cpx-Signaling Pathway'. *Proceedings of the National Academy of Sciences* 99 (4): 2287–92.

Papakostidis, Costas, Nikolaos K. Kanakaris, Juan Pretel, Omar Faour, Daniel Juan Morell, and Peter V. Giannoudis. 2011. 'Prevalence of Complications of Open Tibial Shaft Fractures Stratified as per the Gustilo-Anderson Classification'. *Injury* 42 (12): 1408–15.

Parker, B., S. Petrou, J. P. M. Masters, F. Achana, and M. L. Costa. 2018. 'Economic Outcomes Associated with Deep Surgical Site Infection in Patients with an Open Fracture of the Lower Limb'. *The Bone & Joint Journal* 100-B (11): 1506–10.

Patangia, Dhrati V., Cornelius Anthony Ryan, Eugene Dempsey, Reynolds Paul Ross, and Catherine Stanton. 2022. 'Impact of Antibiotics on the Human Microbiome and Consequences for Host Health'. *MicrobiologyOpen* 11 (1): e1260.

Pattanayak, Prapti, Sachin Kumar Singh, Monica Gulati, Sukriti Vishwas, Bhupinder Kapoor, Dinesh Kumar Chellappan, Krishnan Anand, et al. 2021. 'Microfluidic Chips: Recent Advances, Critical Strategies in Design, Applications and Future Perspectives'. *Microfluidics and Nanofluidics* 25 (12): 99.

Persat, Alexandre. 2017. 'Bacterial Mechanotransduction'. *Current Opinion in Microbiology* 36 (April):1–6.

Peterson, R.Vaughn, and William G Pitt. 2000. 'The Effect of Frequency and Power Density on the Ultrasonically-Enhanced Killing of Biofilm-Sequestered Escherichia Coli'. *Colloids and Surfaces B: Biointerfaces* 17 (4): 219–27.

Png, May Ee, Stavros Petrou, Ruth Knight, James Masters, Juul Achten, and Matthew L. Costa. 2022. 'Economic Outcomes Associated with Deep Surgical Site Infection from Lower Limb Fractures Following Major Trauma'. *Bone & Joint Open* 3 (5): 398–403.

Quan, Kecheng, Jiapeng Hou, Zexin Zhang, Yijin Ren, Brandon W. Peterson, Hans-Curt Flemming, Christian Mayer, Henk J. Busscher, and Henny C. Van Der Mei. 2022. 'Water in Bacterial Biofilms: Pores and Channels, Storage and Transport Functions'. *Critical Reviews in Microbiology* 48 (3): 283–302.

Ramos, Gabriel, Clara Toulouze, Maya Rima, Olivier Liot, Paul Duru, and Yohan Davit. 2023. 'Ultraviolet Control of Bacterial Biofilms in Microfluidic Chips'. *Biomicrofluidics* 17 (2): 024107.

Ribeiro, M., I.B. Gomes, M.J. Saavedra, and M. Simões. 2022. 'Photodynamic Therapy and Combinatory Treatments for the Control of Biofilm-Associated Infections'. *Letters in Applied Microbiology* 75 (3): 548–64.

Rojas, Enrique R, and Kerwyn Casey Huang. 2018. 'Regulation of Microbial Growth by Turgor Pressure'. *Current Opinion in Microbiology* 42 (April):62–70.

Rotello, Vincent M. 2023. 'Nanomaterials for Fighting Multidrug-Resistant Biofilm Infections'. *BME Frontiers* 4 (January):0017.

Ruhal, Rohit, and Rashmi Kataria. 2021. 'Biofilm Patterns in Gram-Positive and Gram-Negative Bacteria'. *Microbiological Research* 251 (October):126829.

Rumbaugh, Kendra P., and Karin Sauer. 2020. 'Biofilm Dispersion'. *Nature Reviews Microbiology* 18 (10): 571–86.

Sabaté Brescó, M., L. O'Mahony, S. Zeiter, K. Kluge, M. Ziegler, C. Berset, D. Nehrbass, R. G. Richards, and T. F. Moriarty. 2017. 'Influence of Fracture Stability on Staphylococcus Epidermidis and Staphylococcus Aureus Infection in a Murine Femoral Fracture Model'. *European Cells & Materials* 34 (November):321–40.

Saeed, Kordo, Parham Sendi, William V. Arnold, Thomas W. Bauer, Débora C. Coraça-Huber, Antonia F. Chen, Hyonmin Choe, et al. 2021. 'Bacterial Toxins in Musculoskeletal Infections'. *Journal of Orthopaedic Research* 39 (2): 240–50.

Sauer, Karin, Paul Stoodley, Darla M. Goeres, Luanne Hall-Stoodley, Mette Burmølle, Philip S. Stewart, and Thomas Bjarnsholt. 2022. 'The Biofilm Life Cycle: Expanding the Conceptual Model of Biofilm Formation'. *Nature Reviews Microbiology* 20 (10): 608–20.

Schaer, Thomas P., Suzanne Stewart, Bryan B. Hsu, and Alexander M. Klibanov. 2012. 'Hydrophobic Polycationic Coatings That Inhibit Biofilms and Support Bone Healing during Infection'. *Biomaterials* 33 (5): 1245–54.

Schindelin, Johannes, Ignacio Arganda-Carreras, Erwin Frise, Verena Kaynig, Mark Longair, Tobias Pietzsch, Stephan Preibisch, et al. 2012. 'Fiji: An Open-Source Platform for Biological-Image Analysis'. *Nature Methods* 9 (7): 676–82.

Shah, Ramesh K., and Alexander Louis London. 1978. *Laminar Flow Forced Convection in Ducts: A Source Book for Compact Heat Exchanger Analytical Data*. Advances in Heat Transfer. Supplement 1. New York: Academic Press.

Shakeri, Amid, Shadman Khan, and Tohid F. Didar. 2021. 'Conventional and Emerging Strategies for the Fabrication and Functionalization of PDMS-Based Microfluidic Devices'. *Lab on a Chip* 21 (16): 3053–75.

Shrestha, Looniva, Hai-Ming Fan, Hui-Ren Tao, and Jian-Dong Huang. 2022. 'Recent Strategies to Combat Biofilms Using Antimicrobial Agents and Therapeutic Approaches'. *Pathogens* 11 (3): 292.

Simpkin, Victoria L, Matthew J Renwick, Ruth Kelly, and Elias Mossialos. 2017. 'Incentivising Innovation in Antibiotic Drug Discovery and Development: Progress, Challenges and next Steps'. *The Journal of Antibiotics* 70 (12): 1087–96.

Singh, Anirudh, Ayush Amod, Priyanshu Pandey, Pranay Bose, M Shivapriya Pingali, Saurabh Shivalkar, Pritish Kumar Varadwaj, Amaresh Kumar Sahoo, and Sintu Kumar Samanta. 2022. 'Bacterial Biofilm Infections, Their Resistance to Antibiotics Therapy and Current Treatment Strategies'. *Biomedical Materials* 17 (2): 022003.

Sivakumar, Rajamanickam, and Nae Yoon Lee. 2020. 'Chemically Robust Succinimide-Group-Assisted Irreversible Bonding of Poly(Dimethylsiloxane)–Thermoplastic Microfluidic Devices at Room Temperature'. *The Analyst* 145 (21): 6887–94.

Song, Fangchao, Megan E. Brasch, Hao Wang, James H. Henderson, Karin Sauer, and Dacheng Ren. 2017. 'How Bacteria Respond to Material Stiffness during Attachment: A Role of *Escherichia Coli* Flagellar Motility'. *ACS Applied Materials & Interfaces* 9 (27): 22176–84.

Stetter, J., G.S. Boge, U. Grönlund, and A. Bergström. 2021. 'Risk Factors for Surgical Site Infection Associated with Clean Surgical Procedures in Dogs'. *Research in Veterinary Science* 136 (May):616–21.

Tang, Linzhi, and Nae Yoon Lee. 2010. 'A Facile Route for Irreversible Bonding of Plastic-PDMS Hybrid Microdevices at Room Temperature'. *Lab on a Chip* 10 (10): 1274.

Thakore, Rachel V., Sarah E. Greenberg, Hanyuan Shi, Alexandra M. Foxx, Elvis L. Francois, Marc A. Prablek, Samuel K. Nwosu, et al. 2015. 'Surgical Site Infection in Orthopedic Trauma: A Case-Control Study Evaluating Risk Factors and Cost'. *Journal of Clinical Orthopaedics and Trauma* 6 (4): 220–26.

Tillander, Jonatan A N, Karin Rilby, Karin Svensson Malchau, Susann Skovbjerg, Erika Lindberg, Ola Rolfson, and Margarita Trobos. 2022. 'Treatment of Periprosthetic Joint Infections Guided by Minimum Biofilm Eradication Concentration (MBEC) in Addition to Minimum Inhibitory Concentration (MIC): Protocol for a Prospective Randomised Clinical Trial'. *BMJ Open* 12 (9): e058168.

Uruén, Cristina, Gema Chopo-Escuin, Jan Tommassen, Raúl C. Mainar-Jaime, and Jesús Arenas. 2020. 'Biofilms as Promoters of Bacterial Antibiotic Resistance and Tolerance'. *Antibiotics (Basel, Switzerland)* 10 (1): 3.

Valvez, Sara, Abilio P. Silva, and Paulo N. B. Reis. 2022. 'Optimization of Printing Parameters to Maximize the Mechanical Properties of 3D-Printed PETG-Based Parts'. *Polymers* 14 (13): 2564.

Varin-Simon, Jennifer, Fabien Lamret, Marius Colin, Sophie C. Gangloff, Céline Mongaret, and Fany Reffuveille. 2021. 'Comparison of Two Cutibacterium Acnes Biofilm Models'. *Microorganisms* 9 (10): 2035.

Varrone, John J., Karen L. De Mesy Bentley, Sheila N. Bello-Irizarry, Kohei Nishitani, Sarah Mack, Joshua G. Hunter, Stephen L. Kates, John L. Daiss, and Edward M. Schwarz. 2014. 'Passive Immunization with Anti-Glucosaminidase Monoclonal Antibodies Protects Mice from Implant-Associated Osteomyelitis by Mediating Opsonophagocytosis of *Staphylococcus Aureus* Megaclusters: PASSIVE IMMUNIZATION PROTECTS MICE FROM MRSA'. *Journal of Orthopaedic Research* 32 (10): 1389–96.

Veerachamy, Suganthan, Tejasri Yarlagadda, Geetha Manivasagam, and Prasad KDV Yarlagadda. 2014. 'Bacterial Adherence and Biofilm Formation on Medical Implants: A Review'. *Proceedings of the Institution of Mechanical Engineers, Part H: Journal of Engineering in Medicine* 228 (10): 1083–99.

Visperas, Anabelle, Daniel Santana, Alison K. Klika, Carlos A. Higuera-Rueda, and Nicolas S. Piuzzi. 2022. 'Current Treatments for Biofilm-associated Periprosthetic Joint Infection and New Potential Strategies'. *Journal of Orthopaedic Research* 40 (7): 1477–91.

Waters, Christopher M., and Bonnie L. Bassler. 2005. 'Quorum Sensing: Cell-to-Cell Communication in Bacteria'. *Annual Review of Cell and Developmental Biology* 21:319–46.

Wildemann, Britt, and Klaus D. Jandt. 2021. 'Infections @ Trauma/Orthopedic Implants: Recent Advances on Materials, Methods, and Microbes-A Mini-Review'. *Materials (Basel, Switzerland)* 14 (19): 5834.

Wilking, James N., Thomas E. Angelini, Agnese Seminara, Michael P. Brenner, and David A. Weitz. 2011. 'Biofilms as Complex Fluids'. *MRS Bulletin* 36 (5): 385–91.

Wu, Wenming, Jing Wu, Jae-Heon Kim, and Nae Yoon Lee. 2015. 'Instantaneous Room Temperature Bonding of a Wide Range of Non-Silicon Substrates with Poly(Dimethylsiloxane) (PDMS) Elastomer Mediated by a Mercaptosilane'. *Lab on a Chip* 15 (13): 2819–25.

Wu, Yuan-Kun, Nai-Chen Cheng, and Chao-Min Cheng. 2019. 'Biofilms in Chronic Wounds: Pathogenesis and Diagnosis'. *Trends in Biotechnology* 37 (5): 505–17.

Xiao, Wanting, Guoren Xu, and Guibai Li. 2021. 'Role of Shear Stress in Biological Aerated Filter with Nanobubble Aeration: Performance, Biofilm Structure and Microbial Community'. *Bioresource Technology* 325 (April):124714.

Xu, Huan, Jing Liu, Zhaohuan Zhang, Qian Tao, Zhenhua Huang, Yingjie Pan, and Yong Zhao. 2022. 'Animal models in bacterial biofilm research: a review'. *Sheng Wu Gong Cheng Xue Bao = Chinese Journal of Biotechnology* 38 (8): 2840–56.

Zhang, Hainan, and Nae Yoon Lee. 2015. 'Non-Silicon Substrate Bonding Mediated by Poly(Dimethylsiloxane) Interfacial Coating'. *Applied Surface Science* 327 (February):233–40.

Zheng, Sherry, Marwa Bawazir, Atul Dhall, Hye-Eun Kim, Le He, Joseph Heo, and Geelsu Hwang. 2021. 'Implication of Surface Properties, Bacterial Motility, and Hydrodynamic Conditions on Bacterial Surface Sensing and Their Initial Adhesion'. *Frontiers in Bioengineering and Biotechnology* 9 (February):643722.

Zimmerli, Werner, and Parham Sendi. 2017. 'Orthopaedic Biofilm Infections'. *APMIS* 125 (4): 353–64.

Scientific publications with review panels:

Biomechanical:

1. **Blondel M**, Machet C, Wildemann B, Abidine Y, Swider P.
   Mechanobiology of bacterial biofilms: implications for orthopedic infection.
   Journal of Orthopaedic Research. 2024. doi: 10.1002/jor.25822

2. Palierne S, **Blondel M**, Swider P, Autefage A.
   Biomechanical comparison of use of two screws versus three screws per fragment with locking plate constructs under cyclic loading in compression in a fracture gap model.
   VCOT. 2022, 35:166-174. doi: 10.1055/s-0042-1744175.

3. Deprey J, **Blondel M**, Saban C, Massenzio M, Gauthier O, Moissonnier P, Viguier E, Cachon T.
   Mechanical evaluation of a novel angle-stable interlocking nail in a gap fracture model
   VetSurg. 2022, 51:1247-1256. doi: 10.1111/vsu.13837.

4. **Blondel M**, Abidine Y, Assemat P, Palierne S, Swider P.
   Identification of effective elastic modulus using modal analysis; Application to canine cancellous bone.
   Journal of Biomechanics. 2020, 110:109972. doi:10.1016/j.jbiomech.2020.109972

Clinical:

5. Porsmoguer C, **Blondel M**, Moissonnier P.
   Surgical treatment of feline intracranial meningiomas: a retrospective study of 26 cases
   Journal of Veterinary Science. 2024, 25(2):e25. doi: 10.4142/jvs.23207

6. Roels J, Genevois JP, Fostier-Humbert M, Porsmoguer C, **Blondel M**, Chanoit G, Fau D, Cachon T.
   Prevalence of elbow dysplasia in 13 dog breeds in France: a retrospective radiographic study (2002–2022).
   American Journal of Veterinary Research. 2024. doi: 10.2460/ajvr.23.12.0290

7. Palierne S, **Blondel M**, Patard F, Autefage A.
   Impacts of tibial plateau levelling osteotomy on the tibial insertion of the medial collateral ligament of the canine stifle joint – A cadaveric study.
   Research in Veterinary Science. 2023, 154:66-72. doi: 10.1016/j.rvsc.2022.11.011.

8. Palierne S, **Blondel M**, Vié K, Autefage A.
   Morphometric assessment of the medial collateral ligament of the canine stifle joint.
   Research in Veterinary Science. 2022, 151:22-26. doi: 10.1016/j.rvsc.2022.06.032.

9. **Blondel M**, Morvan V, Moissonnier P.
   Treatment of an extrahepatic portosystemic shunt by placement of a hydraulic occluder followed by a thin film band in a dog : An eventful story.
   Veterinary Record Case Reports. 2022, e389. doi :10.15406/jdvar.2016.03.00070.

10. Moissonnier P, **Blondel M**, Manou M, Viguier E.
    Transoral ventral tympanic bulla osteotomy in cats: 13 cases (2016-2019).
    JAVMA. 2022, 260:892-898. doi: 10.2460/javma.21.01.0054.

11. Taroni M, Saban C, Baldinger A, **Blondel M**, Marchal T, Viguier E, Cachon T, Carozzo C, Moissonnier P.
    Anatomical features of the canine C2-C3 spinal cord vascular environment.
    American Journal of Veterinary Research. 2022, 83:107-113. doi: 10.2460/ajvr.21.05.0063.

12. Deprey J, Baldinger A, Livet V, **Blondel M**, Taroni M, Lefebvre C, Goy-Thollot I, Moissonnier P, Viguier É, Pouzot-Nevoret C, Carozzo C, Cachon T.
    Risk factors and clinical relevance of positive urine cultures in cats with subcutaneous ureteral bypass.
    BMC Vet Res. 2021, 27;17(1):199. doi: 10.1186/s12917-021-02898-7

13. **Blondel M**, Sonet J, Cachon T, Ségard-Weisse E, Ferrand FX, Carozzo C.
    Comparison of imaging techniques to detect migrating foreign bodies. Relevance of preoperative and intraoperative ultrasonography for diagnosis and surgical removal.
    Vet Surg. 2021, 50:833-842. doi: 10.1111/vsu.13607.

14. Cervone M, **Blondel M**, Moissonnier P, Chabanne L.
    Multiple endocrine neoplasia type 2-like syndrome in a crossbred dog.
    Veterinary Record Case Reports. 2021, 9, e61. doi: 10.1002/vrc2.61.

15. **Blondel M**, Gros L, Lucas MN, Delverdier M, Palierne S.
    Multifocal haematogenous osteomyelitis and septic physitis in a dog.
    Veterinary Record Case Reports. 2020, 8(4):e001207. doi: 10.1136/vetreccr-2020-001207

16. **Blondel M**, Deprey J, Moissonnier P.
    Type IV dermoid sinus, intramedullary dermoid cyst and spina bifida in a Cane Corso.
    JSAP. 2021, 62:810-815. doi: 10.1111/jsap.13240

17. **Blondel M**, Gros L, Semin MO, Delverdier M, Palierne S, Autefage A.
    A case of giant cell tumour of bone in a dog.
    VCOT Open. 2019, 2:e64-e69. doi: 10.1055/s-0039-3400513

18. Asimus E, Palierne S, **Blondel M**, Pollet V, Ferran A, Bousquet-Melou A, Rousselot JF, Autefage A.
    Comparison of hydroalcoholic rubbing and conventional chlorhexidine scrubbing for aseptic skin preparation in dogs.
    Veterinary Surgery. 2019, 48:1466-1472. doi : 10.1111/vsu.13222

19. Bassanino J, Palierne S, **Blondel M**, Reynolds B.
Sublingual sialocele in a cat.
Journal of Feline Medicine and Surgery Open Reports. 2019. doi: 10.1177/2055116919833249

20. **Blondel M**, Decambron A, Delpont V, Maurey C, Manassero M.
Bilateral ectopic ureteroceles in a female dog.
Revue Vétérinaire Clinique. 2017, 52:17-25. doi :10.1016/j.anicom.2016.12.001

21. **Blondel M**, Kohlhauer M, Zilberstein L, Tissier R.
How can we study cardiopulmonary resuscitation and cardiac arrest in animals : a review**.**
J Dairy Vet Anim Res. 2016, 3:37-41. doi: 10.15406/jdvar.2016.03.00070

Oral communications:

Biomechanical:

1. **Blondel M**, Abidine Y, Assemat P, Autefage A, Palierne S, Swider P.
Characterization of effective elastic modulus of canine cancellous bone by using modal analysis.
On-line European Congress of Veterinary Surgeons, July 2020.

2. Abidine Y, Assemat P, Soeparno R, **Blondel M**, Palierne S, Gomez-Brouchet A, Swider P.
Mechanobiological study of biological explants by modal analysis at the tissue scale.
5èmes Journée du GDR MécaBio3570, Toulouse, France, January 2018.

Clinical:

3. Hebrard L, **Blondel M**, Cachon T.
Treatment of medial shoulder instability by video-assisted ligamentoplasty. A retrospective study of 6 cases.
17th Annual VA3, Arthrex Corporate Headquarters, Naples, USA, August 2023.

4. **Blondel M**, Cachon T.
Traitement d'une instabilité médiale de l'épaule sous arthroscopie.
Soirée Arthrex Vet Systems, Arthrex France, Saint- Didier-au-Mont-d'Or, March 2021.

5. **Blondel M**, Sonet J, Nectoux A, Cervone M, Carozzo C.
Torsion caeco-colique associée à une déchirure du mésocôlon chez un Cavalier King Charles.
E-Congrès AFVAC (Association Française des Vétérinaires pour Animaux de Compagnie), December 2020.

6. **Blondel M**, Deprey J, Tortereau A, Couturier J, Moissonnier P.
   Sinus dermoïde de type IV et dermoïde spinal associés à une spina bifida chez un Cane Corso.
   Congrès AFVAC (Association Française des Vétérinaires pour Animaux de Compagnie), Lyon, France, December 2019.

7. Asimus E, Palierne S, **Blondel M**, Pollet V, Ferran A, Bousquet-Melou A, Rousselot JF, Autefage A.
   Evaluation of a new pre-surgical skin asepsis protocol with hydro-alcoholic rubbing compared to classic chlorhexidine scrubbing in dogs.
   5th World Veterinary Orthopaedic Congress ESVOT-VOS, Barcelona, Spain, September 2018.

Continuing education :

Articles:

1. **Blondel M**, Carozzo C.
   Prise en charge des traumatismes thoraciques chez le chat et le chien.
   Le Nouveau Praticien Vétérinaire canine-féline, Hors-série Urgences et Traumatologie chez le chien et le chat 2020, 48 – 54.

2. **Blondel M**, Cachon T.
   Prise en charge des plaies chez le chat et le chien.
   Le Nouveau Praticien Vétérinaire canine-féline, Hors-série Urgences et Traumatologie chez le chien et le chat 2020, 32 – 38.

3. **Blondel M**, Bassanino J, Meynaud P, Asimus E.
   Ablation totale du conduit auditif associée à la trépanation de la bulle tympanique.
   PratiqueVet 2019, 54 : 102 – 105.

4. Bassanino J, **Blondel M**, Asimus E.
   L'otectomie lors de carcinome épidermoïde du pavillon auriculaire.
   PratiqueVet 2019, 54 : 49 – 52.

5. **Blondel M**, Bassanino J, Asimus E.
   Traitement d'une hernie périnéale par transposition du muscle obturateur interne.
   PratiqueVet 2018, 53 : 46 – 49.

6. **Blondel M**, Giansetto T, Asimus E.
   La caudectomie.
   PratiqueVet 2018, 53 : 492 – 495.

7. Teychene A, **Blondel M**, Asimus E.
Amputation du membre pelvien.
PratiqueVet 2018, 53 : 322 – 325.

Oral presentations :

1. « Biomécanique et classification des fractures »
« Coaptation externe »
« Greffe osseuse »
34ème cours AO de traitement des fractures – Cours d'initiation. Marseille, France. March 2024.

2. « Les urétrostomies chez le chat »
« L'urétrostomie périnéale chez le chat : technique chirurgicale »
Enseignement post-universitaire. VetAgro Sup, Campus Vétérinaire de Lyon, France. June 2023.

3. « Particularités anatomiques du chat et conséquences en orthopédie et traumatologie »
« Entorse grave du grasset chez le chat »
« Polyarthrite du chat »
16ème cours de propédeutique, sémiologie et pathologie de l'appareil locomoteur : Le chat sous toutes ses coutures. Bédoin, France. June 2023

4. « Osteoarthritis in feline patients: more common than what you think »
Oral communication – Vetoquinol. Sofia, Bulgaria. April 2023.

5. « Luxations sacro-iliaques et fractures du bassin »
33ème cours AO de traitement des fractures – Cours d'initiation. Marseille, France. January 2023.

6. « Anatomie chirurgicale et biomécanique du grasset »
Enseignement post-universitaire. VetAgro Sup, Campus Vétérinaire de Lyon, France. June 2021.

7. « Hémostase chirurgicale : utilisation de la pince Caiman en pratique »
Enseignement post-universitaire. VetAgro Sup, Campus Vétérinaire de Lyon, France. June 2021.
8. « Luxation de hanches – cas cliniques »
Enseignement post-universitaire. VetAgro Sup, Campus Vétérinaire de Lyon, France. March 2021.

9. « Les examens d'imagerie en neuropathologie médullaire »
« Lecture d'examens d'imagerie en neuropathologie »
Enseignement post-universitaire. VetAgro Sup, Campus Vétérinaire de Lyon, France. October 2019

10. « Syndrome Obstructif des Races Brachycéphales – cas cliniques »
Enseignement post-universitaire. VetAgro Sup, Campus Vétérinaire de Lyon, France. October 2018.

Received: 21 December 2023 | Revised: 14 February 2024 | Accepted: 19 February 2024

DOI: 10.1002/jor.25822

RESEARCH ARTICLE

Journal of Orthopaedic Research®

Mechanobiology of bacterial biofilms: Implications for orthopedic infection

Margaux Blondel[1] | Camille Machet[2] | Britt Wildemann[3] | Yara Abidine[4] | Pascal Swider[4]

[1]Small Animal Surgery Department, Lyon University, VetAgro Sup, Marcy l'Etoile, France

[2]National Veterinary School of Toulouse, Toulouse, France

[3]Experimental Trauma Surgery, Department of Trauma, Hand and Reconstructive Surgery, Jena University Hospital, Friedrich Schiller University Jena, Jena, Germany

[4]Institut de Mécanique des Fluides (IMFT), CNRS & Toulouse University, Toulouse, France

Correspondence

Pascal Swider, Institut de Mécanique des Fluides (IMFT), CNRS & Toulouse University, Toulouse, France.
Email: pascal.swider@imft.fr

Funding information

Deutsche Forschungsgemeinschaft, Grant/Award Numbers: #444711651, RTG 2723 Materials-Microbes-Microenvironments

Abstract

Postoperative bacterial infections are prevalent complications in both human and veterinary orthopedic surgery, particularly when a biofilm develops. These infections often result in delayed healing, early revision, permanent functional loss, and, in severe cases, amputation. The diagnosis and treatment pose significant challenges, and bacterial biofilm further amplifies the therapeutic difficulty as it confers protection against the host immune system and against antibiotics which are usually administered as a first-line therapeutic option. However, the inappropriate use of antibiotics has led to the emergence of numerous multidrug-resistant organisms, which largely compromise the already imperfect treatment efficiency. In this context, the study of bacterial biofilm formation allows to better target antibiotic use and to evaluate alternative therapeutic strategies. Exploration of the roles played by mechanical factors on biofilm development is of particular interest, especially because cartilage and bone tissues are reactive environments that are subjected to mechanical load. This review delves into the current landscape of biofilm mechanobiology, exploring the role of mechanical factors on biofilm development through a multiscale prism starting from bacterial microscopic scale to reach biofilm mesoscopic size and finally the macroscopic scale of the fracture site or bone–implant interface.

KEYWORDS

antibiotic therapy, biofilm, mechanobiology, orthopedic infection

1 | INTRODUCTION

Surgical site infection (SSI) is one of the most dreaded postoperative complications, with a prevalence of approximately 1%–3% in human patients.[1] Among surgical disciplines, orthopedic surgery carries the highest risk of postoperative SSIs, as it is estimated that up to 20% of all SSIs can occur in orthopedic patients.[2] The risk of SSIs is more important for open fractures than for closed fractures, ranging from 8.5% to 14.9% when one-stage treatment can be performed,[3] and exceeding 30% when multiple-staged surgeries are needed.[4] SSIs can lead to delayed bone healing, permanent functional loss, and, in up to 17.6% cases, amputation.[5] Surgical revision is required in more than 80% of SSI cases in orthopedics and more than 75% of SSI cases in traumatology, with success rates varying between 70% and 90%.[6] The consequent economic outcomes are a cause for concern. Indeed, treatment costs associated with these orthopedic complications are more than 2.5 times higher compared to patients without a postoperative SSI,[7] with a difference in health and social care cost exceeding £1500.[8,9] This difference is in part due to the cost associated with revision procedures and to prolonged hospital stays.[7] In veterinary orthopedics, the incidence of SSIs is higher, with rates reaching as high as 30% after surgical repair of an open or a closed

fracture in dogs.[10] The consequences can be as disastrous as those observed in human patients, often necessitating amputation in extreme cases.

The diagnosis of postoperative SSI primarily relies on clinical signs, which can vary depending on the bacteria involved, the route of infection, and the stage of bone healing. Main complaints in human patients include pain, local erythema, and soft tissue swelling, and can be accompanied by wound dehiscence, fistula formation, purulent discharge, and fever.[11] Clinical signs in animals are somewhat similar and include lameness, swelling, heat, pain upon palpation and draining tracts.[10] As in humans, pyrexia is not a consistent finding.[10] Additional diagnostic imaging examinations may support the diagnosis of SSI in human and veterinary patients.[10,11] While radiography can provide information on bone healing and implant stability, it has low sensitivity and specificity in detecting acute osteomyelitis.[12] Advanced imaging modalities, such as high-resolution imaging or positron emission tomography, are therefore necessary. However, a definitive diagnosis of bone infection requires bacterial analysis of deep samples, such as bone or soft tissue.[10,11,13]

Treatment of SSIs associated with implants is a challenge for the surgeon, mainly because infections around implants will frequently lead to the formation of a biofilm.[14,15] In most cases, biofilm elimination requires orthopedic implant removal. However, this cannot be considered an option until bone healing is completed, and amputation should only be considered as a last resort. Therefore, the purposes of treating SSIs are to not only eradicate the infection but also promote successful healing, while minimizing the risks associated with antibiotic resistance. The initial therapeutic approach is identical in human and veterinary patients and consists in combining surgical debridement under general anesthesia to systemic antibiotic administration, associated if needed with local antibiotic therapy. Broad-spectrum antibiotics are initially selected to provide coverage against a wide range of bacteria, and antibiotic therapy may be adjusted eventually according to sensitivity testing. However, the systematic and unreasonable use of antibiotics and their inefficiency once a biofilm has formed have led to the emergence of multidrug resistant organisms.[10,16] Nowadays, antibiotic resistance is considered a major public health issue, especially as antibiotic resistance genes are transmissible by horizontal gene transfer.[16,17]

Bacterial proliferation and biofilm growth are complex multifactorial processes. In this context, investigating bacterial biofilm formation may allow the emergence of alternative therapeutic strategies that do not rely solely on antibiotics. However, significant progress in management and treatment of musculoskeletal infections remains challenging. Indeed, to understand underlying infectious phenomena, it seems crucial to carry out clinical trials bounded by demanding ethical protocols. In addition, inherent complexity of these trials also means that significant induced costs have to be taken into account to achieve clinical relevance.

To contribute, the Orthopedic Research Society (ORS) has organized International Consensus Meetings (ICMs) covering all aspects of musculoskeletal infections in 2018 and 2023, with the aim of documenting expert opinion and defining research priorities.[18–22] In addition, the Host Immunity Section of 2023 ORS ICM identified 45 diagnostic questions to render examination more discriminant and robust. However, some of the questions addressing the effect of implant material and possible biophysical interactions were not answered due to limited resources.[22] In a coordinated way, our review aimed to propose an overall view of biofilm formation and growth, certainly considering material impact but also dynamic effects, including stresses and strains on local responses and the microenvironment. Indeed, the exploration of the roles played by biophysical factors may be of particular interest for cartilage and bone tissues, which are reactive environments subjected to mechanical loading, where permanent exchanges between cell populations, proteins, and chemical factors occur under the action of fluid transports, load bearing, and associated mechanical strain fields. As such, investigating the mechanobiology in both the biofilm and its environment may play a critical role in understanding biofilm development.

This review presents the clinical aspects of SSIs in orthopedic surgery in both animals and humans. The mechanisms underlying bacterial biofilm formation are described. Finally, the role of mechanical factors on biofilm development is discussed, exploring these mechanobiological interactions through a multiscale prism starting from bacterial microscopic scale to reach biofilm mesoscopic size and finally the macroscopic scale of the fracture site or bone–implant interface.

2 | BACTERIAL INFECTION IN ORTHOPEDIC SURGERY

Implants are indispensable in orthopedic surgery, yet they are considered as foreign materials by the body. Furthermore, the local inflammatory environment is modified secondary to trauma, and further amplified by disruption of the skin barrier related to material implantation. These factors collectively increase the risk of bacterial contamination at the surgical site. Once bacteria adhere to an implant, they form surface-adhering biofilms. These biofilms exhibit not only tolerance to the host defense and to antibiotics but also mature over time, preventing bone healing through cytokine-mediated osteoclast differentiation and bone resorption.[23] Bone healing is also influenced by bacterial toxins, which may play detrimental roles in shifting the host response toward bacterial clearance or exaggerated pro-inflammatory reaction. They can contribute to mechanisms leading to biofilm formation and dispersion.[24]

2.1 | Prevalence of bacterial isolates

In human or animal patients suspected of developing bacterial infection secondary to orthopedic surgery, bacterial analysis on five or more deep tissue/implant samples should be performed.[25,26] Infection is confirmed when either a single positive culture test identifies a virulent pathogen, or at least two positive bacterial culture isolate the same pathogens.[27]

Monomicrobial infections involving *Staphylococcus aureus* are most prevalent in human and animal orthopedic patients.[25,26] In fact, *S. aureus* is the most commonly isolated bacterium causing SSIs regardless of time to onset of infection, with the methicillin-resistant strain more frequently encountered than the methicillin-sensitive strain.[10,11,26,28] This Gram-positive bacterium is capable of forming biofilms on an implant or on necrotic bone, of forming abscesses in soft tissues and in bone marrow, and of penetrating into cells and colonizing the osteocyte–canaliculi network of cortical bone. Other skin commensal bacteria can also cause SSIs, such as coagulase-negative staphylococci, *Corynebacterium*, and *Propionibacterium*, as well as enterococci, enterobacterales, streptococcus, and *Candida* spp.[25,26] In human patients, SSIs developing within 2 weeks of surgery are mainly polymicrobial and frequently include enterobacterales and *Enterococcus* spp.[26] Furthermore, the Gram-negative bacteria *Pseudomonas aeruginosa* are also frequently involved, primarily due to their minimal nutritional needs, their tolerance to relatively high temperatures, and their resistance to various antibiotics.[29] It is worth noting that *P. aeruginosa* is responsible for more recurrences and therapeutic failures than *S. aureus*, and that an increased number in multiresistant *P. aeruginosa* infections has been reported.[11] Anaerobes present more frequently in polymicrobial infections, but remain rarely isolated overall.[26,30]

2.2 | Infection in bone healing

Bone healing is achieved through either primary or secondary repair mechanisms.[31] Primary bone healing occurs when stability of the construct is absolute and when strain at the fracture site has been eliminated, which implies anatomic reduction of the fracture, compression of bone fragments, and rigid fixation. When mechanical strain at the fracture site exceeds 2%, secondary bone healing occurs and involves formation of a bone callus.[31]

Bone infection promotes instability and non-union, but an unstable fracture site can also predispose to bone infection.[31] Indeed, clinical and experimental evidence show that a stable internal fixation of a fractured bone leads to less septic complications than an unstable fixation.[32] In fact, stability at the fracture site is considered compromised if bone infection persists for more than 2 weeks.[31]

2.3 | Risk factors for infection

In both human and veterinary medicine, treating bone infection presents a considerable challenge for orthopedic surgeons due to various factors that contribute to the persistence and resilience of these infections. The nature of implants, providing ideal surfaces for bacterial colonization, exacerbates this challenge. Bacteria that colonize fracture sites, such as *S. aureus*, are difficult to eradicate due to their virulence and their capacity to form biofilms.[33,34] Several factors contribute to the development of bacterial biofilms at a fracture site, notably by impairing both adaptive and innate host immunity. Exemplary risk factors for the development of fracture-related infection are shown in Table 1.

TABLE 1 Exemplary risk factors for the development of fracture-related infection (FRI).

General	Humans[17,35–37]	Animal[35]
Fracture type	Hypothermia	Physical status (ASA)
Bacterial strains	Hypoxia	Wound classification
Implant type	Smoking	Anesthesia and surgery time
Soft tissue trauma	Diabetes	Antimicrobial treatment
Environmental and physicochemical conditions[a]	Cardiac failure	Preoperative hair clipping
	Previous surgeries	Number of people present in the operating theater
	Immunodeficiency	
	Hypertension	Hypotension and the presence of endocrine disease
	Obesity	

Abbreviation: ASA, American Society of Anesthesiologists.

[a]Such as necrotic debris, hypoxia, attenuated immune response, fluid flow, circulating proteins.

In summary, postoperative orthopedic SSIs are a major health issue in human and veterinary medicine. Despite the identification of the common bacteria involved in SSIs and the main risk factors, these infections remain challenging to diagnose and treat, in large part due to the development of biofilms within the surgical site. Therefore, a comprehensive understanding of biofilm formation is critical for the emergence of new therapeutic methods that do not rely solely on antibiotics.

3 | MECHANISMS OF BACTERIAL BIOFILM FORMATION

Bacterial biofilm formation is a dynamic and multifactorial process. A biofilm is a community of microorganisms embedded in a hydrated matrix rich in self-produced extracellular polymeric substances (EPS) and in contact with a surface.[14] EPS are composed of proteins, polysaccharides, lipids, and extracellular DNA providing mechanical resistance, protection against antibiotics and immune cells, tolerance to dehydration, and constitute a carbon source to microorganisms.[29]

All bacteria are capable of forming biofilms, but the mechanisms governing adhesion to a surface, growth and maturation, and dispersion are inherent to each bacterium.[29] Indeed, bacterial genotype determines its ability to form a biofilm on a given surface and each bacterium has a preferred surface and an optimal pH and temperature for growth. For example, *S. aureus* adheres particularly well to metal, which explains why it is the most common isolate found in SSI post-orthopedic surgery.[10,11,28]

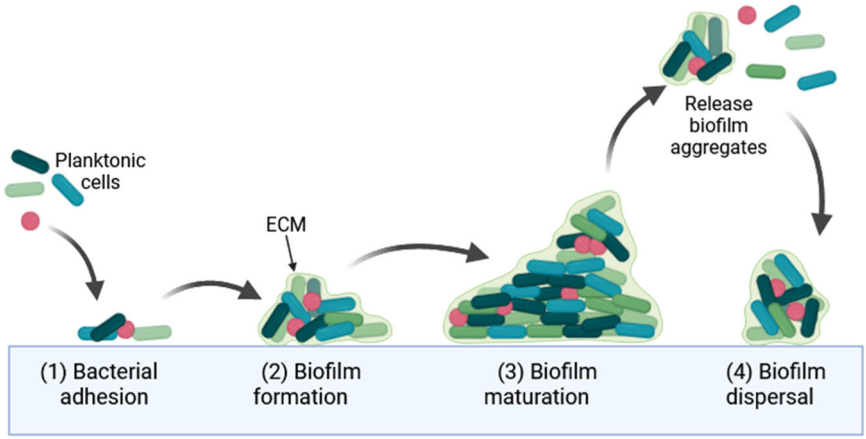

FIGURE 1 Stages of biofilm formation (modified from Shrestha et al.[29]). Following adhesion onto a surface, bacteria multiply and become embedded within a self-produced extracellular matrix rich in extracellular polymeric substances, thus forming a biofilm. This biofilm matures over time and ultimately becomes a three-dimensional structure. By the end of maturation, the biofilm undergoes a process known as dispersal, characterized by the detachment of bacterial cells (figure created with Biorender).

Biofilm formation is commonly considered to occur in four main stages as described in Figure 1: (1) reversible to irreversible bacterial adhesion to a surface; (2) bacterial growth and biofilm formation; (3) biofilm maturation; and (4) detachment and dispersion of bacteria.[37,38]

3.1 | Bacterial adhesion

Biofilm development is initiated by the adhesion of single bacteria onto a surface due to physical forces such as Van der Waals forces and electrostatic interactions. Reversible adhesion of the bacterium to the surface occurs due to weak interactions involving mechanosensing, the ability of a cell to sense mechanical cues of its microenvironment, including surface properties.[36,39] After mechanotransduction of the sensed signal, the production of intracellular signaling molecules occurs, thus fortifying the adhesion and making it irreversible.[39]

Adhesion onto the surface is influenced not only by the bacterium itself but also by the environmental characteristics and the surface properties.[11,40] Indeed, components of bacterial surfaces may affect initial adhesion. While lipopolysaccharides comprising the outer membrane of Gram-negative bacteria play a key role in this process, Gram-positive bacteria are deprived of an outer membrane and rely mostly on cell wall glycoproteins such as teichoic acid.[41] Furthermore, each bacterium has a specific affinity for a surface depending on its topology, chemical composition, charge, and hydrophobicity, but also depending on environmental factors such as temperature, pH, electrolytes concentration, flow, and presence of antibiotics.[39] Adhesion is most effective when electrostatic potentials and hydrophobicity between the bacterium and the surface are opposite and similar, respectively.[36]

3.2 | Biofilm formation

Following adhesion, bacteria multiply and form numerous microcolonies embedded in multiple layers among an exopolysaccharide matrix composed of EPS.[36,42] This extracellular matrix (ECM) provides the mechanical stability of a biofilm and the protection for the community of cells against environmental stresses.[43] The ECM provides hydration, nutrient storage, and protection from external environmental conditions, including mechanical forces, osmolarity fluctuations, and antimicrobial treatments. Similar components are found within the matrixes of Gram-negative and Gram-positive bacteria, such as extracellular DNA, polysaccharides, and amyloid-type proteins. These latter proteins are required for biofilm formation but also play roles in biofilm maturation and dispersion.[41]

Biofilm growth is initiated by mechanotransduction and chemical signaling within the matrix. The different bacterial microcolonies are separated by channels in which fluid and molecules circulate.[42] Biofilm growth is also influenced by genotypic factors, physicochemical factors, stochastic processes, determinist phenomena, mechanical processes, molecular exchanges, and temporal modifications.[39] Bis-3′-5′-cyclic dimeric guanosine monophosphate (c-di-GMP) is a key regulator in biofilm formation of Gram-negative bacteria, while its role remains to be established in Gram-positive bacteria.[41]

3.3 | Biofilm maturation

Maturation of the biofilm involves the formation of pores and channels, which serve as a circulatory system for distributing oxygen, water, and nutrients, and evacuating waste, and allows the circulation of molecules produced by bacteria.[44] Such intercellular signaling system, known as quorum sensing (QS), enables inter-bacteria communication via chemotaxis and directly affects their physiological state.[45] Molecules involved in QS are different between Gram-positive and -negative bacteria.[41]

3.4 | Biofilm detachment and dispersion

The final stage of biofilm formation is the detachment and dispersion of planktonic cells.[38] It is initiated by several mechanisms that allow

bacterial release from the biofilm matrix and dispersion into surrounding environment for further infection. Mechanical stress is one of the primary factors that triggers detachment. The stress can result from shear forces and wearing secondary to fluid flow. When subjected to these stresses, biofilms can become disrupted leading to the release of individual or clusters of bacteria.[46] Bacteria can also produce enzymes and tension-active agents, which can induce degradation of or detachment from the ECM.[39] Once parts of biofilms are detached, bacteria are able to disperse throughout the organism. They eventually reach the circulatory system and can cause systemic infections.[47]

Each stage of the complex biofilm formation is governed and is regulated by mechanobiological factors, the mechanisms by which they detect and respond to mechanical cues from their environment.[48]

Enzymatic degradation of the ECM may cause biofilm dispersion in both Gram types of bacteria.[41] For example, *P. aeruginosa* produces alginate lyases secondary to stress.[42] Moreover, bacteria attached to a surface can change the condition and become motile again.[39] Regulation of biofilm dispersion may differ between Gram-positive and Gram-negative bacteria.[41] A priori, mechanical stimuli could also influence toxin release, but this open question could merit dedicated multidisciplinary and multiscale explorations.

4 | MULTISCALE MECHANOBIOLOGY OF BIOFILM DEVELOPMENT

While a healing bone is constantly subjected to mechanical stresses, little is known about the impact of this mechanical environment on biofilm development.[49–51] Recent advances in high-resolution imaging techniques and bacterial studies have shed light on bacteria and biofilm mechanobiology. Studies have shown that bacteria sense mechanical stimuli through different receptors and effectors, which enable them to adapt, deform, and attach to or detach from a surface.[50,52] Some mechanical stimuli may even support biofilm development as a defense strategy in a hostile environment.[53] As the biofilm grows and matures, bacteria are embedded in the self-produced ECM whose composition can change in response to mechanical forces, significantly impacting the overall stability of biofilms. These mechanobiological interactions thus occur at all three scales: bacteria, biofilm, and implant, as illustrated in Figure 2.

4.1 | Mechanical factors at the microscopic scale of bacteria

Mechanosensitivity, the capacity to sense and respond to mechanical cues, plays a crucial role in the physiological response of bacteria and their survival.[52,54,55] Though studies have identified a direct link between bacterial initial accumulation and motility to the surface properties,[56–58] the mechanisms of how bacteria perceive and interact with the substrates are poorly understood. The bacterial cell envelope is a key element of mechanosensitivity, providing not only mechanical stability due to its turgor pressure but also functioning as a sensory interface, allowing bacteria to sense and respond to external mechanical cues such as changes in osmotic pressure and substrate stiffness and topography (Figure 2A).[56–62] For example, in *Escherichia coli*, the NlpE-Cpx transmembranous system activates the virulence factor regulation upon contact between the bacterial envelope and a surface.[63] Other bacteria respond to mechanical forces through membrane depolarization, which is responsible for a calcium influx, translating mechanical forces into intracellular ionic concentration.[64] As a response to the mechanical cues, mechanosensitive channels transduce the mechanical stimuli into cellular responses, regulating ion fluxes and cytoplasmic pressure. Another mechanism is based on cell surface components such as adhesins, which undergo conformational changes when subjected to tension, as seen in *E. coli* adhesin FimH, thereby reinforcing the bond between the bacterium and the surface.[65,66] This mechanism is known as *catch bond* and is responsible for *a stick and roll* motion of the bacterium on a surface. *S. aureus* can also reinforce its adhesion to a surface when external forces increase.[67] On the contrary, mechanical forces can destroy a cell-binding site, further proving that mechanosensitivity plays a crucial role in bacterial adhesion.[68] The exact mechanisms underlying detection, signaling, and responses by membranous receptors are still to be discovered.

Bacterial motility, a fundamental aspect of bacterial behavior, is closely linked to mechanobiology. Some bacteria have extensions, such as flagella or pili, which can serve as mechanosensory systems and enable the bacteria to sense the surface and respond according to the structure of the surface, its topography and stiffness.[69,70] Flagella-driven propulsion adapts to changes in fluid viscosity and flow by using the coordination of motor proteins within the bacterial cell envelope. The activation system of bacterial flagella is composed of a stator combined to a rotor, which is responsible for rotation and torque. Conformational changes of the stator's components are caused by the proton-motive force, and induce rotation of the rotor and of the flagellum consequently.[54] In *E. coli*, flagella adapt rotation speed and torque according to resistances met by the stator.[52,71] Adaptation happens mainly through positive feedback: if a force counteracts flagella rotation, for example, due to an increase in fluid viscosity, other subunits of the stator are recruited to increase the speed of rotation.[54,71] When bacteria encounter a surface, the physical interaction with the surface can change the rotation of the flagella. This alteration in flagella rotation allows bacteria to detect the surface and respond by modulating their motility. They may exhibit behaviors such as swimming along the surface, attaching to it, or changing direction to explore the surface features.

Type IV pili are motorized filaments present on the surface of many Gram-positive and Gram-negative bacteria. They are involved in motility and adhesion on surfaces, and they have been shown to have a critical role in bacterium motility. The molecular motor of type IV pilus is composed of different subunits which hydrolyze ATP to polymerize and depolymerize other subunits.[72] When type IV pilus is in contact with a surface, it detects a traction force and

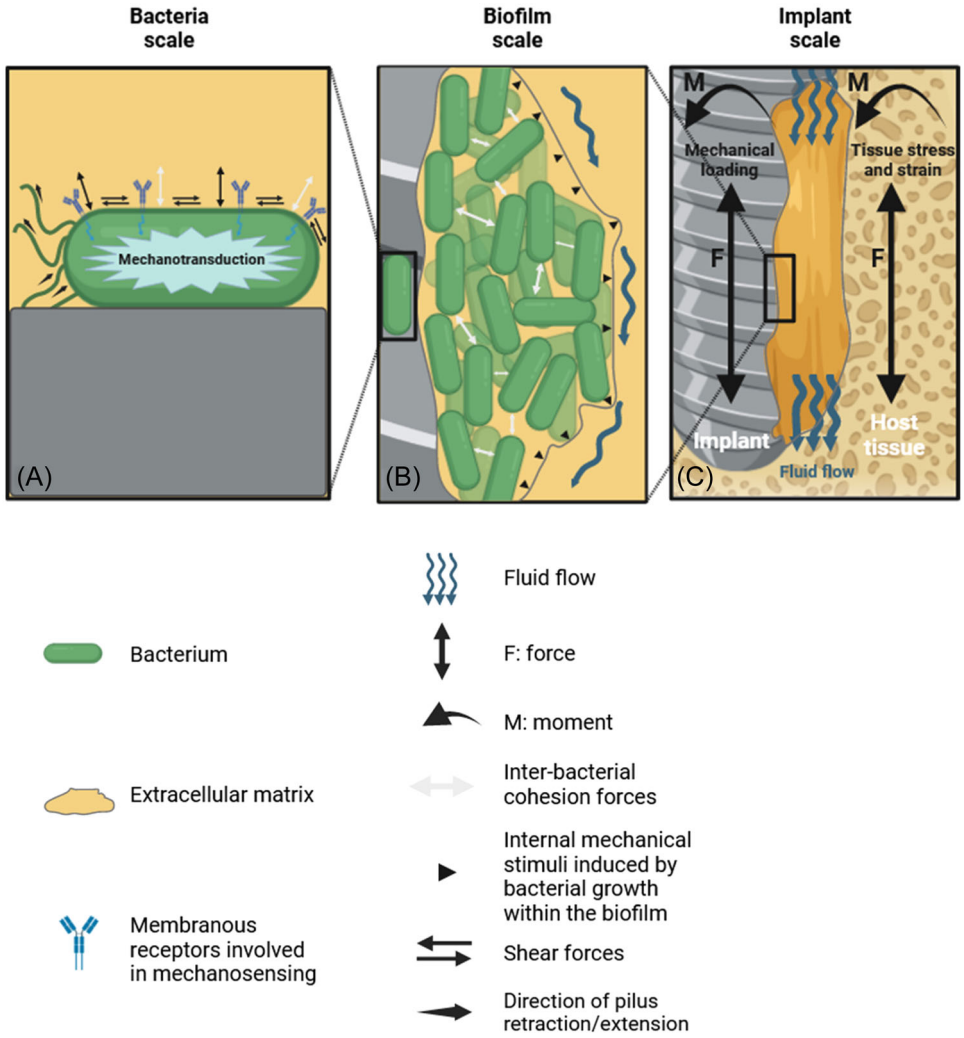

FIGURE 2 Mechanobiological interactions from bacterium to implant surface. (A) At the microscopic scale, the isolated bacterium perceives mechanical signals thanks to its membranous receptors, its bacterial envelope, and its surface organelles. (B) At the biofilm scale, bacterial growth within the self-produced extracellular matrix induces internal mechanical stimuli and increases inter-bacterial cohesion forces. (C) At the macroscopic scale, mechanical loading of the implant and host tissue behavior affects bone implant interface (BII) (figure created with Biorender).

retracts, thus attracting the bacterium against the surface. This mechanism is known as *twitching motility* and enables bacteria to move on a surface.[72] If the bacterium is subjected to increasing fluid flow and friction forces, the retraction force of the pilus is even greater.

Further research has suggested that bacteria also respond to acoustic cycled waves.[73] Specific acoustic waves appear to aggregate bacteria together and promote biofilm formation. Although the underlying mechanisms remain unexplained, concomitance with bacterial population increases might play a role. Indeed, increasing tension in bacteria might activate mechanosensitive channels of the cell membrane with a specific impact upon bacterial wall turgor pressure.[73] Biofilms also exhibit frequency-dependent responses. For instance, growth of *P. aeruginosa* and *S. aureus* biofilms are enhanced when exposed to 800 and 1600 Hz cycles for 48 h, respectively.[73] Conversely, low frequencies might either stimulate or inhibit biofilm growth in *E. coli* depending on exposure duration.[74]

4.2 | Mechanical factors at the mesoscopic scale of biofilm

While bacterial mechanosensing occurs predominantly on the microscale, biofilms size can range from micrometers, like dental plaques, up to centimeters, such as SSIs, which can be visible to the naked eye. This shift in scale from individual bacteria to biofilms brings new challenges and insights to the mechanobiology. At the biofilm scale, internal mechanical stimuli induced by bacterial growth can be considered (Figure 2B). The self-produced biofilm matrix not only maintains cohesion between bacterial cells but also links them to the underlying surface.[14] This cohesion is substantial for biofilm survival, as it protects the bacterial community against chemical, biological, and mechanical stresses. From a mechanical perspective, the biofilm behaves like a hydrated colloidal gel with rigid bacteria and a viscous matrix.[39] This structure grants viscoelastic properties to biofilms, resulting in both solid-like and

liquid-like responses, enabling them to withstand mechanical forces such as fluid shear through energy dispersion and mechanical stress distribution and adapting to their mechanical environment.[75] Indeed, mechanical cues can trigger changes in the production of EPS components altering the viscoelasticity of the biofilm through gene expression.[75] For instance, one could hypothesize that bacteria residing within an overly rigid matrix may produce matrix-destroying enzymes to reduce local elasticity so as to pursue bacterial growth. Conversely, bacteria may increase the production of matrix components when they perceive a local increase in elasticity, rendering their environment more rigid. Regardless of the conditions, bacterial cells arrangement within a biofilm influences their mode of interaction and communication, and impacts therefore QS and biofilm growth.[54]

Fluid flow and associated shear forces play pivotal roles, as they affect biofilm composition. Indeed, biofilms grown under a flow are thicker and denser.[39] Moreover, two biofilms originated from the same initial planktonic inoculum exhibit different compositions depending on whether bacterial growth occurs in a laminar or turbulent flow.[54] Turbulent flows seem to promote growth of a thin and dense biofilm, whereas laminar flows promote the formation of a more homogeneous, thicker and less dense biofilm.[39] Mechanical forces associated with both types of flow can affect the transport of signaling molecules and nutrients, and are likely to deform or damage the matrix, thus promoting adhesion or dispersion.[54]

4.3 | Mechanical factors at the macroscopic scale of fracture or implant fixation

Little is known about how mechanical forces influence the risk of infection at the bone implant interface (BII) (Figure 2C). At this scale, mechanical stresses and loading patterns significantly affect the dynamics and persistence of infections in and around orthopedics implants and can lead to fracture. A priori, clinical practice is considering that instability of the fracture site promotes infection,[11] and that conversely, stable fracture sites are less prone to fracture related infection and heal more rapidly.[31]

Some experimental studies showed contradictory results depending on bacteria phenotypes and animal species. It has been shown that femoral osteosynthesis with rigid fixation enabled eradication of inoculated *S. epidermitis* at the fracture site in mice, whereas infection was persisting with a compliant fixation. However, the authors showed that the mouse strain and the type of bacteria affected these results, especially with *S. aureus* resulting in more severe infections.[32]

Biomechanical analysis and computational modeling have been developed to understand the properties and behavior of biofilms at BII.[76,77] While these models provide valuable insights for optimal fixation configurations and prediction of outcome, these studies are still relatively new and a need for collaborations between scientists working with numerical models and clinicians is needed.

5 | CONCLUSION

Postoperative SSIs remain one of the common complications in orthopedic and musculoskeletal surgery in both human and veterinary surgery. Even though risk factors and commonly involved bacteria have been identified, these infections are challenging to treat because they are often associated with development of biofilms. Mechanics play not only a role in bone healing, but also affect bacteria and biofilm formation on implants. As such, each stage of biofilm formation is regulated by mechanical factors. While bacteria response to mechanical cues is well documented and the subject of many recent studies in interdisciplinary fields, an important gap in knowledge exists on the mechanobiology of infectious sites in BII. A comprehensive understanding of the mechanobiology of biofilms at these different scales is crucial for the development of innovative therapeutic strategies.

AUTHOR CONTRIBUTIONS

Pascal Swider and Margaux Blondel conceived and designed the review. Margaux Blondel, Camille Machet, Britt Wildemann, Yara Abidine, and Pascal Swider reviewed the literature and drafted the manuscript. Pascal Swider, YaraAbidine, Britt Wildemann, and Margaux Blond elcritically revised the manuscript. All authors have read and approved the final submitted manuscript.

ACKNOWLEDGMENTS

The authors would like to thank Sophie Palierne for her contribution to research projects involving Toulouse Veterinary School and IMFT UMR CNRS. The authors would like to acknowledge the support of the Deutsche Forschungsgemeinschaft (#444711651, RTG 2723 Materials-Microbes-Microenvironments) to Britt Wildemann.

ORCID

Britt Wildemann http://orcid.org/0000-0002-8365-1188
Pascal Swider http://orcid.org/0000-0001-6780-9830

REFERENCES

1. Calderwood MS, Anderson DJ, Bratzler DW, et al. Strategies to prevent surgical site infections in acute-care hospitals: 2022 update. *Infect Control Hosp Epidemiol*. 2023;44(5):695-720.
2. Motififard M, Teimouri M, Shirani K, Hatami S, Yadegari M. Prevalence of bacterial surgical site infection in traumatic patients undergoing orthopedic surgeries: a cross-sectional study. *Int J Burns Trauma*. 2021;11(3):191-196.
3. Gopal S, Majumder S, Batchelor AGB, Knight SL, De Boer P, Smith RM. Fix and flap: the radical orthopaedic and plastic treatment of severe open fractures of the tibia. *J Bone Joint Surg Br*. 2000; 82(7):959-966.
4. Mathews JA, Ward J, Chapman TW, Khan UM, Kelly MB. Single-stage orthoplastic reconstruction of Gustilo-Anderson Grade III open tibial fractures greatly reduces infection rates. *Injury*. 2015; 46(11):2263-2266.
5. Papakostidis C, Kanakaris NK, Pretel J, Faour O, Morell DJ, Giannoudis PV. Prevalence of complications of open tibial shaft fractures stratified as per the Gustilo-Anderson classification. *Injury*. 2011;42(12):1408-1415.

6. Thakore RV, Greenberg SE, Shi H, et al. Surgical site infection in orthopedic trauma: a case-control study evaluating risk factors and cost. *J Clin Orthop Trauma*. 2015;6(4):220-226.
7. Badia JM, Casey AL, Petrosillo N, Hudson PM, Mitchell SA, Crosby C. Impact of surgical site infection on healthcare costs and patient outcomes: a systematic review in six European countries. *J Hosp Infect*. 2017;96(1):1-15.
8. Png ME, Petrou S, Knight R, Masters J, Achten J, Costa ML. Economic outcomes associated with deep surgical site infection from lower limb fractures following major trauma. *Bone Joint Open*. 2022;3(5):398-403.
9. Parker B, Petrou S, Masters JPM, et al. Economic outcomes associated with deep surgical site infection in patients with an open fracture of the lower limb. *Bone Joint J*. 2018;100-B(11):1506-1510.
10. Gieling F, Peters S, Erichsen C, Richards RG, Zeiter S, Moriarty TF. Bacterial osteomyelitis in veterinary orthopaedics: pathophysiology, clinical presentation and advances in treatment across multiple species. *Vet J*. 2019;250:44-54.
11. Fang C, Wong T-M, Lau T-W, To KK, Wong SS, Leung F. Infection after fracture osteosynthesis—Part I: Pathogenesis, diagnosis and classification. *J Orthopaed Surg*. 2017;25(1):230949901769271.
12. Funk SS, Copley LAB. Acute hematogenous osteomyelitis in children. *Orthop Clin North Am*. 2017;48(2):199-208.
13. McNally M, Govaert G, Dudareva M, Morgenstern M, Metsemakers WJ. Definition and diagnosis of fracture-related infection. *EFORT Open Rev*. 2020;5(10):614-619.
14. Costerton JW, Stewart PS, Greenberg EP. Bacterial biofilms: a common cause of persistent infections. *Science*. 1999;284(5418):1318-1322.
15. Kennedy DG, O'Mahony AM, Culligan EP, O'Driscoll CM, Ryan KB. Strategies to mitigate and treat orthopaedic device-associated infections. *Antibiotics*. 2022;11(12):1822.
16. Bowler P, Murphy C, Wolcott R. Biofilm exacerbates antibiotic resistance: is this a current oversight in antimicrobial stewardship? *Antimicrob Resist Infect Control*. 2020;9(1):162.
17. Uruén C, Chopo-Escuin G, Tommassen J, Mainar-Jaime RC, Arenas J. Biofilms as promoters of bacterial antibiotic resistance and tolerance. *Antibiotics*. 2020;10(1):3.
18. Saeed K, McLaren AC, Schwarz EM, et al. 2018 international consensus meeting on musculoskeletal infection: summary from the biofilm workgroup and consensus on biofilm related musculoskeletal infections. *J Orthop Res*. 2019;37(5):1007-1017.
19. Schwarz EM, Parvizi J, Gehrke T, et al. 2018 international consensus meeting on musculoskeletal infection: research priorities from the general assembly questions. *J Orthop Res*. 2019;37(5):997-1006.
20. Hickok NJ, Li B, Oral E, et al. The 2023 Orthopedic Research Society's international consensus meeting on musculoskeletal infection: summary from the in vitro section. *J Orthop Res*. 2023. In press. doi:10.1002/jor.25774
21. Jennings JA, Arts JJ, Abuhussein E, et al. 2023 International consensus meeting on musculoskeletal infection: summary from the treatment workgroup and consensus on treatment in preclinical models. *J Orthop Res*. 2023. In press. doi:10.1002/jor.25765
22. Schwarz EM, Archer NK, Atkins GJ, et al. The 2023 Orthopaedic Research Society's International Consensus Meeting on musculoskeletal infection: Summary from the host immunity section. *J Orthop Res*. 2023. In press. doi:10.1002/jor.25758
23. Moriarty TF, Metsemakers W-J, Morgenstern M, et al. Fracture-related infection. *Nat Rev Dis Primers*. 2022;8(1):67.
24. Saeed K, Sendi P, Arnold WV, et al. Bacterial toxins in musculoskeletal infections. *J Orthop Res*. 2021;39(2):240-250.
25. González-Martín M, Silva V, Poeta P, Corbera JA, Tejedor-Junco MT. Microbiological aspects of osteomyelitis in veterinary medicine: drawing parallels to the infection in human medicine. *Vet Q*. 2022;42(1):1-11.
26. Depypere M, Sliepen J, Onsea J, et al. The microbiological etiology of fracture-related infection. *Front Cell Infect Microbiol*. 2022;12:934485.
27. Metsemakers W, Morgenstern M, McNally MA, et al. Fracture-related infection: a consensus on definition from an international expert group. *Injury*. 2018;49(3):505-510.
28. Morgenstern M, Erichsen C, Militz M, et al. The AO trauma CPP bone infection registry: epidemiology and outcomes of *Staphylococcus aureus* bone infection. *J Orthop Res*. 2021;39(1):136-146.
29. Shrestha L, Fan H-M, Tao H-R, Huang J-D. Recent strategies to combat biofilms using antimicrobial agents and therapeutic approaches. *Pathogens*. 2022;11(3):292.
30. Gitajn I, Werth P, O'Toole RV, et al. Microbial interspecies associations in fracture-related infection. *J Orthop Trauma*. 2022;36(6):309-316.
31. Foster AL, Moriarty TF, Zalavras C, et al. The influence of biomechanical stability on bone healing and fracture-related infection: the legacy of Stephan Perren. *Injury*. 2021;52(1):43-52.
32. SabatéBrescó M, O'Mahony L, Zeiter S, et al. Influence of fracture stability on *Staphylococcus epidermidis* and *Staphylococcus aureus* infection in a murine femoral fracture model. *Eur Cell Mater*. 2017;34:321-340.
33. Zimmerli W, Sendi P. Orthopaedic biofilm infections. *APMIS*. 2017;125(4):353-364.
34. Cheung GYC, Bae JS, Otto M. Pathogenicity and virulence of *Staphylococcus aureus*. *Virulence*. 2021;12(1):547-569.
35. Stetter J, Boge GS, Grönlund U, Bergström A. Risk factors for surgical site infection associated with clean surgical procedures in dogs. *Res Vet Sci*. 2021;136:616-621.
36. Filipović U, Dahmane RG, Ghannouchi S, et al. Bacterial adhesion on orthopedic implants. *Adv Colloid Interface Sci*. 2020;283:102228.
37. Wu Y-K, Cheng N-C, Cheng C-M. Biofilms in chronic wounds: pathogenesis and diagnosis. *Trends Biotechnol*. 2019;37(5):505-517.
38. Sauer K, Stoodley P, Goeres DM, et al. The biofilm life cycle: expanding the conceptual model of biofilm formation. *Nat Rev Microbiol*. 2022;20(10):608-620.
39. Krsmanovic M, Biswas D, Ali H, Kumar A, Ghosh R, Dickerson AK. Hydrodynamics and surface properties influence biofilm proliferation. *Adv Colloid Interface Sci*. 2021;288:102336.
40. Corder J, Munuera L, Folgueira MD. Influence of bacterial strains on bone infection. *J Orthop Res*. 1996;14(4):663-667.
41. Ruhal R, Kataria R. Biofilm patterns in Gram-positive and Gram-negative bacteria. *Microbiol Res*. 2021;251:126829.
42. Jamal M, Ahmad W, Andleeb S, et al. Bacterial biofilm and associated infections. *J Chin Med Assoc*. 2018;81(1):7-11.
43. Wilking JN, Angelini TE, Seminara A, Brenner MP, Weitz DA. Biofilms as complex fluids. *MRS Bull*. 2011;36(5):385-391.
44. Quan K, Hou J, Zhang Z, et al. Water in bacterial biofilms: pores and channels, storage and transport functions. *Crit Rev Microbiol*. 2022;48(3):283-302.
45. Waters CM, Bassler BL. Quorum sensing: cell-to-cell communication in bacteria. *Annu Rev Cell Dev Biol*. 2005;21:319-346.
46. Veerachamy S, Yarlagadda T, Manivasagam G, Yarlagadda PK. Bacterial adherence and biofilm formation on medical implants: a review. *Proc Inst Mech Eng H*. 2014;228(10):1083-1099.
47. Rumbaugh KP, Sauer K. Biofilmdispersion. *Nat Rev Microbiol*. 2020;18(10):571-586.
48. Dumont S, Prakash M. Emergent mechanics of biological structures. *Mol Biol Cell*. 2014;25(22):3461-3465.
49. Jara J, Alarcón F, Monnappa AK, et al. Self-adaptation of *Pseudomonas fluorescens* biofilms to hydrodynamic stress. *Front Microbiol*. 2021;11:588884.
50. Araújo GRS, Viana NB, Gómez F, Pontes B, Frases S. The mechanical properties of microbial surfaces and biofilms. *Cell Surf*. 2019;5:100028.

51. Xu H, Liu J, Zhang Z, et al. [Animal models in bacterial biofilm research: a review]. *Sheng Wu Gong Cheng Xue Bao = Chin J Biotechnol*. 2022;38(8):2840-2856.
52. Chawla R, Gupta R, Lele TP, Lele PP. A skeptic's guide to bacterial mechanosensing. *J Mol Biol*. 2020;432(2):523-533.
53. Bottagisio M, Barbacini P, Bidossi A, et al. Phenotypic modulation of biofilm formation in a *Staphylococcus epidermidis* orthopedic clinical isolate grown under different mechanical stimuli: contribution from a combined proteomic study. *Front Microbiol*. 2020;11:565914.
54. Dufrêne YF, Persat A. Mechanomicrobiology: how bacteria sense and respond to forces. *Nat Rev Microbiol*. 2020;18(4):227-240.
55. Gordon VD, Wang L. Bacterial mechanosensing: the force will be with you, always. *J Cell Sci*. 2019;132(7):jcs227694.
56. Song F, Brasch ME, Wang H, Henderson JH, Sauer K, Ren D. How bacteria respond to material stiffness during attachment: a role of *Escherichia coli* flagellar motility. *ACS Appl Mater Interfaces*. 2017;9(27):22176-22184.
57. Zheng S, Bawazir M, Dhall A, et al. Implication of surface properties, bacterial motility, and hydrodynamic conditions on bacterial surface sensing and their initial adhesion. *Front Bioeng Biotechnol*. 2021;9:643722.
58. Gomez S, Bureau L, John K, Chêne EN, Débarre D, Lecuyer S. Substrate stiffness impacts early biofilm formation by modulating *Pseudomonas aeruginosa* twitching motility. *eLife*. 2023;12:e81112.
59. Auer GK, Weibel DB. Bacterial cell mechanics. *Biochemistry*. 2017;56(29):3710-3724.
60. Rojas ER, Huang KC. Regulation of microbial growth by turgor pressure. *Curr Opin Microbiol*. 2018;42:62-70.
61. Harper CE, Hernandez CJ. Cell biomechanics and mechanobiology in bacteria: challenges and opportunities. *APL Bioeng*. 2020;4(2):021501.
62. Maier B. How physical interactions shape bacterial biofilms. *Annu Rev Biophys*. 2021;50(1):401-417.
63. Otto K, Silhavy TJ. Surface sensing and adhesion of *Escherichia coli* controlled by the Cpx-signaling pathway. *Proc Natl Acad Sci USA*. 2002;99(4):2287-2292.
64. Bruni GN, Weekley RA, Dodd BJT, Kralj JM. Voltage-gated calcium flux mediates Escherichia coli mechanosensation. *Proc Natl Acad Sci USA*. 2017;114(35):9445-9450.
65. Anderson BN, Ding AM, Nilsson LM, et al. Weak rolling adhesion enhances bacterial surface colonization. *J Bacteriol*. 2007;189(5):1794-1802.
66. Nilsson LM, Thomas WE, Sokurenko EV, Vogel V. Elevated shear stress protects *Escherichia coli* cells adhering to surfaces via catch bonds from detachment by soluble inhibitors. *Appl Environ Microbiol*. 2006;72(4):3005-3010.
67. Kerrigan SW, Clarke N, Loughman A, Meade G, Foster TJ, Cox D. Molecular basis for *Staphylococcus aureus*-mediated platelet aggregate formation under arterial shear in vitro. *Arterioscler Thromb Vasc Biol*. 2008;28(2):335-340.
68. Chabria M, Hertig S, Smith ML, Vogel V. Stretching fibronectin fibres disrupts binding of bacterial adhesins by physically destroying an epitope. *Nat Commun*. 2010;1(1):135.
69. Kreve S, Reis ACD. Bacterial adhesion to biomaterials: what regulates this attachment? A review. *Jpn Dent Sci Rev*. 2021;57:85-96.
70. Asp ME, Thanh M-TH, Dutta S, Comstock JA, Welch RD, Patteson AE. Mechanobiology as a tool for addressing the genotype-to-phenotype problem in microbiology. *Biophys Rev*. 2023;4(2):021304.
71. Persat A. Bacterial mechanotransduction. *Curr Opin Microbiol*. 2017;36:1-6.
72. Burrows LL. *Pseudomonas aeruginosa* twitching motility: type IV pili in action. *Annu Rev Microbiol*. 2012;66(1):493-520.
73. Murphy MF, Edwards T, Hobbs G, Shepherd J, Bezombes F. Acoustic vibration can enhance bacterial biofilm formation. *J Biosci Bioeng*. 2016;122(6):765-770.
74. Martirosyan V, Ayrapetyan S. Comparative study of time-dependent effects of 4 and 8 Hz mechanical vibration at infrasound frequency on *E. coli* K-12 cells proliferation. *Electromagn Biol Med*. 2015;34(4):293-297.
75. Nguyen H, Ybarra A, Başağaoğlu H, Shindell O. Biofilm viscoelasticity and nutrient source location control biofilm growth rate, migration rate, and morphology in shear flow. *Sci Rep*. 2021;11(1):16118.
76. Acemel RD, Govantes F, Cuetos A. Computer simulation study of early bacterial biofilm development. *Sci Rep*. 2018;8(1):5340.
77. Ferreira JA, De Oliveira P, Silva PM. Computational simulation of bacterial infections in surgical procedures: an exploratory study. In: Pinelas S, Graef JR, Hilger S, eds. *Differential and difference equations with applications*. Springer International Publishing; 2020:413-425. http://link.springer.com/10.1007/978-3-030-56323-3_32

How to cite this article: Blondel M, Machet C, Wildemann B, Abidine Y, Swider P. Mechanobiology of bacterial biofilms: implications for orthopedic infection. *J Orthop Res*. 2024;1-9. doi:10.1002/jor.25822

RÉPUBLIQUE FRANÇAISE
Liberté
Égalité
Fraternité

Université de Toulouse

Titre : Mécanobiologie des biofilms : influence de facteurs mécaniques sur la prolifération bactérienne par une approche expérimentale in-vitro

Mots clés : Biofilm, Mécanobiologie, Microfluidique, Pseudomonas aeruginosa, Infection, Chargement dynamique, Méthodes expérimentales

Résumé : L'infection postopératoire est une complication redoutée tant en chirurgie orthopédique humaine que vétérinaire, pouvant avoir des conséquences lourdes en termes de morbidité, de coûts et de récidives. Son éradication est particulièrement difficile, notamment à cause du développement de biofilms sur les implants utilisés. Les bactéries au sein d'un biofilm sont en effet tolérantes aux antibiotiques, ce qui explique les nombreux échecs thérapeutiques lorsqu'une antibiothérapie seule est utilisée. L'exploration des facteurs influant sur le développement de ces biofilms, en particulier l'impact de contraintes mécaniques fluides et solides auxquelles l'os en cours de cicatrisation est en permanence soumis, permettrait de développer des stratégies thérapeutiques alternatives aux antibiotiques, et de minimiser les risques d'antibiorésistances. L'hypothèse centrale de ce travail a consisté à supposer qu'un stimulus mécanique pouvait modifier la prolifération bactérienne et la formation du biofilm. La première partie de cette thèse s'attache à décrire les aspects cliniques de l'infection bactérienne en chirurgie orthopédique humaine et vétérinaire, ainsi que les mécanismes de formation d'un biofilm. La mécanobiologie sous-jacente au développement d'un biofilm est ensuite discutée dans une approche multi-échelle, de la bactérie au tissu biologique, et les stratégies thérapeutiques complémentaires ou alternatives aux antibiotiques sont présentées. La deuxième partie présente le dispositif expérimental original développé dans cette étude. Un dispositif microfluidique pouvant être soumis à un moment de flexion et permettant la formation d'un biofilm bactérien a été conçu. Ce dispositif a consisté en l'assemblage d'une puce contenant un micro-canal moulé dans du PDMS, et d'une lamelle flexible en PETG. Un système mécanique générant une force de flexion cyclique de fréquence et d'amplitude contrôlables (0 – 2.5 Hz et 0 – 3.10 mm, respectivement) a également été conçu. Les équations gouvernant la réponse cinématique du dispositif ont été fournies. La troisième partie du document présente et discute les résultats préliminaires obtenus dans l'étude in vitro. Afin de quantifier le développement du biofilm, les puces en PDMS ont été inoculées avec une souche de P. aeruginosa contenant un plasmide exprimant une protéine fluorescente. Les dispositifs microfluidiques ainsi inoculés ont ensuite été soumis à un moment de flexion (condition dynamique), et la réponse statique a été utilisée comme contrôle. La microscopie en épifluorescence a permis de comparer la fluorescence des puces dynamiques à celle des puces statiques. Les résultats préliminaires ont montré que la flexion cyclique pouvait impacter le développement des biofilms. D'une part, les biofilms se sont formés de façon aléatoire le long des micro-canaux soumis à la flexion, contrairement à ceux formés dans les micro-canaux statiques pendant ce même laps de temps. D'autre part, la taille et l'intensité de la fluorescence des biofilms formés ont également été impactées par la flexion, l'intensité restant inchangée entre les images capturées à 24h et 48h mais la taille augmentant. En comparaison avec les résultats statiques, cette dernière observation suggère que la flexion pourrait altérer la composition des biofilms, en particulier en diminuant la concentration bactérienne. En conclusion, la méthodologie proposée dans ce travail de thèse tend à valider l'hypothèse initiale au regard de la sensibilité mécanobiologique des biofilms bactériens, en particulier sous stimuli mécaniques à l'état d'équilibre. Ce document propose un cadre expérimental reproductible permettant d'évaluer l'impact d'un cycle dynamique sur le développement d'un biofilm bactérien, et éventuellement de tester des stratégies thérapeutiques dans un environnement contrôlé.

Title: Mechanobiology of biofilms: impact of mechanical factors on bacterial proliferation by an experimental approach in vitro

Key words: Biofilm, Mechanobiology, Microfluidics, Pseudomonas aeruginosa, Infection, Dynamic loading, Experimental methods

Abstract: Postoperative infection is a dreaded complication in human and veterinary orthopedics which can be associated with significant consequences in terms of morbidity, costs and recurrence. Its eradication is difficult, especially due to the development of biofilms on implants used. As a matter of fact, bacteria within a biofilm are tolerant to antibiotics, thus explaining the high number of therapeutic failures when antibiotic therapy alone is used. Investigating factors that could affect biofilm development, and particularly exploring the impacts of the solid and fluid mechanical stresses to which a healing bone is permanently submitted, could allow developing therapeutic strategies alternative to antibiotics and minimize the risk of antibiotic resistances. The main hypothesis of this work consisted in supposing that a mechanical stimulus could modify bacterial proliferation and biofilm formation. The first part of this work is based on describing the clinical aspects of bacterial infection in human and veterinary orthopedic surgery, as well as the mechanisms of biofilm formation. A multiscale approach of the mechanobiology underlying biofilm development is then discussed, starting from the bacterium to reach the biological tissue, and the therapeutic strategies alternative or additional to antibiotics are presented. In the second part, the original experimental workbench developed in this study is presented. A microfluidic device capable of sustaining a bending moment while still allowing bacterial biofilm growth was conceived. It consisted in a chip containing a microchannel molded into PDMS bonded to a flexible PETG coverslip. A mechanical system capable of generating a cyclic bending moment of controlled frequency and amplitude (0 – 2.5 Hz and 0 – 3.10 mm, respectively) was also conceived. The equations governing the kinematical response of the device were provided. The third part of the document presents and discusses the preliminary results of the in vitro study. To quantify biofilm development, PDMS chips were inoculated with a strain of P. aeruginosa containing a fluorescent protein-expressing plasmid. The microfluidic devices thus inoculated were then submitted to a bending moment (dynamic condition), and the static response was used as control. Imaging with epifluorescence microscopy was performed to compare fluorescence in the static chips with that in the dynamic chips. Preliminary results showed that cyclic bending may influence biofilm development. On the one hand, biofilms formed rather randomly along the microchannels submitted to bending, contrary to those formed in the static microchannels during the same period of time. On the other hand, biofilms size and fluorescence intensity were also affected by bending, with intensity remaining unchanged between microscopic images obtained at 24h and at 48h and size increasing. Compared to static results, this latter observation suggests that bending may alter biofilm composition, especially by decreasing bacterial concentration. In conclusion, the methodology presented in this thesis tends towards validating the initial hypothesis regarding the mechanobiological susceptibility of biofilms, in particular under steady state dynamical stimuli. This work suggests a reproducible experimental framework allowing to assess the impact of a dynamic cycle on bacterial biofilm development, and eventually to test therapeutic strategies in a controlled environment.